International
Progress Report

IPR-09-13

Äspö Hard Rock Laboratory

Prototype Repository

Acoustic emission and ultrasonic monitoring results from deposition hole DA3545G01 in the Prototype Repository between April 2008 and September 2008

D. Duckworth
J. Haycox
W.S. Pettitt
Applied Seismology Consultants

March 2009

Svensk Kärnbränslehantering AB
Swedish Nuclear Fuel
and Waste Management Co

Box 250, SE-101 24 Stockholm
Phone +46 8 459 84 00

Äspö Hard Rock
Laboratory

Report no.
IPR-09-13
No.
F63K
Author
D. Duckworth
J. Haycox
W.S. Pettitt
Date
March 2009
Checked by
Lars-Erik Johannesson
R.P. Young
Date
2009-08-27
Approved
Anders Sjöland
Date
2009-09-01

Äspö Hard Rock Laboratory

Prototype Repository

Acoustic emission and ultrasonic monitoring results from deposition hole DA3545G01 in the Prototype Repository between April 2008 and September 2008

D. Duckworth
J. Haycox
W.S. Pettitt
Applied Seismology Consultants

March 2009

Keywords: Field test, Prototype Repository, Acoustic emission, Ultrasonic monitoring, P-wave velocity, S-wave velocity, Rock fractures, Rock properties

Executive summary

This report describes results from acoustic emission (AE) and ultrasonic monitoring around a canister deposition hole (DA3545G01) in the Prototype Repository Experiment at SKB's Hard Rock Laboratory (HRL), Sweden. The experiment has been designed to simulate a disposal tunnel in a real deep repository environment for storage of high-level radioactive waste. The test consists of a 90m long, 5m diameter sub-horizontal tunnel excavated in dioritic granite. The monitoring aims to examine changes in the rock mass caused by an experimental repository, in particular due to thermal stresses induced from canister heating and pore pressures induced from tunnel sealing.

Two techniques are utilised here to investigate the processes occurring within the rock mass around the deposition hole: ultrasonic survey and acoustic emission monitoring. Ultrasonic surveys are used to 'actively' examine the rock. Velocity changes are measured between transmitter-receiver pairs using a cross-correlation technique that allows a velocity resolution of $\pm 2 ms^{-1}$. Amplitude and velocity changes on the ray-paths can then be interpreted in terms of changes in the material properties of the rock. Calculations using the velocities can determine the changes in dynamic moduli, Young's modulus and Poisson's ratio, to give direct indications of the properties of the rock through which the ray-paths travel. Crack density and saturation can also be calculated to determine changes in crack properties in the damaged and disturbed zones. AE monitoring is a 'passive' technique similar to earthquake monitoring but on a much smaller distance scale (source dimensions of millimetres). AEs occur on fractures in the rock when they are created or when they propagate.

Ultrasonic monitoring has been conducted at the Prototype Repository since September 1999. During excavation, monitoring of both deposition holes in section 2 of the Prototype Tunnel was undertaken to delineate zones of stress related fracturing and quantitatively measure fracturing in the damaged zone. A permanent ultrasonic array was installed in the rock mass in June 2002 around deposition hole DA3545G01.

The period covered by this report is between 1st April and 30th September 2008. The pulsing system malfunctioned on the 17th December 2007, so there is no survey data after this time through to July 2008, when a maintenance visit to the HRL was performed by an ASC Geophysicist. The passive AE data are not reliant on the pulsing system therefore the data coverage remained continuous throughout this period. The system was not operating for both ultrasonic and AE data between 31st August and 27th November 2008. In this period the system was refurbished and upgraded, and re-installed during a site visit by an ASC Geophysicist.

In total there were 60 located AE events (Figure I) for the portion of this period for which there was data captured. All AE events have good waveforms with clear P- and S-wave arrivals. The rate of AE triggering decreased from the previous monitoring period, with an average of 0.38 triggers recorded each day. In this report we have examined the relationship between the AE activity and nearby blasting activities occurring during excavation of a neighbouring tunnel close to the Prototype Experiment. We have found no direct correlation between the timing of increased AE triggering and blasting in this report, although a time dependent effect resulting from the new excavation cannot be ruled out.

A study of the spatial distribution of AEs shows that there are primarily three distinct clusters, labelled A, B, and D during this period. Events in the individual clusters are located close enough together to be considered to occur along the same feature. Cluster A is made up of 29 events located on the SE side, Cluster B (12 events) is located on the SW side and Cluster D (4 events) is located NE of deposition hole DA3545G01. Some minor activity is observed in the same volumes as have been observed in the past: Cluster C (3 events) and Cluster T (2 events). Clusters A and B have been observed over the past two years [e.g. *Zolezzi et al.,* 2007 and 2008; *Duckworth et al*., 2008]. Cluster D was identified in the last report by *Duckworth et al.,* [2008] and is located in a region that was active during the initial phases of the experiment [*Pettitt et al.,* 2000] although not at the precise depths we have observed recently. Cluster A locates in a region of low-compressive or tensile stress and Cluster B locates in a region of high compressive stress induced around the excavation [*Pettitt et al.,* 1999]. The clustering of AEs around the deposition hole is a recurring feature in the data from the Prototype Repository. They are thought to be occurring at these positions due to the presence of pre-existing micro-cracks generated during excavation.

Due to the lack of survey data during this period, we have assembled the data recorded here, from July and August 2008, with data recorded during the previous recording period so as to evaluate any significant changes across the time when no recording was performed. Velocity analysis reveals changes in P- and S-wave velocity that closely mimic one another but with larger variations observed for P-waves (Figure II). The maximum changes in average velocity are ~1ms^{-1} for P-waves and ~0.4ms^{-1} for S-waves, with changes across the monitoring period generally occurring in the range of ±0.4ms^{-1} for P-waves and ±0.1ms^{-1} for S-waves. The magnitudes of the average velocity changes are significantly smaller than the velocity uncertainty of 2ms^{-1} estimated for ultrasonic measurements, however, changes on individual ray-paths may be more pronounced. For example, the greatest magnitude change in velocity is observed on the ray-path between transmitter three and receiver nine (on the 18th August 2008), when P-wave velocity decreases by ~10ms^{-1}. Similar changes are also noted in P- and S-wave amplitudes.

Both P- and S-waves show the same velocity variations on each of the category ray-paths during the period that data were actively recorded (23rd July to 31st August 2008). For P-waves, ray-path 'C1' exhibits the greatest variation with average changes in the region of 0.6ms^{-1} and a maximum change of ~1.7ms^{-1}. For S-waves, category 'Far' exhibits the most variation with average changes of ~0.3ms^{-1} and a maximum change of 0.6ms^{-1}. Overall, P-wave velocities display more variation than S-wave. The maximum change in amplitude is ~0.2dB for both P- and S-waves with average changes in the region of 0.05dB – 0.1dB. The small changes in velocity and amplitude reflect the stable environmental (i.e. temperature and pressure) conditions in and around the canister deposition hole over the period monitored.

Over the 6-month monitoring period there is a small decrease in temperature of ~7°C. Pressure variations are observed during the period that no survey measurements were performed, but result in a small total pressure change when the system returns to being operational (decrease of ~0.8MPa). These changes have had very small accumulated effects on the P- and S-wave velocities and amplitudes measured, and are not significant compared to the uncertainties or to changes measured in previous monitoring periods. AE rates and changes in ultrasonic survey parameters have remained relatively small indicating that the rock mass around the deposition holes has remained stable throughout this report period.

There are over five years of ultrasonic survey measurements at the Prototype experiment with velocity and amplitude measurements conducted through a number of variations in pressure and temperature conditions. We believe it would now be beneficial to perform an additional integrated interpretation of changes in these measurements with available data on the thermal and hydro-mechanical conditions in the repository, in order to better understand the rock response in the immediate vicinity of the deposition hole. This could help resolve whether pressure or temperature, or an optimal combination of the two, has a leading role in reducing crack density (and hence permeability) and thus provide a best practise for working conditions of a future repository.

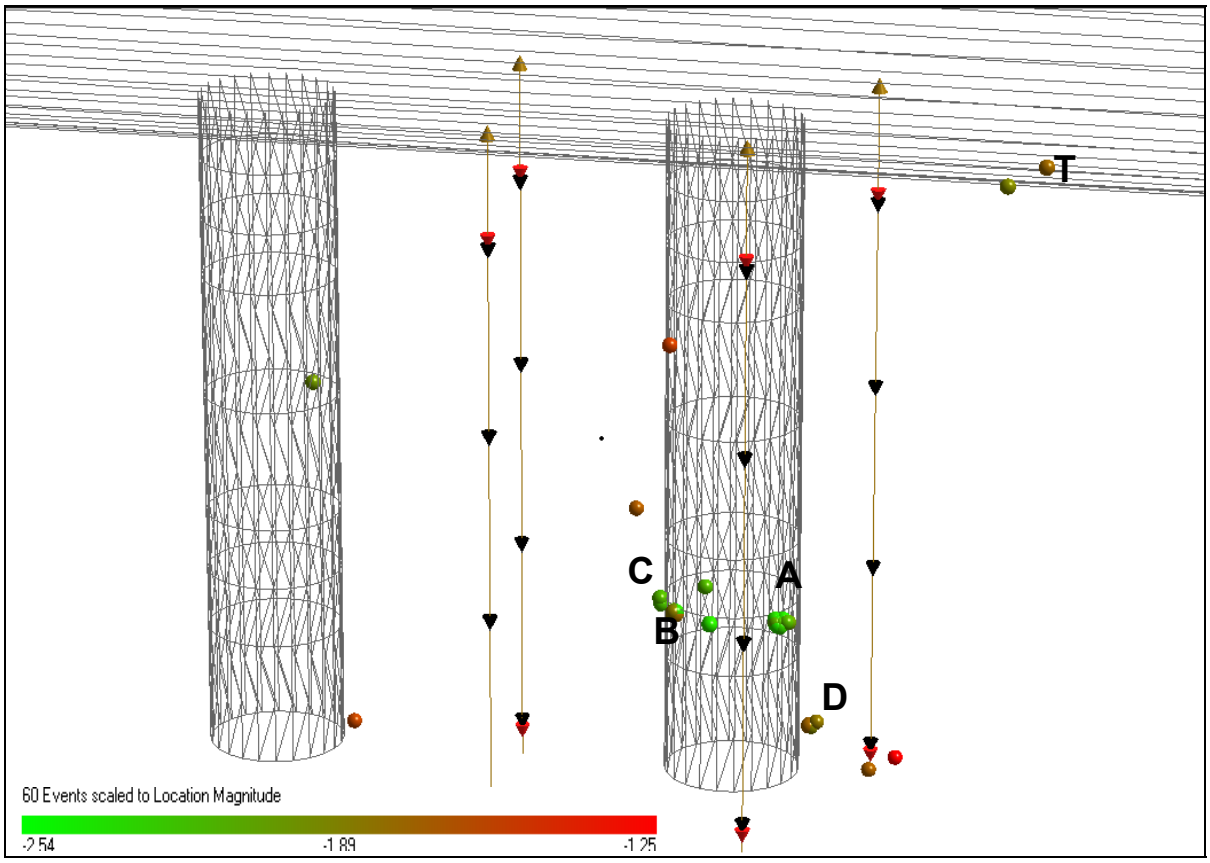

Figure I: *Located AE events observed around the deposition hole for this monitoring period. Events are scaled to location magnitude.*

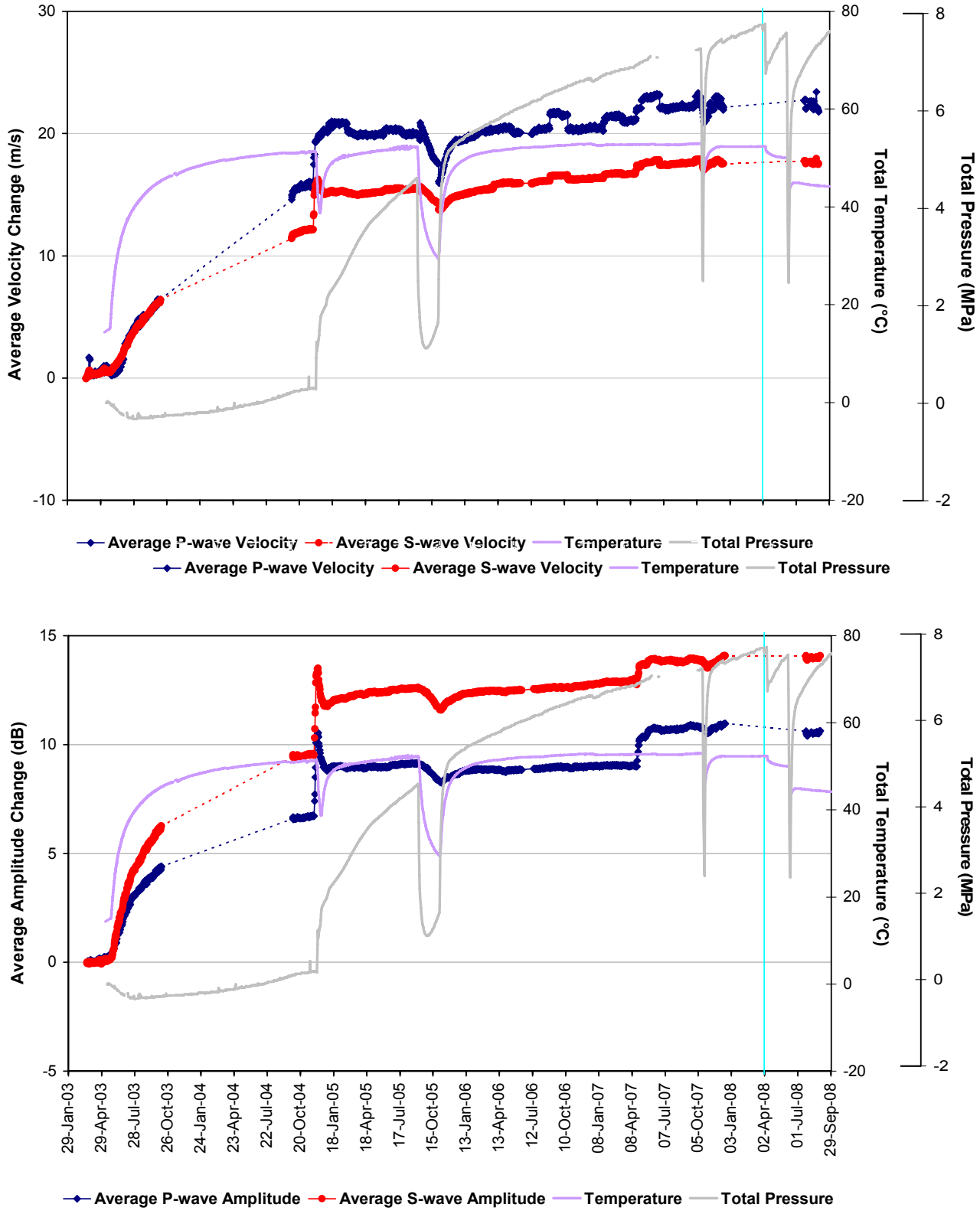

Figure II: *Average velocity and amplitude changes since the start of the heating and pressurisation phase at the Prototype Repository. The vertical blue line indicates the start of the period analysed in this report (1st March 2008 – 30th September 2008).*

Sammanfattning

Denna rapport beskriver resultaten från AE-mätningar (**A**coustic **E**mission) och ultaljudsmätningar runt deponeringshål DA3545G01 i prototypförvaret vid SKB:s Hard Rock Laboratory. Experimentet har designats för att simulera en deponeringstunnel i ett verkligt djupförvar för högaktivt radioaktivt avfall. Det består av en 90 m lång horisontell tunnel med en diameter på 5 m, uttagen ur en dioritisk granit. Syftet med mätningen är att undersöka förändringar i bergmassan som orsakats av en experimentell förvarsmiljö, speciellt med avseende på värmespänning från uppvärmning av kapseln och portryck orsakade av förseglingen av tunneln.

Två tekniker används för att undersöka de processer som förekommer i bergmassan runt deponeringshålet; ultraljudsmätning och AE-mätningar. Ultraljudsmätning används för att ”aktivt” undersöka berget. Hastighetsförändringar mäts mellan sändare - givare genom att utnyttja en kors-korrelationsteknik som möjliggör en mätnoggrannhet på ± 2 ms^{-1}. Förändringar i amplitud och hastighet hos signalen när den passerat genom bergmassan längs olika signalvägar relativt deponeringshålen, (”ray path”) har sedan använts för att undersöka förändringar i bergegenskaperna. Hastigheterna användas för att bestämma förändringar i dynamisk modul, elasticitetsmodul och tvärkontraktionstal som ger direkta indikationer på egenskaperna på berget genom vilket vågen passerar. Sprickdensitet och vattenmättnadsgrad kan också beräknas för att fastställa förändringar i sprickornas egenskaper i de skadade och störda zonerna. AE-mätning är en ”passiv” teknik som liknar jordbävningsövervakning men på en mycket mindre avståndsskala (dimensioner på källan i millimetrar). AE uppkommer hos bergssprickor när de bildas eller när de rör sig.

Ultraljudsmätningar har utförts i projektet Prototype Repository sedan september 1999. Mätningar gjordes runt de båda deponeringshålen i sektion 2 under borrningen av dessa. Syftet med mätningarna var att beskriva zoner med spänningsrelaterade sprickor och kvantitativt mäta sprickutbildningen i den störda zonen runt deponeringshålen. Ett permanent ultraljudssystem installerades i berget runt deponeringshål DA3545G01 i juni 2002.

Denna rapport behandlar mätningar under perioden 1:a april till 30:e september 2008. Systemet som generar pulser slutade fungera den 17:e december 2007 och därför finns inga mätdata från ultraljudsmätningarna efter den tidpunkten fram till juli 2008 då service gjordes på systemet av en geofysiker från ASC. AE-mätningarna är inte beroende av systemet som genererar pulser varför dessa mätningar gjordes kontinuerligt under hela mätperioden. Systemet för mätning av både ultraljud och AE fungerade inte under perioden 31:e augusti och 27:e november 2008. Under denna perioden förbättrades, uppgraderades och ominstallerades systemet vid ett platsbesök av en geofysiker från ASC.

Totalt lokaliserades 60 AE (Figur I) under den del av mätperioden data samlades in. Alla AE har en bra vågform med tydlig ankomst av P- och S-vågorna. Takten på AE minskade jämfört med den tidigare mätperioden. Antalet AE i medeltal per dag var 0.38. I denna rapport undersöker vi förhållande mellan AE-aktiviteter och aktiviteter i samband med sprängning för uttag av en närliggande tunnel. Vi har inte funnit någon direkt korrelation mellan tidpunkter av ökande AE och sprängningsaktiviteter i denna rapport, även om en tidsberoende effekt av tunnledrivningen inte kan uteslutas.

En studie av den rumsliga fördelningen av AE under denna period visar att det finns fyra distinkta kluster, med beteckningarna A, B, och D. Händelser i det enskilda klustret är lokaliserade så nära varandra att de kan anses uppträda på samma anomali. Kluster A består av 29 händelser lokaliserade till SE sidan, Kluster B (12 händelser) är lokaliserat till SW sidan och Kluster D (4 händelser) är lokaliserat till NE sidan av deponeringshål DA3545G01. Mindre aktivitet har observerats i samma volymer som tidigare: Kluster C (3 händelser) och Kluster T (2 händelser). Kluster A och B har observerats under de senaste 2 åren [*Zolezzi et al.,* 2007 och 2008; *Duckworth et al*., 2008]. Kluster D identifierades i den senaste rapporten [*Duckworth et al*., 2008] och den ligger i en region som var aktiv under initialskedet av försöket [*Pettitt et al.,* 2000] även om djupet ner till aktiviteterna varierar. Kluster A ligger i regioner med låga tryckspänningar eller med dragspänningar medan Kluster B ligger i regioner med höga kompressionsspänningar som inducerades vid uttaget av deponeringshålet [Pettitt et al. 1999]. Uppkomsten av kluster av AE runt deponeringshålet är ett återkommande drag i data från Prototypeförsöket. De anses uppstå i dessa positioner på grund av närvaro av mikrosprickor som uppstod under uttaget av deponeringshålet.

På grund av brist på mätdata under denna mätperiod har vi sammanställt data som insamlats under juli till augusti 2008 med data från den föregående mätperioden i syfte att kunna utvärdera eventuella signifikanta förändringar under perioden när ingen datainsamling gjordes. Analyser av hastigheterna för P- och S-vågorna visar att de liknar varandra men med större variationer observerade för P-vågorna (Figur II). Den största förändringen i medelhastigheten är ~1ms^{-1} för P-vågorna och ~0.4 ms^{-1} för S-vågorna. Förändringen över mätperioden i hastigheten är i storleksordningen ±0.4 ms^{-1} för P-vågorna och ±0.1 ms^{-1} för S-vågorna. Magnituden på förändringarna i medelhastigheterna är signifikant mindre än osäkerheten i mätningarna på 2ms^{-1} uppskattat från ultraljudsmätningar. Emellertid kan förändringar i hastigheten för en enskild signalväg vara mer uttalade. Som exempel uppmättes den största förändringen i hastighet för signalvägen mellan sändare tre och mottagare nio till en minskning för P-vågen på ~10ms^{-1} (uppmätt den18:e augusti 2008). Liknande förändringar noteras också för amplituderna för P- och S-vågorna.

Både P- och S-vågor uppvisar samma variationer i hastighet för varje kategori av signalvägar under perioden data samlades in (23:e juli till den 31:e augusti 2008). För P-vågorna uppvisar signalvägen ”C1” den största variationen med förändringar i medeltal på 0.6ms^{-1} och en maximal förändring på ~1.7ms^{-1}. För S-vågorna uppvisar signalvägen ”Far” den största variationen med förändringar i medeltal på ~0.3ms^{-1} och en maximal förändring på 0.6ms^{-1}. På det hela taget uppvisar P-vågen större hastighetsförändringar jämfört med S-vågen. Den maximala förändringen i amplitud är ~0.2dB för både P- och S-vågorna med en medelförändring i intervallet 0.05dB – 0.1dB. De små förändringarna i hastighet och amplitud avspeglar de stabila förhållandena vad gäller temperatur och tryck i och runt deponeringshålet under denna mätperiod.

Under senaste 6-månaders mätperiod sjönk temperaturen med ~7°C. Variation i trycket kunde observeras under tiden när inga akustiska mätningar gjordes men resulterade i små förändringar i totaltrycket när mätsystemet fungerade igen. (minskning med ~0.8MPa). Dessa förändringar har haft mycket små ackumulerade effekter på P- och S-vågornas uppmätta hastigheter och amplituder och är inte signifikanta i jämförelse med osäkerheterna eller förändringar uppmätta under tidigare mätperioder. Frekvensen av AE och förändringar i mätvärden från ultraljudsmätningarna har varit relativt små vilket indikerar att bergmassan runt deponeringshålen har förblivit stabil under denna mätperiod.

Över fem års ultrasonicmätningar vid Prototypeförvaret har genomförts innefattande hastighets- och amplitudmätningar. Mätningarna har gjorts vid varierande tryck- och temperaturförhållanden. Det vore fördelaktigt om man nu kunde genomföra en ytterligare integrerade tolkning av förändringarna i dessa mätningar med tillgänglig data gällande termiska och hydromekaniska förhållanden i förvaret i syfte att bättre kunna förstå bergets beteende i närheten av deponeringshålet. En sådan analys kan hjälpa till lösa frågeställningen huruvida tryck eller temperatur eller en optimal kombination av de två parametrarna har en betydande roll i reduktionen av sprickdensitet (och medföljande permeabilitet) och därför sörja för en bästa uppskattning gällande funktionen av ett framtida förvar.

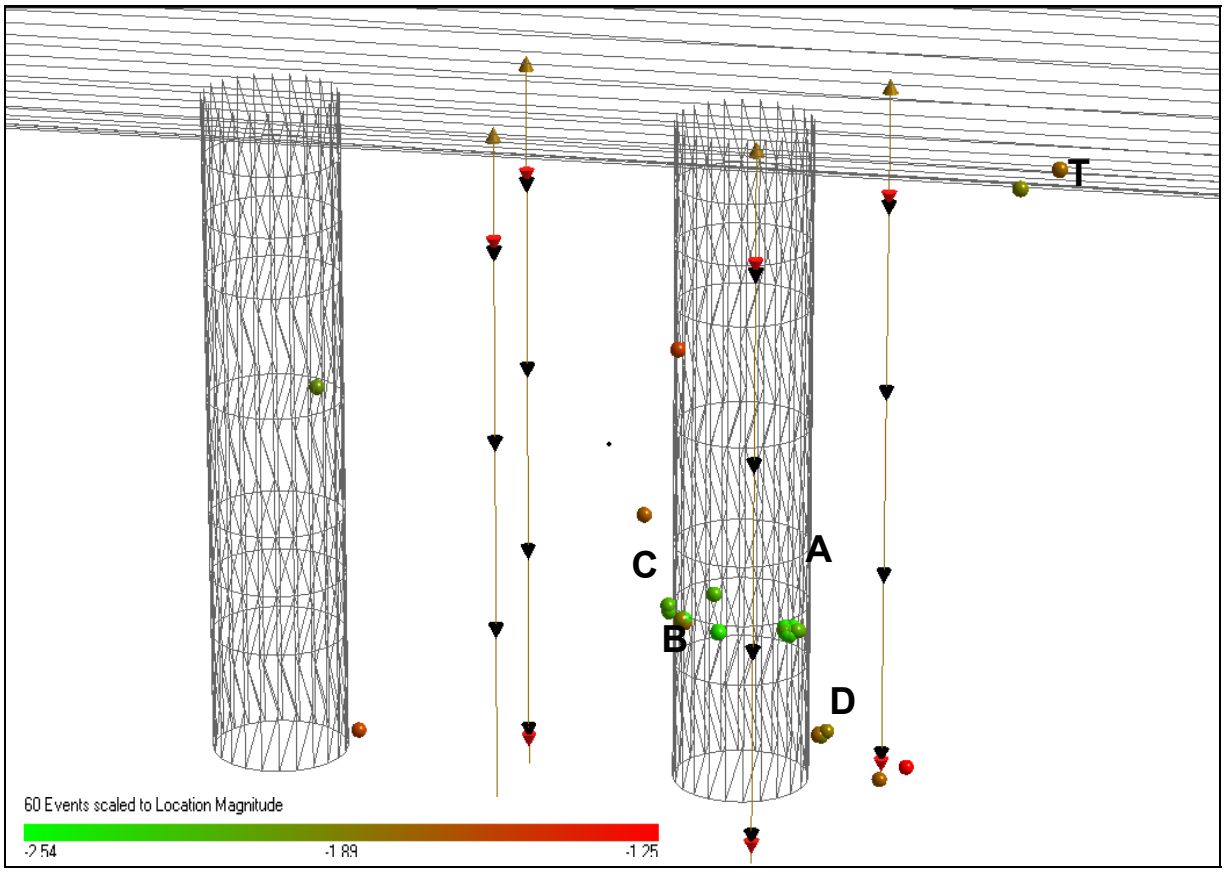

Figur I: *Lokaliserade AE observerade runt deponeringshålet under denna mätperiod.*

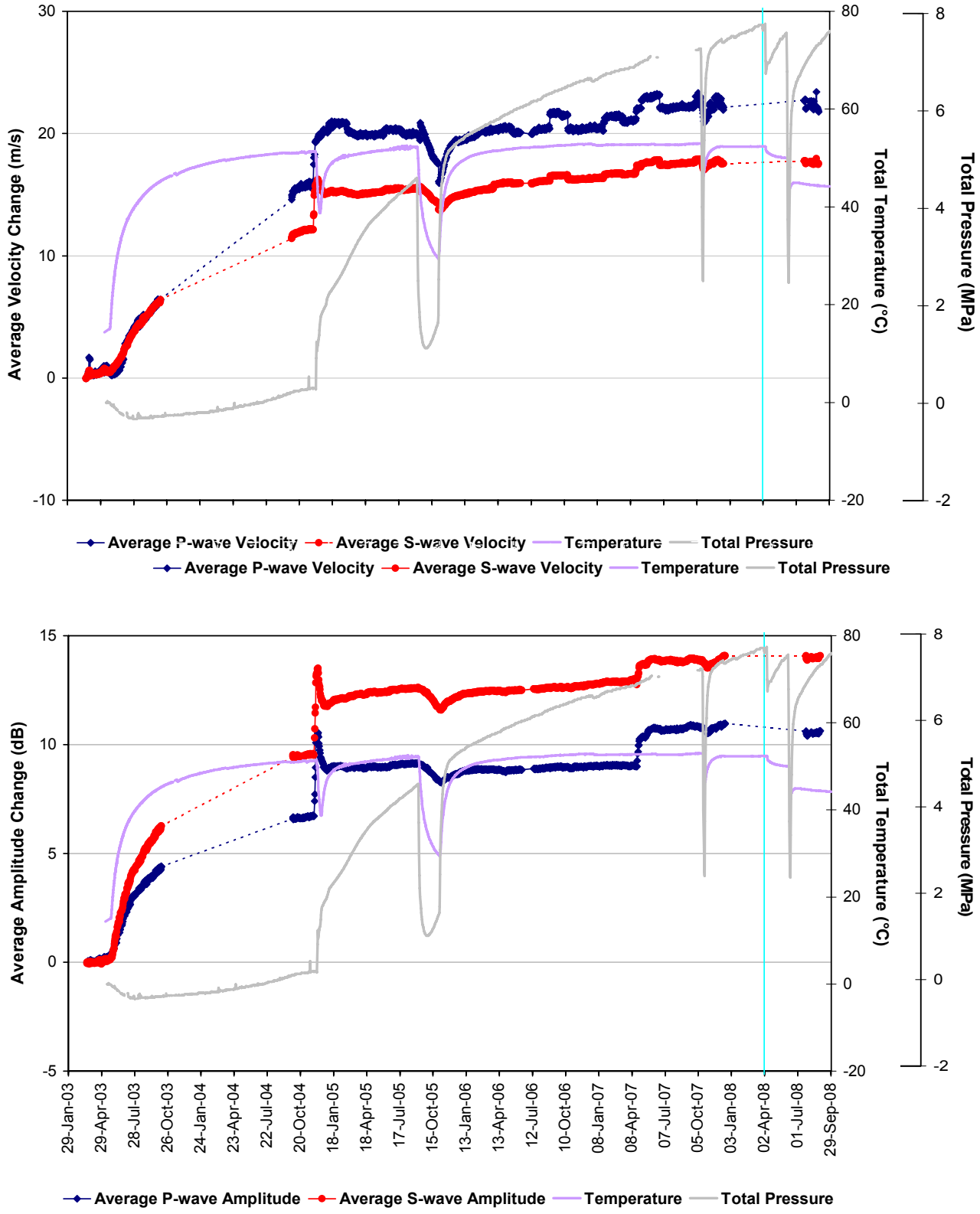

Figur II: *Förändringar i medelhastighet och medelamplitud sedan starten av uppvärmningen och trycksättningen av Prototyp Repository. Den vertikala blå linjen indikerar början på perioden som analyserats i denna rapport (1:a mars 2008 – 30:e september 2008).*

Contents

Table of Figures

Table of Tables

1 Introduction

This report describes results from acoustic emission (AE) and ultrasonic monitoring around a canister deposition hole (DA3545G01) in the Prototype Repository Experiment at SKB's Hard Rock Laboratory (HRL), Sweden. The monitoring aims to examine changes in the rock mass caused by an experimental repository environment, in particular due to thermal stresses induced from canister heating and pore pressures induced from tunnel sealing. Monitoring of this volume has previously been performed during excavation [*Pettitt et al.,* 1999], and during stages of canister heating and tunnel pressurisation [*Haycox et al.,* 2005a and 2005b; *Haycox et al.,* 2006a and 2006b; *Zolezzi et al.,* 2007 and *Duckworth et al.,* 2008]. Further information on this monitoring can be found in Appendix I. This report covers the period between 1st April 2008 and 30th September 2008 and is the seventh instalment of the 6-monthly processing and interpretation of the results from the experiment.

The Prototype Repository Experiment (Figure 1-1) has been designed to simulate a disposal tunnel in a real deep repository for disposal of high-level radioactive waste. Its objective is 'to test and demonstrate the integrated function of the repository components under realistic conditions on a full scale and to compare results with models and assumptions'. The experiment consists of a 90m long, 5m diameter sub-horizontal tunnel excavated in dioritic granite using a Tunnel Boring Machine (TBM). The rock mass has two main discontinuous sets of sparse, en-echelon fractures [*Patel et al.,* 1997]. The Prototype Repository design incorporates six full-scale canister deposition holes which have been excavated vertically into the floor of the tunnel using a TBM converted to vertical boring. Each deposition hole measures 1.75m in diameter and approximately 8.8m in length. Simulated waste canisters, encased in a bentonite buffer, have been placed into each deposition hole and heated from within by specially designed electric heaters to simulate disposed radioactive material at elevated temperatures. The tunnel was then backfilled using a mixture of bentonite and crushed rock, and sealed using concrete plugs. A range of measurements are made in and around the tunnel and deposition holes.

AE and ultrasonic monitoring are tools for remotely examining the extent and severity of damage and disturbance around an excavation. This can be induced by the excavation method itself; by the redistribution of stresses (loading or unloading) resulting from the void or by environmental affects such as heating, saturation or pressurisation. Acoustic techniques are particularly adept at assessing the Excavation Damaged or Disturbed Zone (EDZ) as they allow it to be mapped spatially and temporally with high resolution, and they allow the effect on the rock mass to be quantifiably measured. Furthermore, acoustic techniques allow investigations to be conducted remotely, without the need for potentially damaging coring. *Young and Pettitt* [2000] give a review of AE and ultrasonic results from a number of experiments conducted in different underground environments.

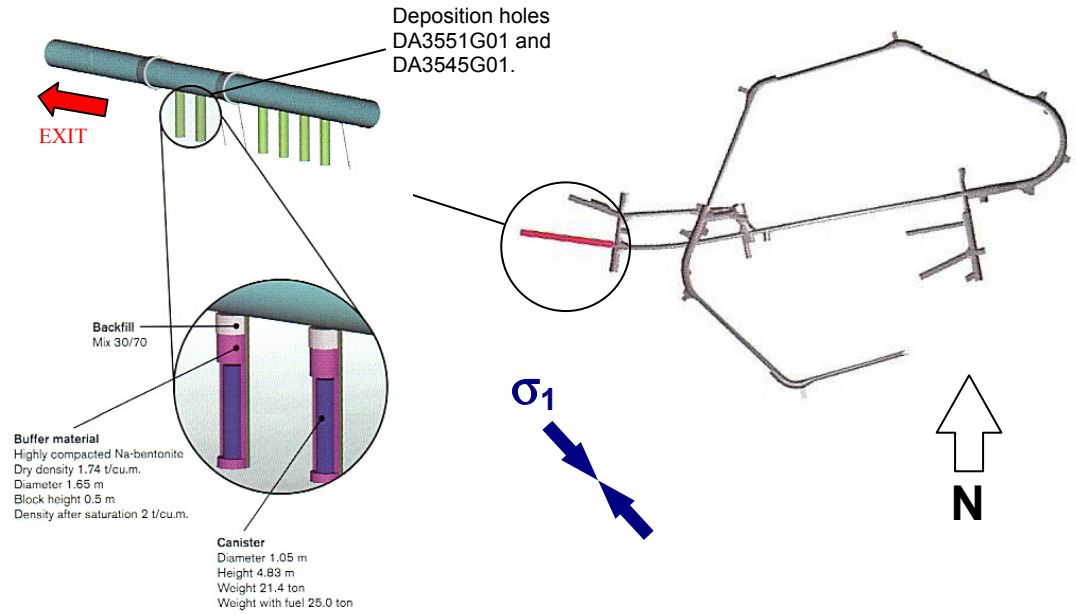

Figure 1-1: *Plan view of the experimental tunnels at the Äspö HRL and the location of the Prototype Repository. A schematic illustration of the final experimental set up is shown with canisters and bentonite clay buffer installed in the 1.75m diameter deposition holes. Note the entrance of the tunnel is towards the left. Graphics are modified from SKB [1999].*

- AE monitoring is a 'passive' technique similar to earthquake monitoring but on a much smaller distance scale (source dimensions of millimetres). AEs occur on fractures in the rock sample when they are created or when they move. The data acquisition system triggers on AEs when they occur and records full-waveform information that can then be used to delineate the amount, time, location and mechanism fracturing.

- Ultrasonic surveys are used to 'actively' examine the rock. In this case an array of transmitters sends signals to an array of receivers. Amplitude and velocity changes on the ray-paths can be interpreted in terms of changes in the material properties of the rock. Calculations using the velocities can determine changes in dynamic moduli, Young's modulus and Poisson's ratio, to give direct indications of the properties of the rock through which the ray-paths travel. Crack density and saturation can also be calculated to determine changes in crack properties in the damaged and disturbed zones.

Appendix II provides detailed descriptions of the data acquisition and processing used during this and past monitoring periods. The ultrasonic array consists of twenty-four ultrasonic transducers configured as eight transmitters and sixteen receivers installed into four instrumentation boreholes using specially designed installation frames sealed within slightly expansive grout. The array is designed to provide good coverage for AE locations and provide 'skimming' ray-paths so as to sample the rock immediately adjacent to the wall of the deposition hole. ASC's InSite Seismic Processor [*Pettitt and Young,* 2007], has been used to automatically process both the AE and ultrasonic survey data. Appendix III A and Appendix III B give the processing parameters used. Data

from daily ultrasonic surveys have been automatically picked and arrivals cross-correlated to a reference survey for high-precision measurements of P- and S-wave velocity changes throughout the experiment. Arrivals of AEs have been manually picked and three dimensional source locations have been calculated.

A power supply malfunction in the pulsing system occurred between 17th December 2007 and 23rd July 2008 and resulted in a gap in ultrasonic survey data with AE data continuing to be recorded. The system ceased operating between 31st August and 27th November 2008 and resulted in a gap in both ultrasonic and AE data (Figure 1-2). The system was returned to ASC for refurbishment and upgrade and was successfully reinstalled at the HRL.

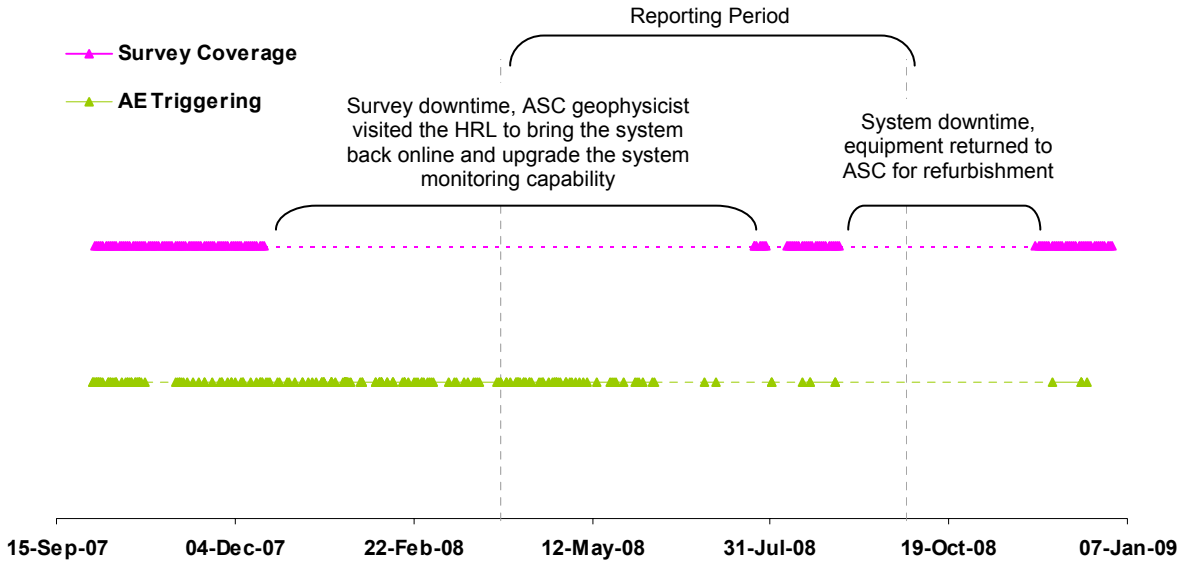

Figure 1-2: *Time-line showing the periods when the acquisition system was operational. AE coverage is almost continuous with only one gap in the data record between 31st August and 27th November, 2008 when the equipment ceased operating (blue rectangle). Ultrasonic survey coverage is sparser with one major gap in the data stream between 17th December 2007 and 23rd July 2008 due to a power supply malfunction in the pulsing system (yellow rectangle), and also the same gap between 31st August and 27th November 2008 when the system ceased operating.*

2 Specific Objectives

This six-month period of ultrasonic monitoring in the Prototype Repository Experiment has been undertaken with the following objectives:

- Produce accurate source locations for AEs so as to delineate the spatial and temporal extent of any brittle micro-cracking within the rock mass around the deposition hole and locate any movements on pre-existing macroscopic fractures;
- Conduct regular ultrasonic surveys to assess the effect of heating and other environmental changes on the velocity and amplitude of transmitted ultrasonic waves;
- Investigate changes in dynamic moduli and crack density to show how the properties of the rock volume around the deposition hole change throughout the experiment;
- Relate the AE and ultrasonic measurements to the measured *in situ* stress regime and other operating parameters such as temperature and fluid pressure;
- Compare AE activity with blasting records to establish if there is a correlation between increased AE activity and nearby blasting;
- Outline how the results from this reporting period relate to previous monitoring periods and into the overall experimental aims and objectives.

3 Results

3.1 Acoustic Emissions

The parameters used to process AEs are displayed for reference in Appendix III. In total there were 60 triggered events all of which have been located successfully. All of the events have good waveforms with clear P- and S-wave arrivals. The estimated uncertainty for the locations of these events around the deposition hole is less than 5cm, determined using calibration 'hits' performed within the deposition holes after excavation (see Appendix II for further details).

A trigger is described as an event that has been acquired by the monitoring system, but may not be of sufficient energy or 'quality' to be located during the processing procedure. Noisy events, those that appear masked by electrical, environmental, or man-made noise, have been removed from the dataset allowing a more accurate representation of the fracturing occurring within the rock. The temporal distribution of the 60 AE events is shown in Figure 3-1. There is a significant reduction in AE rate during the period June-July 2008 following a consistent fall in rate from March 2008. The average number of located AEs per day throughout this monitoring period is 0.38, indicating there may be a return to an activity level that was present before the constant (although low-level) increase in activity observed over the past two years (Table 3-1).

Table 3-1: Average daily number of located AEs for the six monthly report periods starting 1st October 2004 and finishing with the end of this report period on 30th September 2008.

Time Period	Average Number of Events per Day
1st October 2004 to 31st March 2005	0.32
1st April 2005 to 30th September 2005	0.21
1st October 2005 to 31st March 2006	0.27
1st April 2006 to 30th September 2006	0.80
1st October 2006 to 31st March 2007	0.40
1st April 2007 to 30th September 2007	0.63
1st October 2007 to 31st March 2008	0.90
1st April 2008 to 30th September 2008	0.38

We have tested to see if significant increases in AE activity are due to blasting activities occurring during excavation of a neighbouring tunnel close to the Prototype Experiment. Figure 3-2 shows the blasting records plotted alongside the AE trigger rate over the last year. We can see that there is no direct correlation between the timing of blasting and increased AE activity, although a time dependent effect resulting from the new excavation cannot be ruled out.

Figure 3-3 shows the locations of AEs relative to the physical features of the Prototype Repository. Instrumentation boreholes are represented by the brown vertical lines, and the tunnel and deposition hole are represented by the grey wireframe structures. Almost all of the 60 events are tightly clustered around the deposition hole. Several events locate away from the deposition hole and two locate close to the tunnel floor in the same volume as 'Cluster T' was observed in the previous report [*Duckworth et al.,* 2008]. Example waveforms, recorded on different channels, from each of the clusters are shown in Figure 3-4 and demonstrate the high quality data that are recorded using the array.

Cluster A consists of 29 AE events and is located on the SE side of deposition hole DA3545G01 with a centre located at approximately N, E, D = (268.7, 921.1, 455.1) (Table 3-2) and has been observed in previous monitoring periods [*Haycox et al*., 2006a and 2006b; *Zolezzi et al.,* 2007 and 2008 and *Duckworth et al.,* 2008]. The events in this cluster occur along the S3 ray-path category (Figure 3-3), which passes through a region of low-compressive or tensile stresses (Figure 3-14), and are close enough together to be considered as occurring on the same feature (Figure 3-5). The temporal distribution of these events is presented in Figure 3-6 and shows that they occur throughout the monitoring period.

Cluster B consists of 12 AE events located on the SW side of deposition hole DA3545G01 (Figure 3-5) and are very tightly grouped together with an average location of N, E, D = (269.1, 919.7, 455.1) (Table 3-3). The same cluster was observed in the previous report by *Duckworth et al*., [2008]. The events in Cluster B stop at the end of May 2008 (Figure 3-6). The cluster occurs in a volume associated with the S1 ray-path category which passes through a region characterised by high compressive stress (Figure 3-14). Three events are located in the same position where Cluster C was observed in the previous report.

Cluster D (Figure 3-5) occurs in the high compressive stress region diametrically opposite to clusters B and C during excavation. The events in this cluster represent a volume around the deposition hole, recently activated in the previous reporting period. The average event location in this cluster (consisting of 4 events) is N, E, D = (270.3, 921.6, 457.2) (Table 3-4). The temporal distribution of these events is presented in Figure 3-7 and shows that they occur early in the monitoring period.

Table 3-2: Spatial distribution of the 29 events located in Cluster A.

	Northing (m)	Easting (m)	Depth (m)
Minimum	268.67	921.01	455.05
Maximum	268.77	921.19	455.14
Mean	268.73	921.07	455.10
Standard Deviation	0.027	0.040	0.025

Table 3-3: Spatial distribution of the 12 events located in Cluster B.

	Northing (m)	Easting (m)	Depth (m)
Minimum	269.06	919.68	455.06
Maximum	269.13	919.75	455.11
Mean	269.08	919.73	455.09
Standard Deviation	0.019	0.020	0.019

Table 3-4: *Spatial distribution of the 4 events located in Cluster D.*

	Northing (m)	Easting (m)	Depth (m)
Minimum	270.19	921.50	457.11
Maximum	270.32	921.67	457.24
Mean	270.27	921.58	457.17
Standard Deviation	0.045	0.063	0.044

Figure 3-8 shows plan views of events recorded during excavation, the initial phase of heating, the previous monitoring period and this monitoring period. The majority of the events are located in the NE and SW quadrants. These regions are subject to increased compressive stresses, as identified from the in-situ stress field by *Pettitt et al.,* [1999]. Smaller clusters are observed in the orthogonal regions of low-compressive or tensile stress. This pattern is consistent throughout the excavation and heating phases.

The events in Clusters A, B and C are located in the same volumes as clusters observed in previous monitoring periods and are thus occurring along the same structures. The events could be a continuation of activity in the damaged zone, created either by movement on pre-existing micro-cracks or as a result of extension or formation of new micro-cracks in the existing damaged region. Cluster D represents a recently active region observed by *Duckworth et al.,* [2008]. Events have been seen to occur here during the earlier stages of the experiment [*Pettitt et al.,* 1999] but not at the precise depths evident in this and the previous report. The events could be caused by the continuation or inter-connection of pre-existing micro-cracks or possibly by the formation of a new network of micro-cracks in the existing damaged region.

Figure 3-9 shows AE magnitudes for the five response periods discussed in Table 4-1 from the beginning of heating and pressurisation. During the latest six-month reporting there has been a slight increase in both the peak magnitude and overall distribution of magnitudes compared to the previous report period, but remain below the highest magnitudes observed in the initial phases of heating and pressurisation (response periods 1 and 2).

Most of the event locations are consistent with previous results, and low magnitudes characterise the entire acoustic emission data set, therefore we can assume that the rock mass around the deposition holes has remained relatively stable throughout this six-month period.

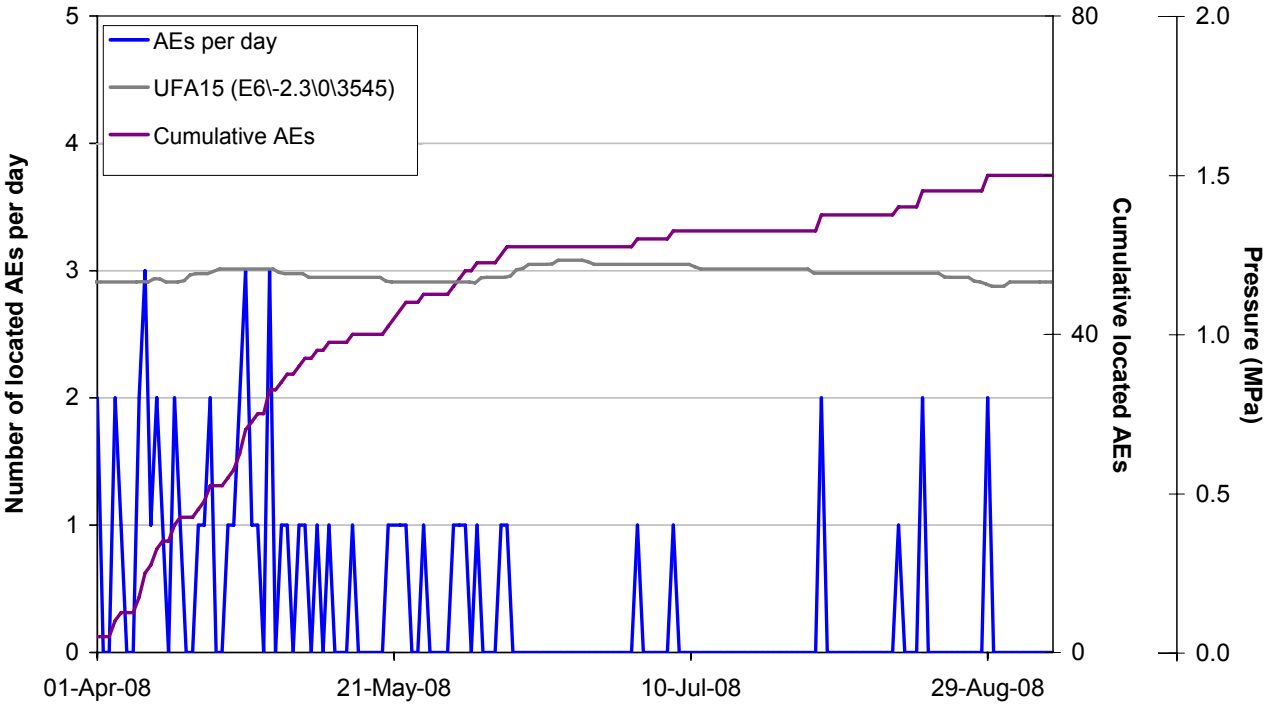

Figure 3-1: *Temporal distribution of the 60 AEs observed during this report period. The number of events per day is shown on the left axis and indicated by the blue line and cumulative number of AE events is shown on the right-hand axis and indicated by the purple line. Also shown is the pore-water pressure (measured on instrument UFA15) in the tunnel backfill over the deposition hole.*

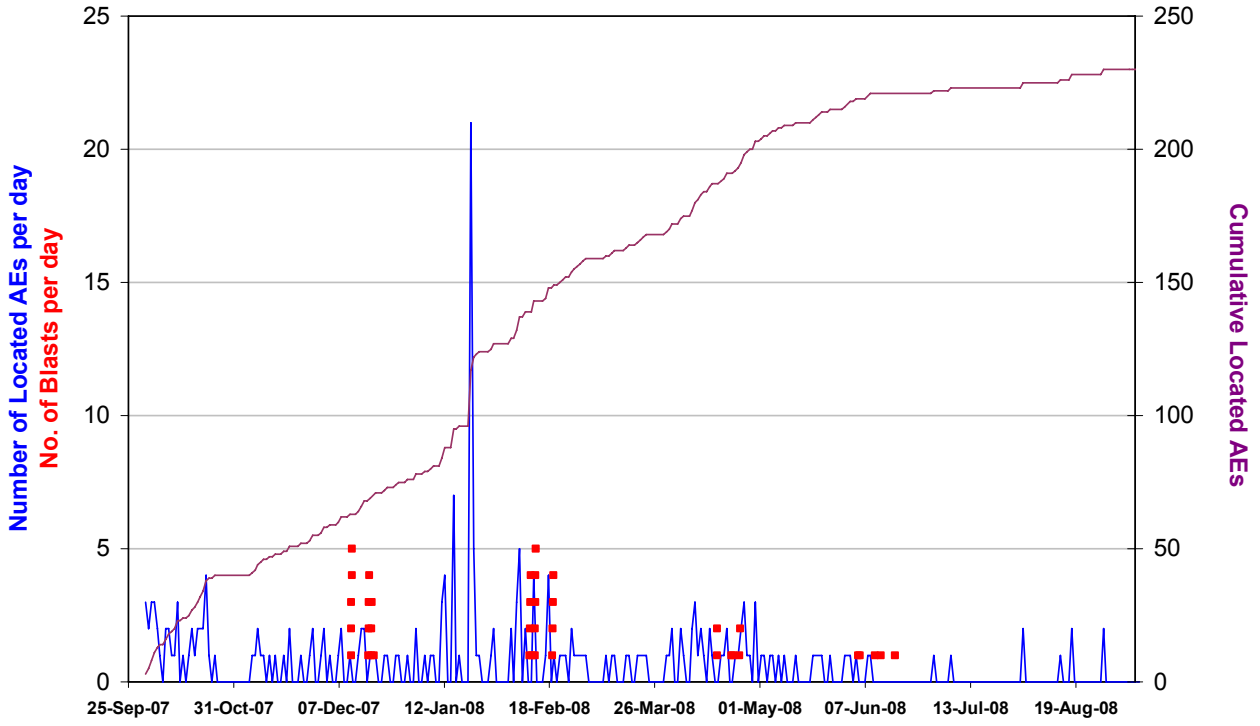

Figure 3-2: *Temporal distribution of the total number of AEs observed over the last year. The number of events per day (blue line) and cumulative number of events (purple line) are plotted alongside blasting records (red squares).*

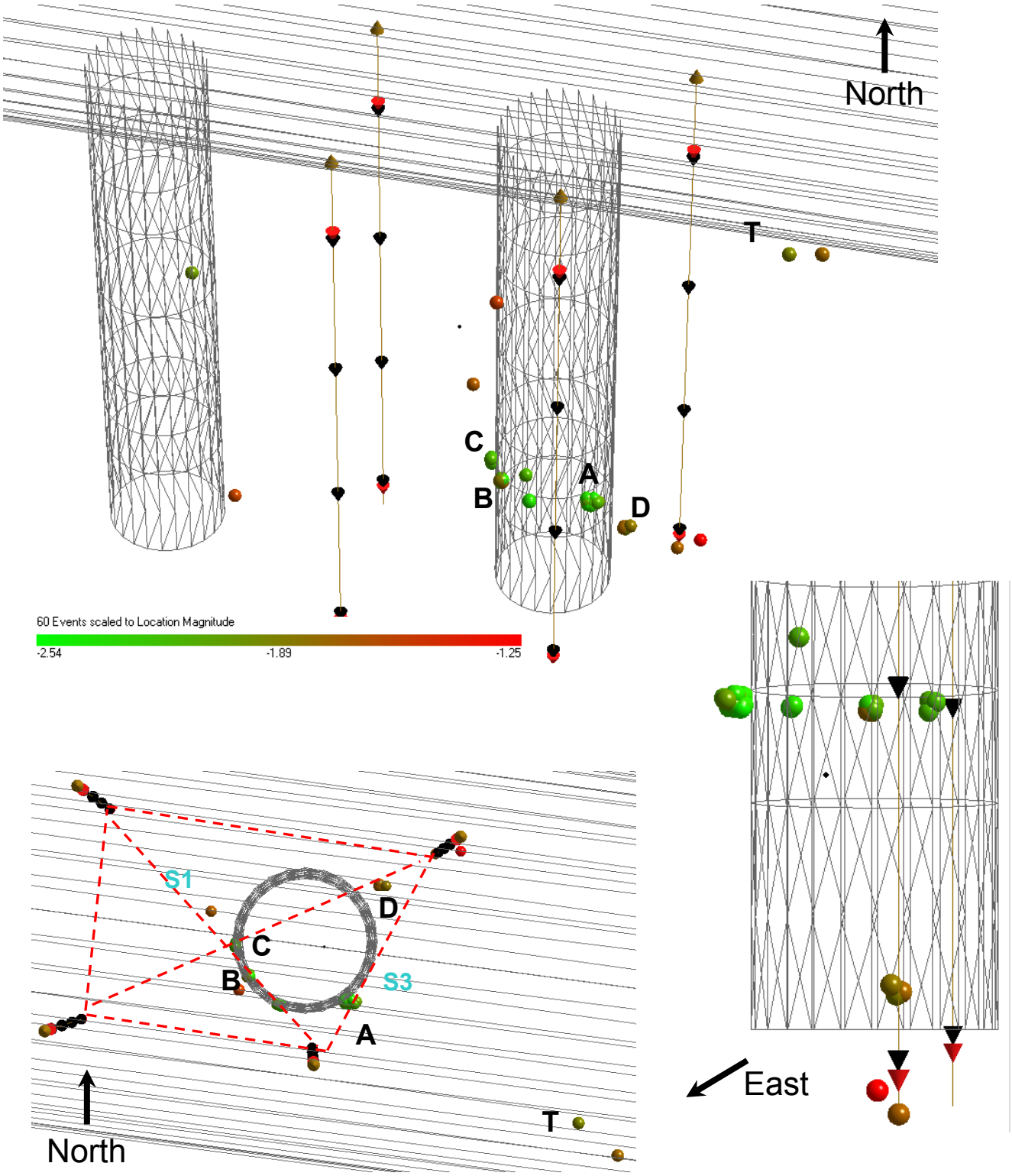

Figure 3-3: *Three views showing the clustered AE activity located around deposition hole DA3545G01. (Top: Oblique view looking north; Bottom left: Plan view with the five category ray-paths used in the ultrasonic survey shown relative to the deposition hole; Bottom right: Close-up view of the deposition hole.) Events are scaled to location magnitude (coloured bar, inset).*

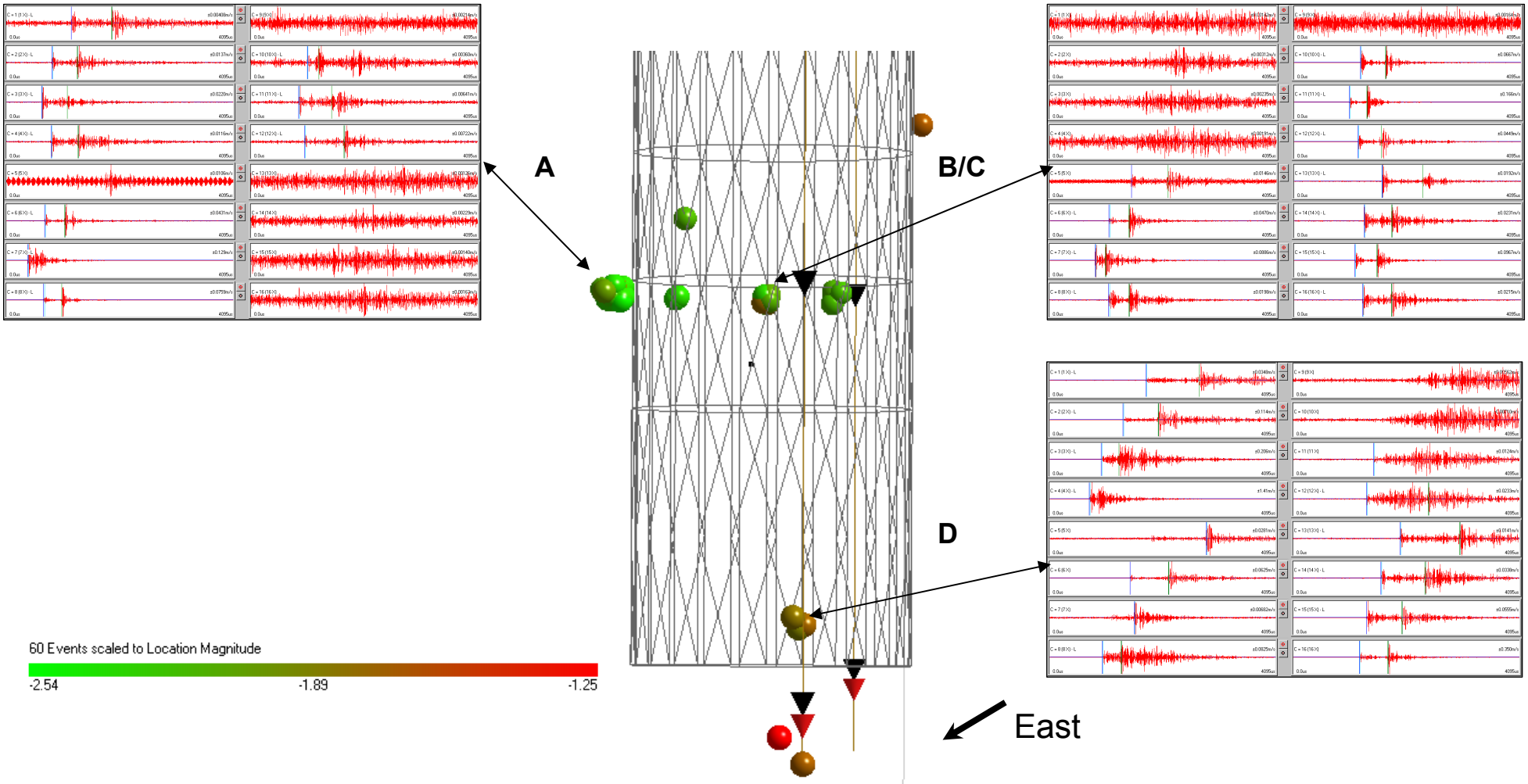

Figure 3-4: *Waveforms for a selected event from each of the four clusters shown in relation to a transverse view of AE activity. Events are scaled to location magnitude (coloured bar, inset).*

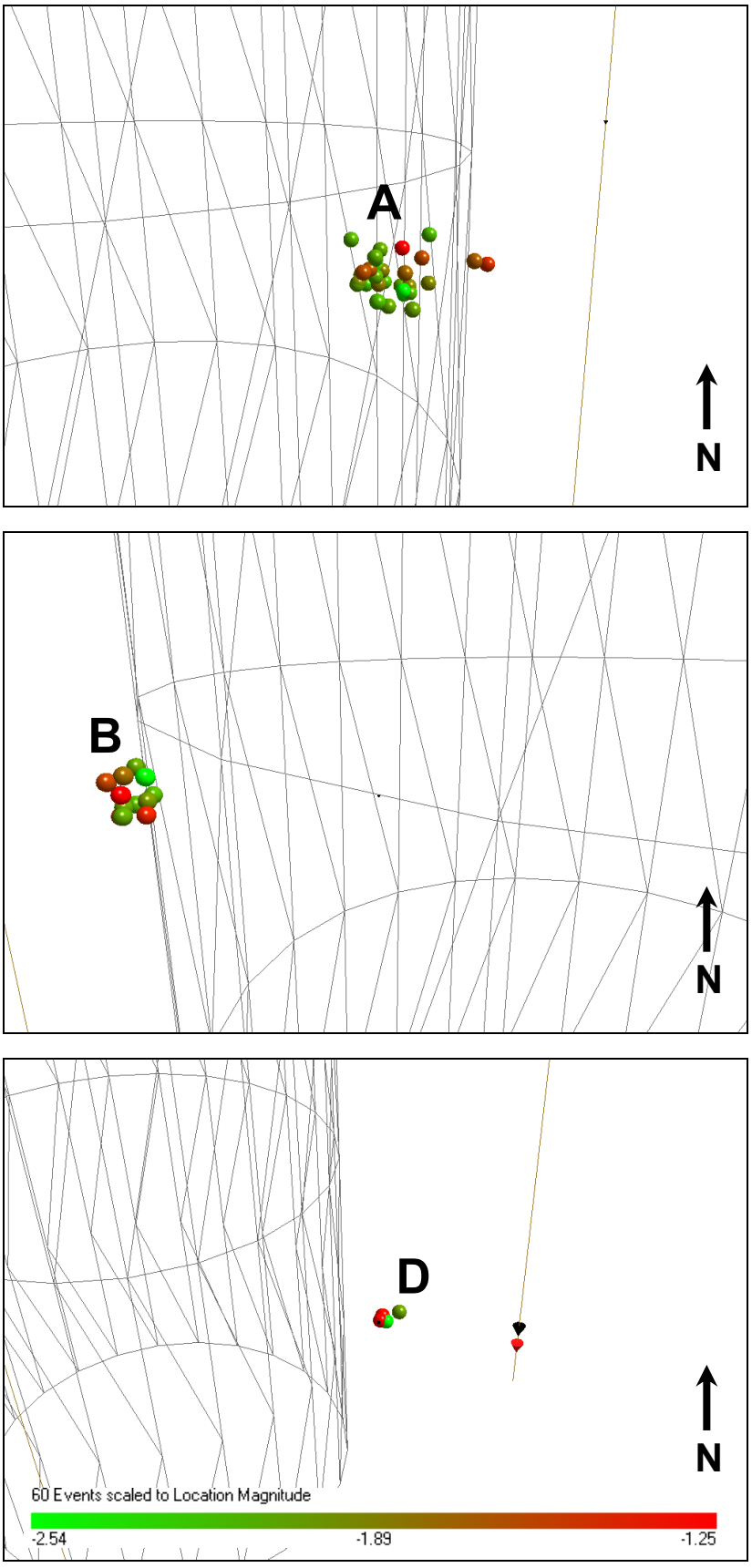

Figure 3-5: *Close up views of Cluster A (top) containing 29 events, Cluster B (middle) containing 12 events and Cluster D (bottom) containing 4 events. Events are scaled to location magnitude (coloured bar, inset).*

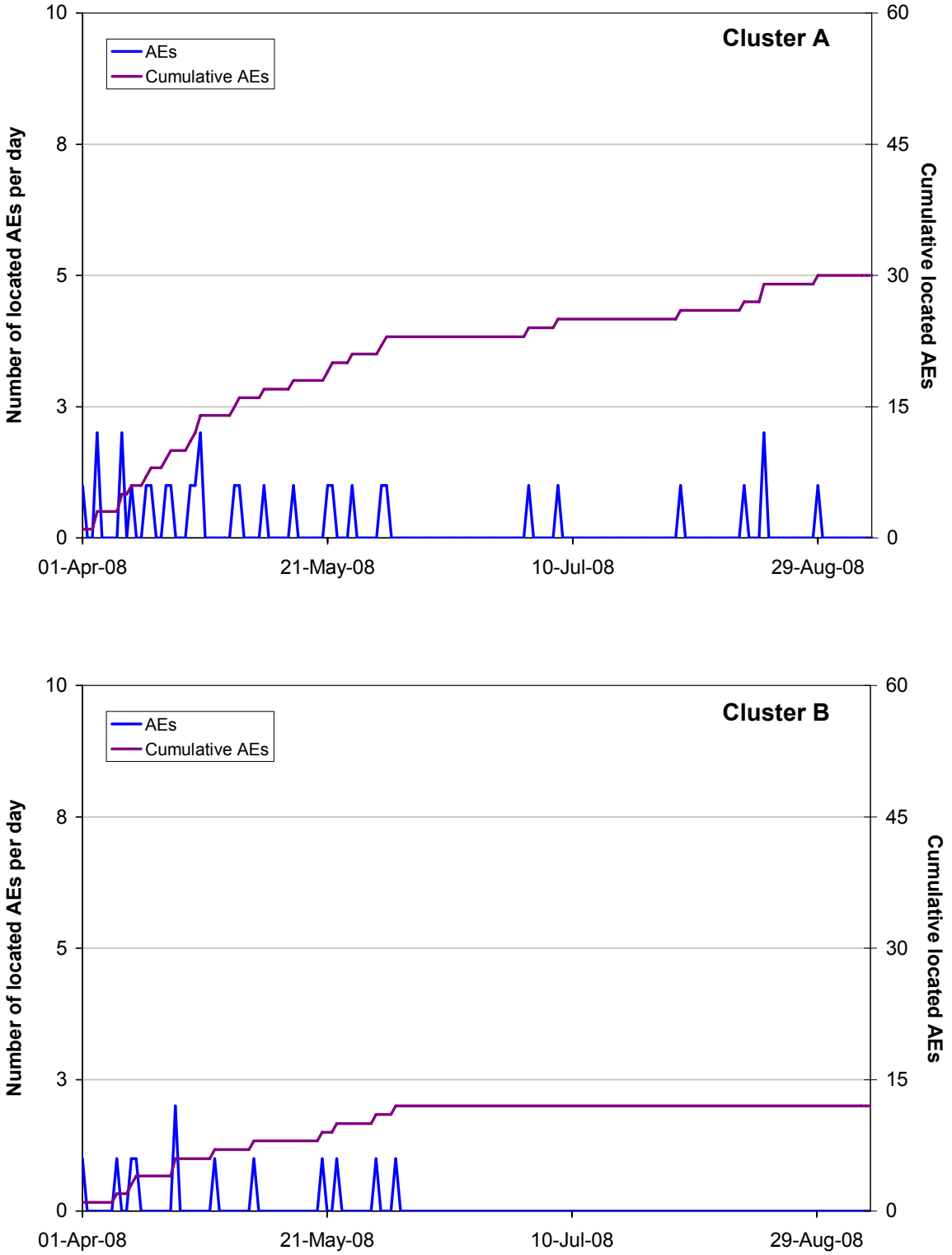

Figure 3-6: *Temporal distribution of located AEs in clusters: Cluster A (top) and Cluster B (bottom). Plots show the number of events (blue line) per day on left axes and cumulative number (purple line) of events for the entire monitoring period on right axes.*

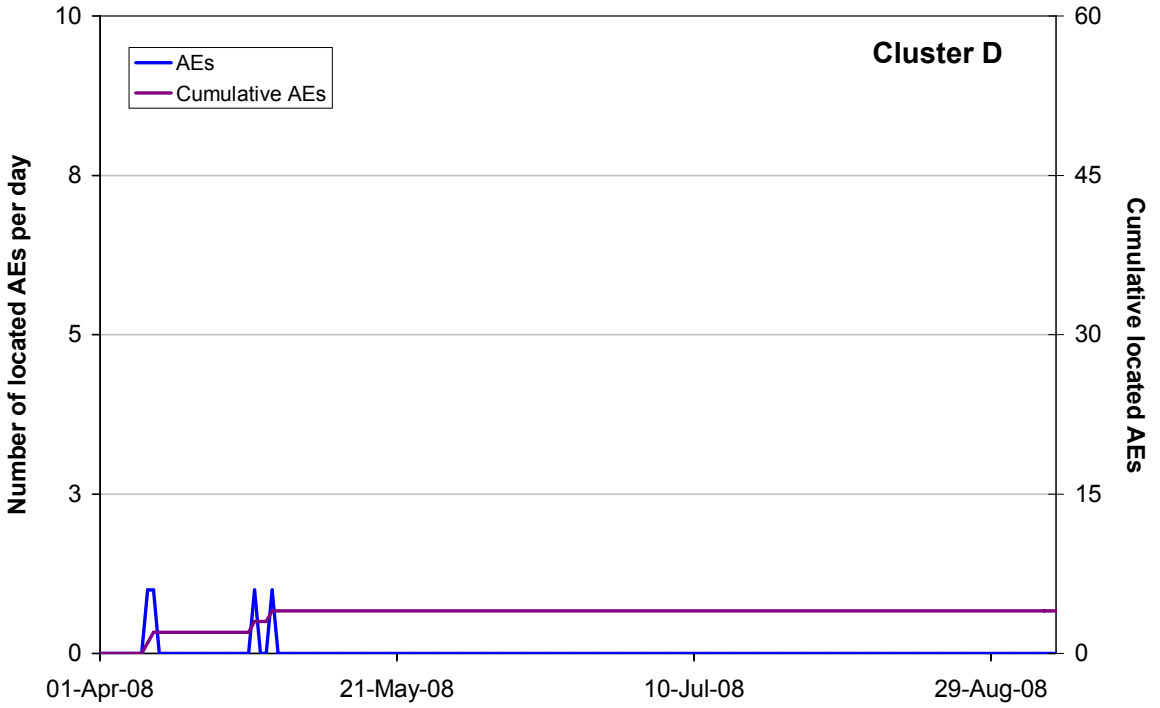

Figure 3-7: *Temporal response plot of located AEs in the identified clusters for Cluster D. Shown are the number of events per day (blue line) on left axis and cumulative number of events (purple line) for the entire monitoring period on right axis.*

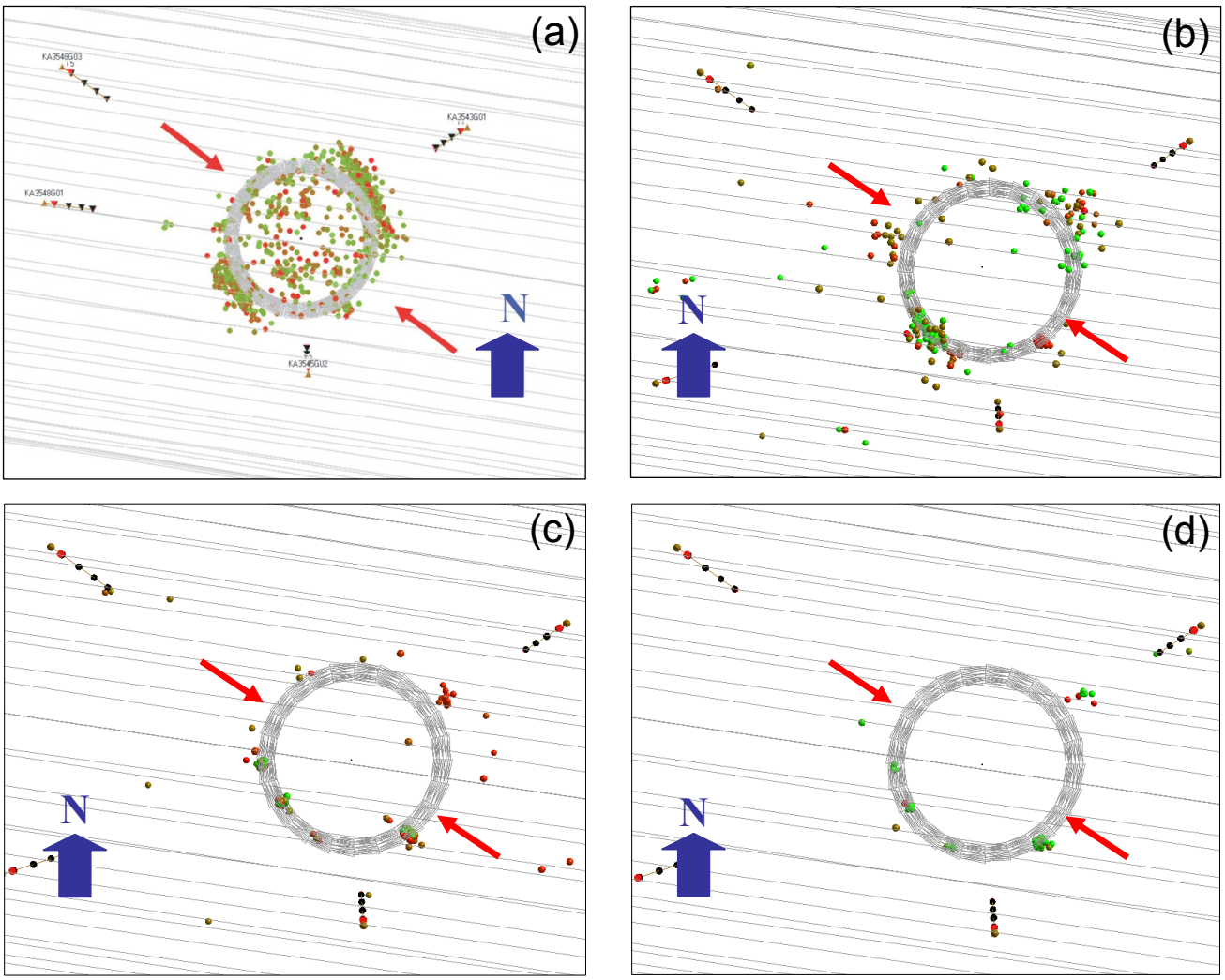

Figure 3-8: *Plan view of total AEs located around deposition hole DA3545G01 during (a) the excavation phase [Pettitt et al., 1999], (b) monitoring during heating through to 01/04/2007, (c) previous monitoring phase from 01/10/2007 until 31/03/2008, and (d) this monitoring phase from 01/04/2008 until 30/09/2008. The red arrows mark the orientation of principle stresses.*

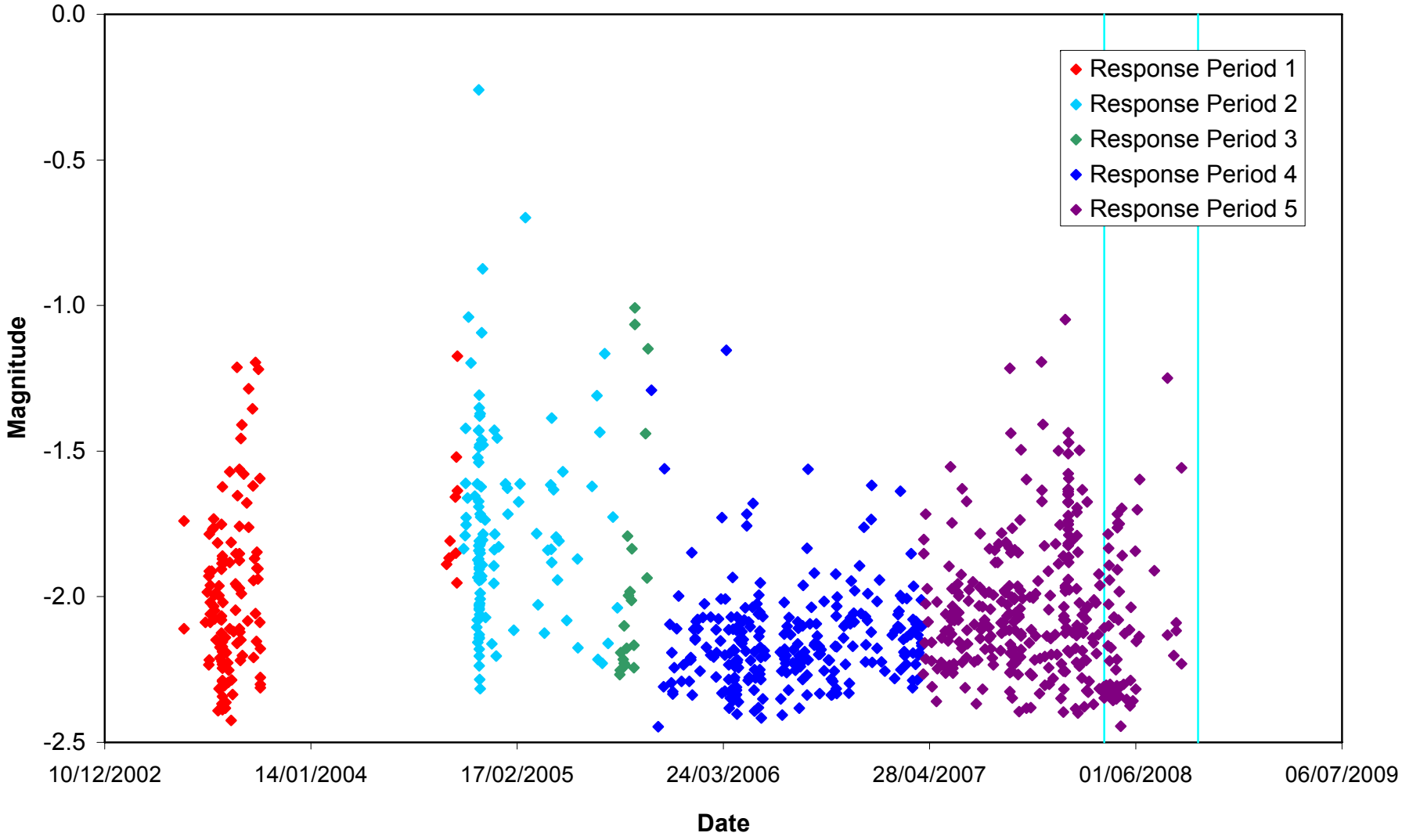

Figure 3-9: *Chart displaying AE magnitudes recorded from the beginning of heating and pressurisation. Events are coloured by response period as defined in Table 4-1. During this latest period (indicated by the blue vertical lines) both the peak magnitude and distribution is comparable to the previous period, but remain below the highest magnitudes observed in the initial phase of heating (response periods 1 and 2).*

3.2 Ultrasonic surveys

Environmental conditions in the tunnel and around the deposition holes can be ascertained from temperature and pressure measurements from sensors embedded within the rock. The numerical data are supplied by SKB. The temperature of the rock surrounding the deposition hole is shown in Figure 3-10 and describes a steady decrease of ~1°C until 6th June 2008 when an average 5°C temperature drop is recorded across all instruments. This drop occurs during a time when no ultrasonic survey data was recorded.

The total pressure in the backfill above deposition hole DA3545G01 is shown in Figure 3-11a. The pressure recorded on each of the instruments in the backfill above the deposition hole DA354G01 is fairly stable throughout the entire period (Figure 3-11a). The pressure ranges from a maximum of ~1.2MPa recorded on instrument PXP0UFA15 to a minimum of ~0.85MPa recorded on instrument PXP0UFA16.

The total pressure in the rock adjacent to deposition hole DA3545G01 is displayed in Figure 3-11b. We see that the pressure here displays much larger variations, most notably the drop in pressure that starts on the 5th June 2008 reaching a period low around the 10th June 2008 recorded by all of the instruments. The maximum pressure drop is ~8MPa recorded by instrument UB610 whilst the smallest pressure drop is ~1.5MPa recorded by instrument PB601. This pressure drop coincides with the temperature drop observed in the same rock mass (Figure 3-10).

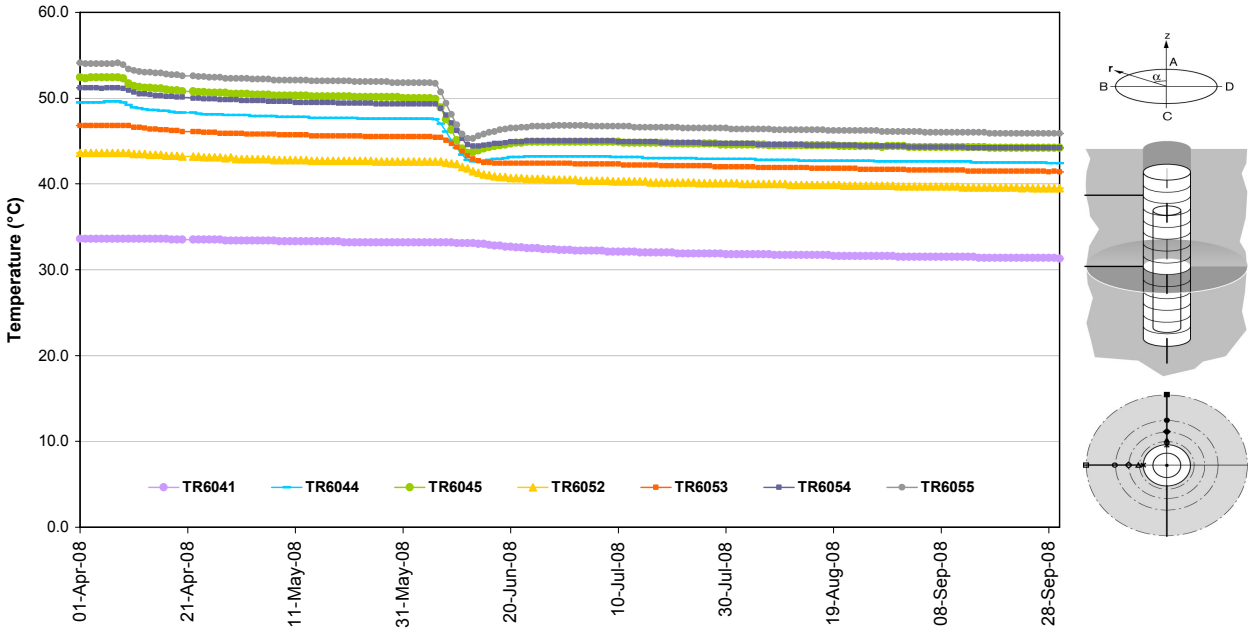

Figure 3-10: *Temperature of the rock mass around deposition hole DA3545G01 for the period between 1st April 2008 and 30th September 2008. The sensors are positioned mid-way up the deposition hole at different depths through the rock mass (see right-hand inset) [Goudarzi, 2007].*

Velocity changes are measured between transmitter-receiver pairs by cross-correlating (CCR) data from the daily ultrasonic surveys. A reference survey, taken from previous monitoring periods, is used to process the ultrasonic results. The reference survey was recorded on 8th December 2004 and has had first P- and S-wave arrivals manually picked from the waveforms [*Haycox et al.,* 2006a]. Data presented in this reporting

period will use the same reference survey so that results from previous periods can be accurately compared. Using the cross-correlation procedure reduces uncertainty and allows a high-resolution analysis to be performed, with an estimated uncertainty of ± 2 ms^{-1} between surveys on individual ray-paths, and hence small changes in velocity to be observed. This is extremely important when changes in rock properties occur over only a small section (~5%) of the ray-path.

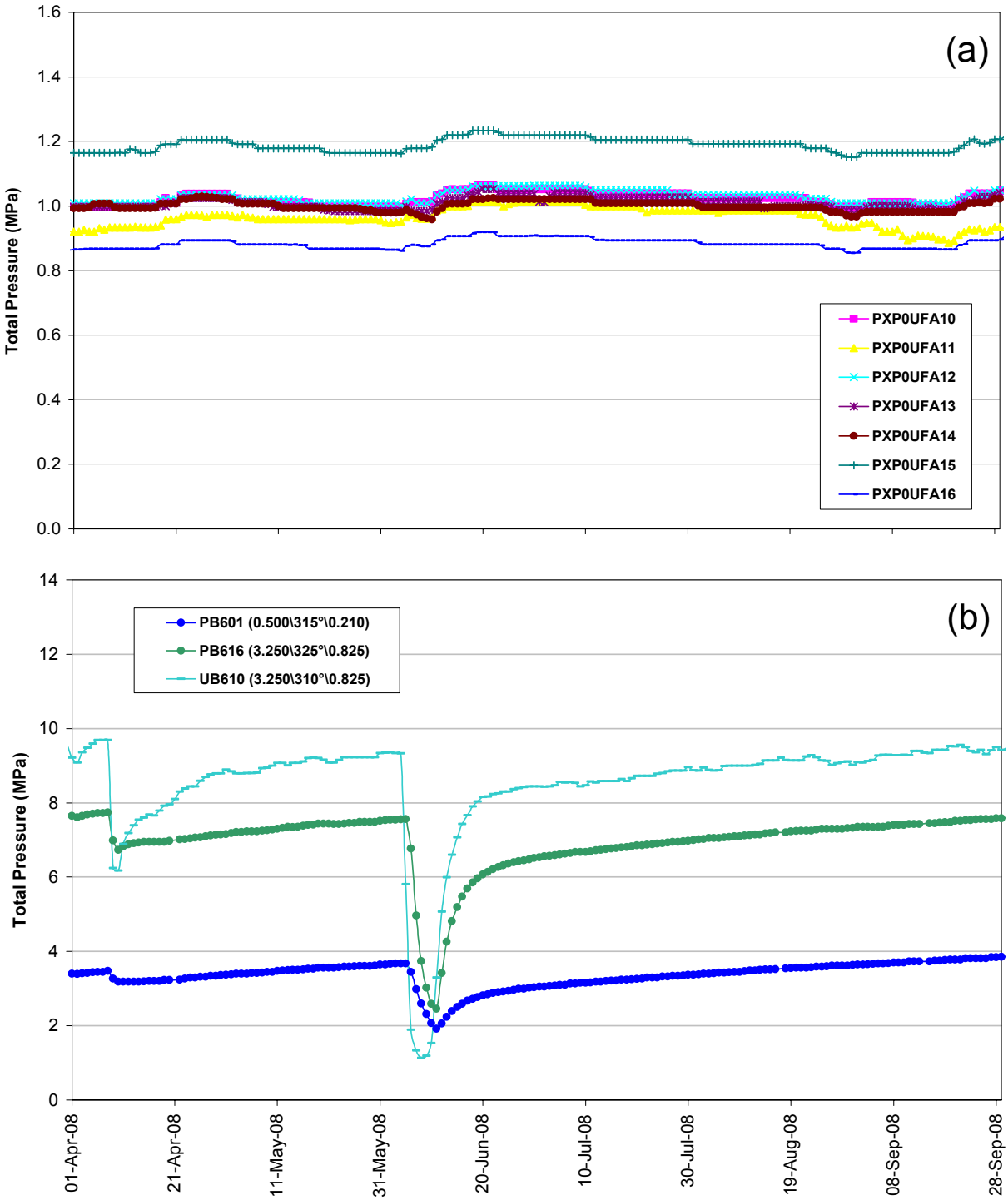

Figure 3-11: *Total pressure in (a) the backfill over deposition hole DA3545G01 and (b) the rock adjacent to deposition hole DA3545G01 for the period between 1st April 2008 and 30th September 2008.*

Average P- and S-wave velocity changes during this and the last report period are shown in Figure 3-12a. Due to the lack of survey data during this period, we have assembled the data recorded here from July and August 2008 with data recorded during the previous recording period so as to evaluate any significant changes across the time when no recording was performed.

Average P- and S-wave velocities for this report period alone are shown in Figure 3-13a. Overall, P-and S-wave velocity changes closely mimic one another but with larger magnitude changes evident for P-waves. The maximum changes in velocity are ~1ms^{-1} for P-waves and ~0.4ms^{-1} for S-waves, with average changes in the region of 0.4ms^{-1} for P-waves and 0.1ms^{-1} for S-waves. Individual, i.e. point to point, variations in velocity are greater than those observed by *Duckworth et al.,* [2008] during the last report period but the maximum and minimum values are very similar. The small changes in velocity and amplitude may reflect the stable environmental (i.e. temperature and pressure) conditions in and around the canister deposition hole.

The magnitudes of the average velocity changes are significantly smaller than the velocity resolution of 2ms^{-1} estimated for ultrasonic measurements, however, changes on individual ray-paths may be more pronounced. For example, the greatest magnitude change in velocity is observed on the ray-path between transmitter three and receiver nine (on the 18th August 2008), when P-wave velocity decreases by ~10ms^{-1}.

Amplitude changes are very small throughout the period of data coverage (Figure 3-13b) and changes in P-wave amplitudes closely mimic the changes in S-wave amplitudes. The maximum change in amplitude is ~0.2dB for both P- and S-waves with average changes in the region of 0.1dB. These changes are smaller than those reported by *Duckworth et al.,* [2008] during the last report period when S-wave amplitudes increased by ~0.5dB and P-wave amplitudes increased by ~0.3dB. The amplitude values at the onset of this report period are ~0.2dB lower than the final values recorded before the equipment malfunctioned on 17th December 2007; these changes are minor but could be related to the drop in pressure and temperature that occurs on the 4th June 2008 (Figure 3-12b).

Pettitt et al., [1999] categorised ray-paths from ultrasonic surveys into six types depending on their orientation with respect to the deposition hole and the in-situ stress field (Figure 3-14). Ultrasonic results are interpreted in terms of the disturbed and damaged regions around the void during the excavation phase of the experiment. *Pettitt et al.,* [2000] undertook three-dimensional elastic stress modelling to describe these zones of stress.

Figure 3-15a-d shows the velocity changes recorded along the S3 category of ray-paths. Category S3 ray-paths pass within centimetres of the deposition hole through the excavation damaged zone, in a region of low compressive or tensile stress. These particular ray-paths have been chosen because they provide a comparison of velocity changes along the length of the deposition hole. Each plot is accompanied by a schematic diagram showing a perspective of the region through which the ray-path passes and also the transmitter-receiver configuration. In general, there is very little change in S-wave velocities recorded along the S3 category of ray-paths, and only small (2 - 3ms^{-1}) changes in P-wave velocities.

Figure 3-16a-d shows velocity changes recorded along the S1 category of ray-paths. These ray-paths pass through a region of compressive stress and permanent damage close to the wall of the deposition hole and are imaged by relatively high AE activity during periods of excavation. Velocity changes are very similar to those along the S3 category ray-paths, with very little change observed in S-wave velocity and minor (2 - 3ms^{-1}) changes observed in P-wave velocity.

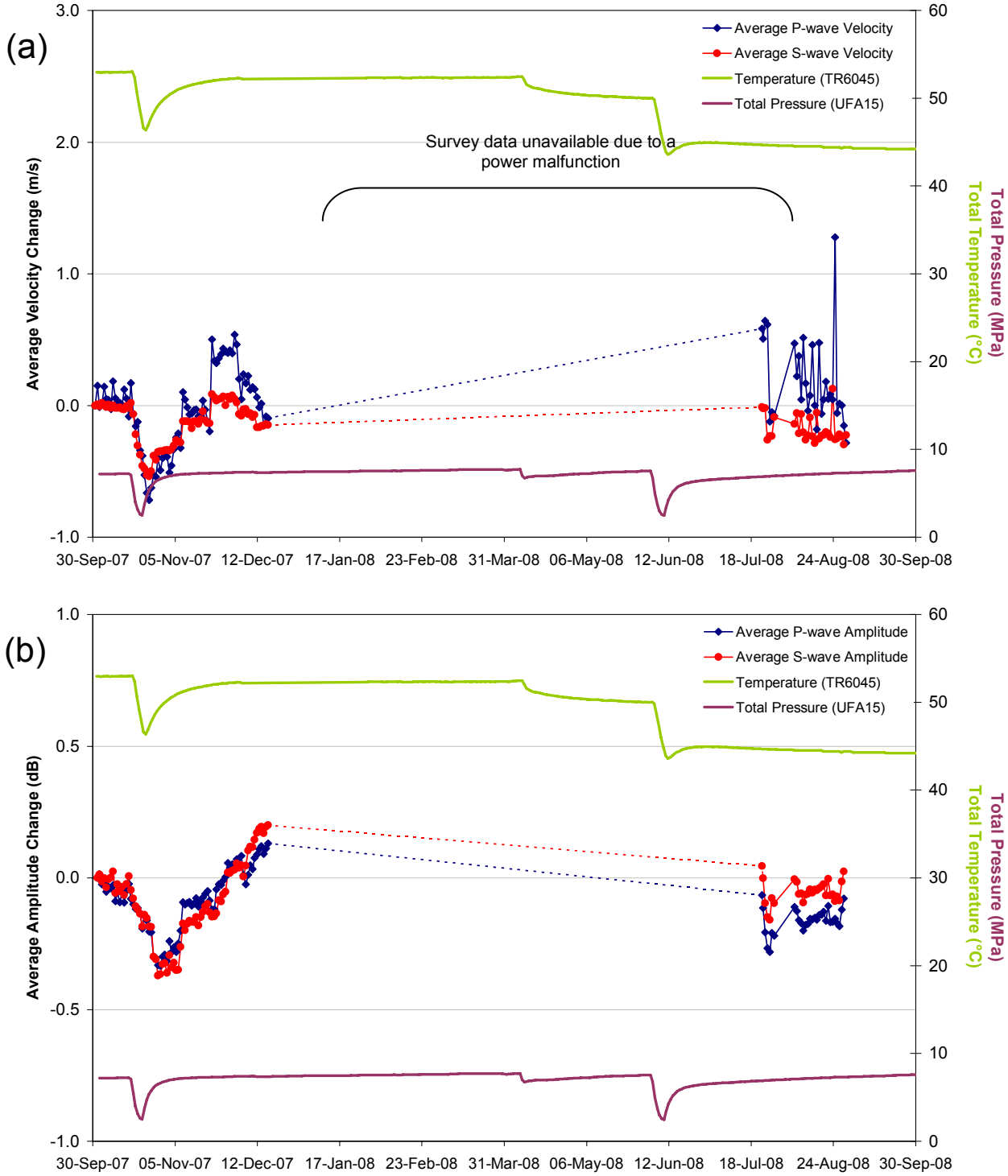

Figure 3-12: *Average P- and S-wave (a) velocity change (ms^{-1}) and (b) amplitude change (dB), for the period between 1st October 2007 (start of the previous report period) and 30th September 2008 (end of this report period). Temperature of the surrounding rock mass (TR6045) and total pressure in the backfill (UFA15) are displayed on the secondary axes. Note that the graph includes the previous period up until 17th December (when survey data stopped due to a power malfunction) and includes the available data for this period from 23rd July until 31st August, 2008 (after which the equipment ceased operating and no further data was recorded for this period).*

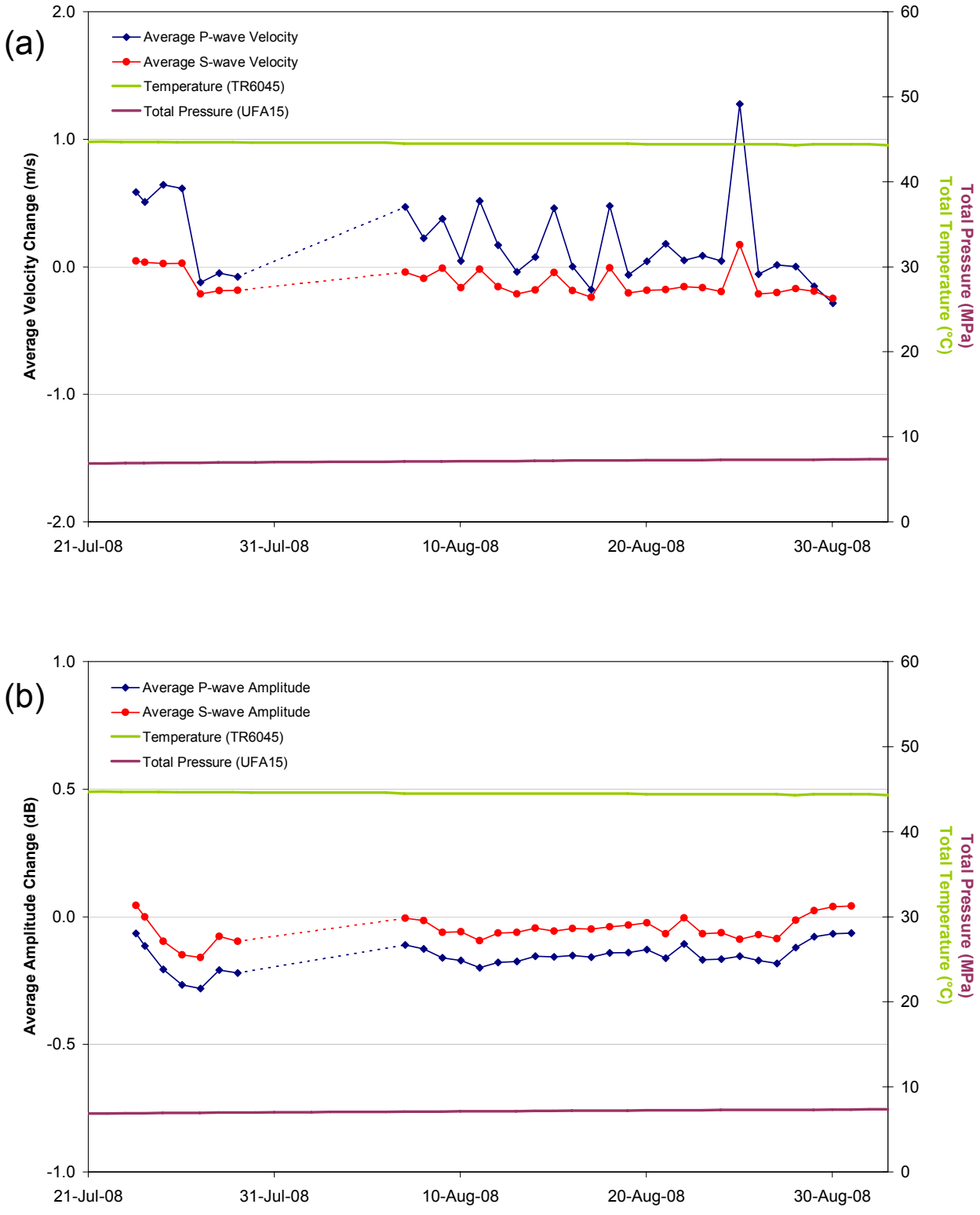

Figure 3-13: *Average P- and S-wave (a) velocity change (ms^{-1}) and (b) amplitude change (dB) for the period that data was captured during this report period (23rd July to 31st August 2008). Temperature of the surrounding rock mass (green line) and total pressure in the backfill over the deposition hole (purple line) are shown on the secondary axes.*

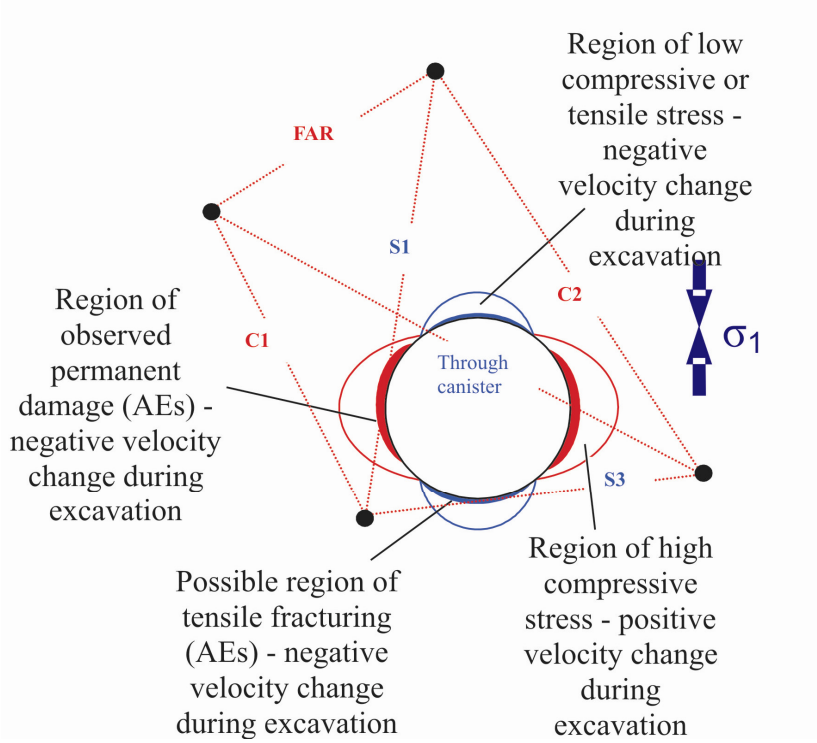

Figure 3-14: *Interpretation of the ultrasonic results during excavation in terms of disturbed and damaged regions around the deposition hole. Zones of induced stress are inferred from elastic modelling and the σ_1 orientation, after Pettitt et al., [1999].*

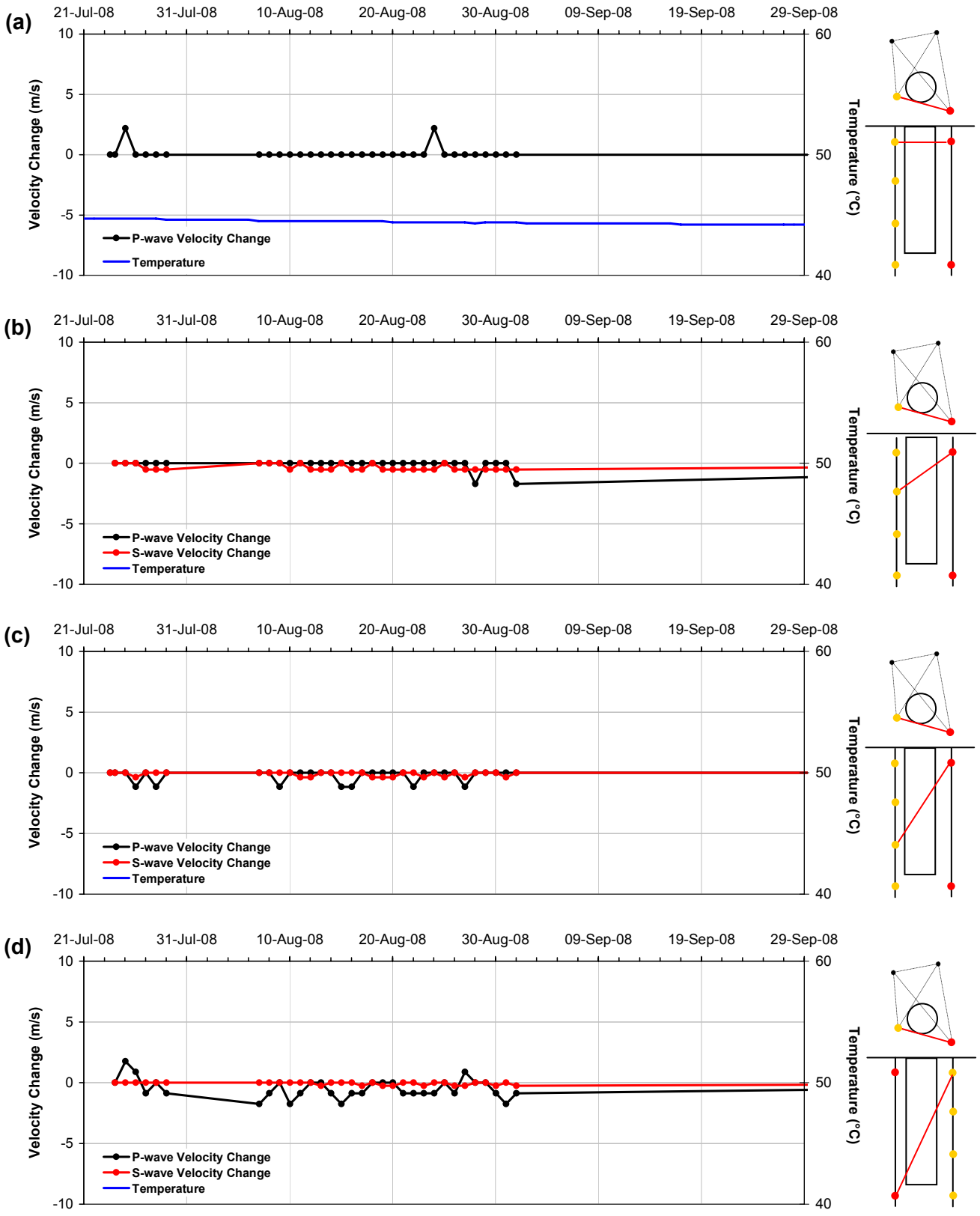

Figure 3-15: *Velocity changes measured on ray-path category S3 (Figure 3-14) for deposition hole DA3545G01. Ray-paths shown are from transmitter (t_n) to receiver (r_n) for (a) t_n=1, r_n=5; (b) t_n=1, r_n=6; (c) t_n=1, r_n=7 and (d) t_n=4, r_n=1. Schematic diagrams on the right indicate the relative positions of transmitter (red) and receiver (gold). Temperature (TR6045, blue line) is displayed on the secondary axes.*

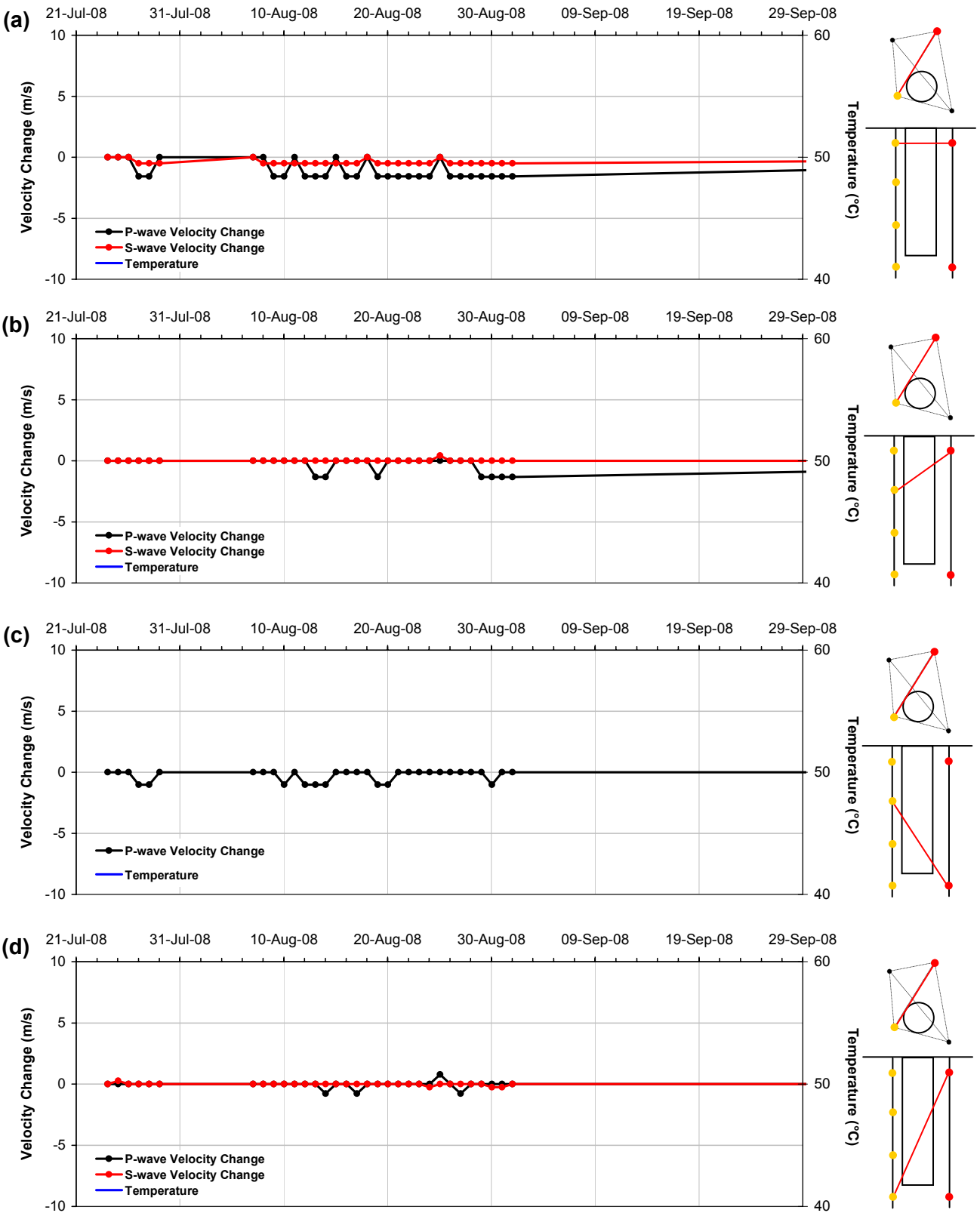

Figure 3-16: *Velocity changes measured on ray-path category S1 (Figure 3-14) for deposition hole DA3545G01. Ray-paths shown are from transmitter (t_n) to receiver (r_n) for (a) t_n=7, r_n=5; (b) t_n=7, r_n=6; (c) t_n=7, r_n=7 and (d) t_n=7, r_n=8. Schematic diagrams on the right indicate the relative positions of transmitter (red) and receiver (gold). Temperature (TR6045, blue line) is displayed on the secondary axes.*

In order to accurately analyse small and consistent changes in the recorded measurements, we compare the average velocity changes across each of the ray-path categories described in Figure 3-14. All of the ray-path categories show the same general trend (Figure 3-17a-b). Both P- and S-wave velocities are fairly consistent, during the period for which data were actively recorded (23rd July to 31st August 2008), showing the same variations on all of the category ray-paths. For P-waves, ray-path C1 exhibits the greatest variation with average changes in the region of $0.6ms^{-1}$ and a maximum change of $\sim 1.7ms^{-1}$. For S-waves, category Far exhibits the most variation with average changes of $\sim 0.3ms^{-1}$ and a maximum change of $0.6ms^{-1}$. Overall, P-wave velocities display more variation than S-wave.

The amplitude changes across the five category ray-paths are shown in Figure 3-18. The trend is very similar for each of the ray-paths and very similar for both P- and S-waves (as noted earlier in Figure 3-13). Point-to-point variations in amplitudes are of the order of 0.05 - 0.10dB with a maximum overall variation of ~0.2dB.

Figure 3-19 and Figure 3-20 show the changes in rock properties calculated using average velocities and amplitudes for the five category ray-paths. Young's Modulus (Figure 3-19a) describes the stiffness of the rock mass, Poisson's Ratio (Figure 3-19b) is the ratio of latitudinal to longitudinal strain, Crack Density (Figure 3-19c) is a measure of the extent of fracturing per unit volume and Saturation (Figure 3-19d) relates to the number of cracks per unit volume containing fluids. Crack Density and Saturation of the rock mass are determined using the method of *Zimmerman and King* [1985], as described in Appendix II.

Young's Modulus shows the same trend as P- and S-wave velocity, including the outlying point occurring on 18th August 2008 (Figure 3-19a). Poisson's ratio exhibits very little change throughout the entire data record and shows the same general trend as P- and S-wave amplitude. Crack density shows opposing behaviour to that of Young's Modulus with the outlying point on 18th August 2008 being opposite in sign (Figure 3-19c). Saturation exhibits a similar overall trend to P-wave velocity (Figure 3-17d) but with much greater variation than any of the other parameters. The largest response is evident in categories C1 and Far for Young's Modulus, Poisson's Ratio, Crack Density, and Saturation.

During the period for which data were actively recorded (23rd July to 31st August 2008) the velocity and amplitude variations along each of the category ray-paths are small compared to the last report period. Average changes in velocity are $\sim 0.6ms^{-1}$ for P-waves and $\sim 0.3ms^{-1}$ for S-waves whilst average changes in amplitude are ~0.1dB for both P- and S-waves. The variations are particularly relevant for those rays travelling along paths relating to categories C1 and Far. There is no change in the environmental conditions in the tunnel and around the deposition hole, so the small variations in velocity and amplitude observed may be due to resolution restrictions when taking ultrasonic measurements. With no short-term changes in temperature and pressure this report period is comparably stable.

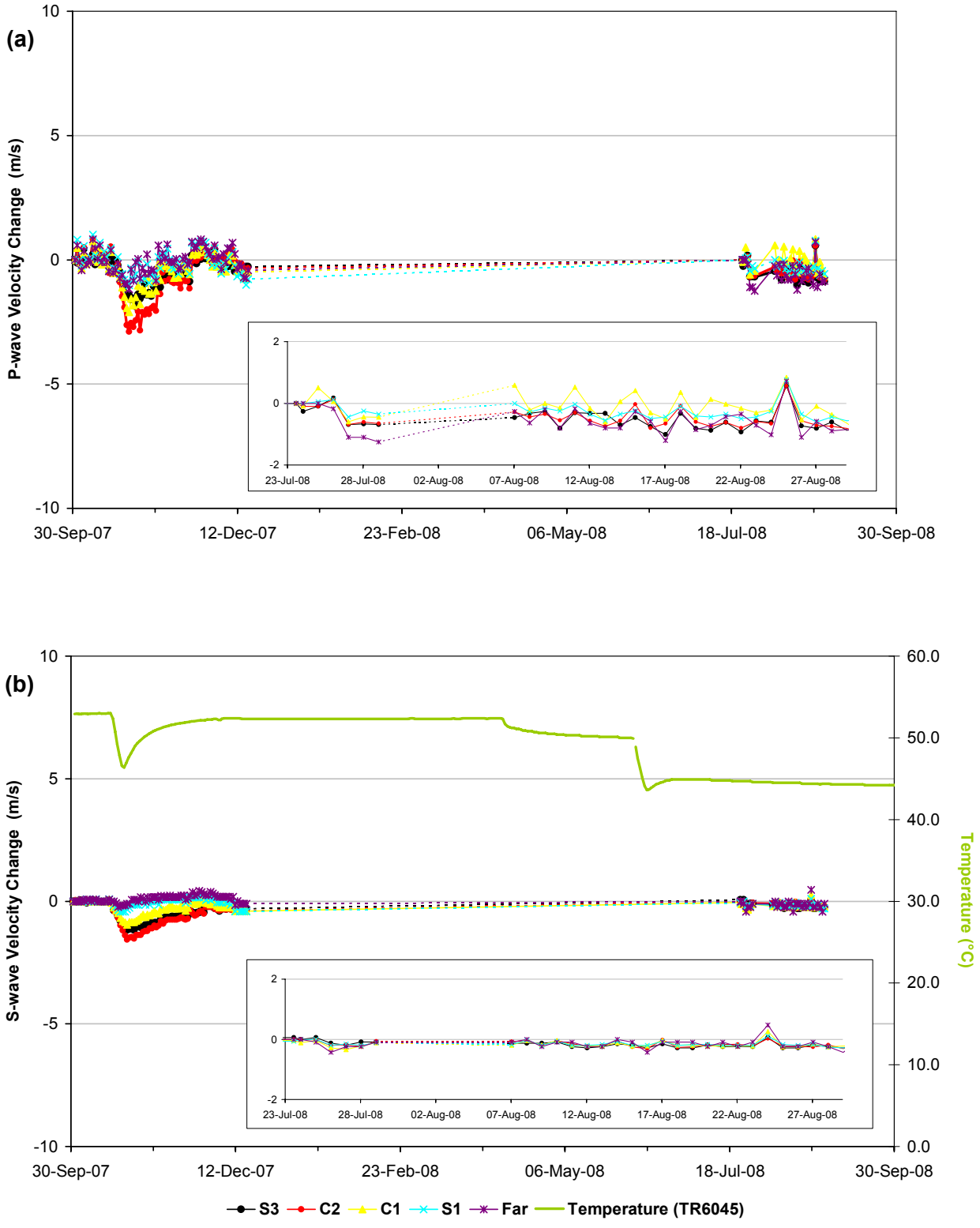

Figure 3-17: *Average velocity changes for the five category ray-paths (S1, S3, C1, C2, Far) around deposition hole DA3545G01 for (a) P-waves and (b) S-waves. Inset shows the data from this report period.*

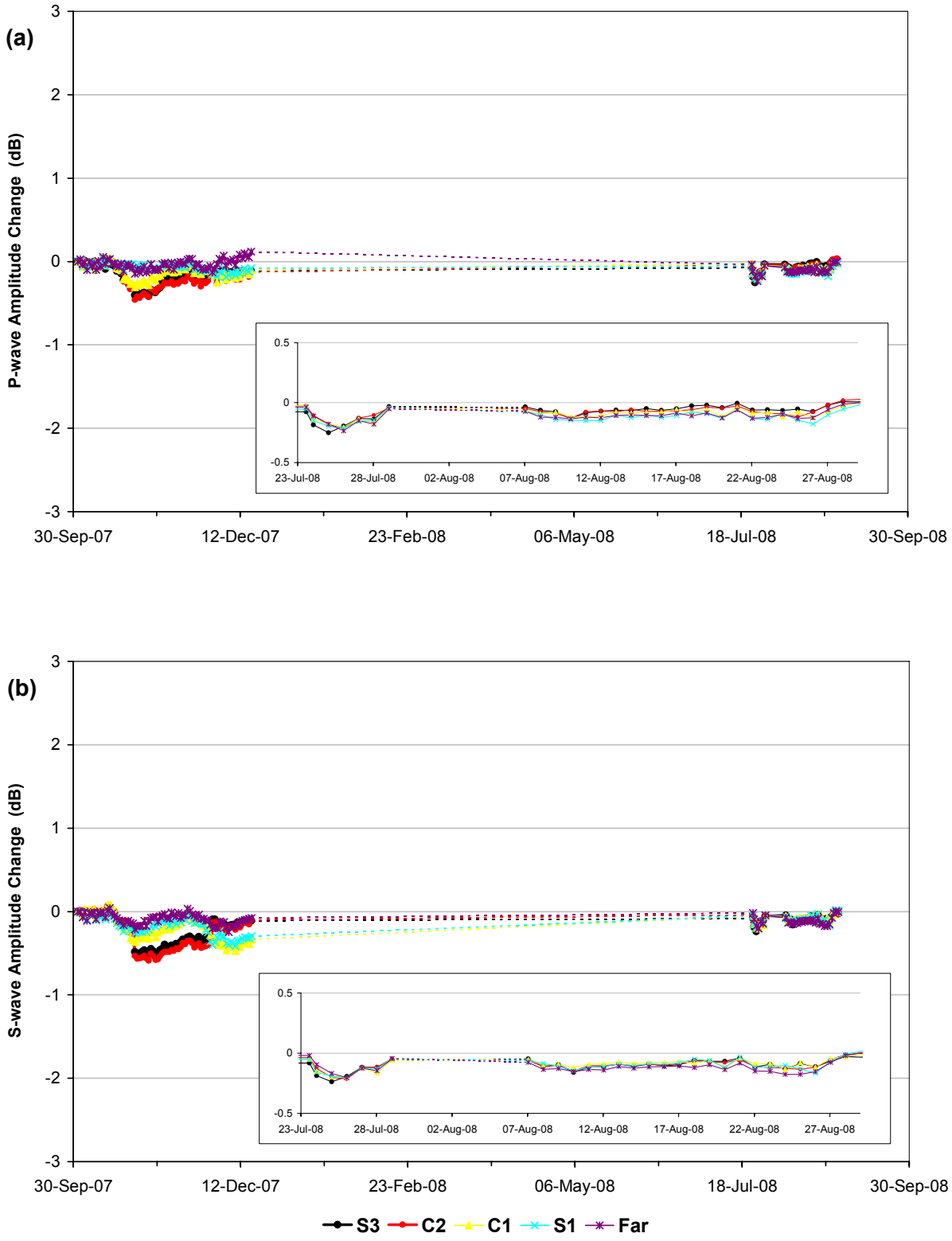

Figure 3-18: *Average amplitude changes for the five category ray-paths (S1, S3, C1, C2, Far) around deposition hole DA3545G01 over the past year; (a) for P-waves with data from this period shown inset and (b) S-waves with data from this period shown inset.*

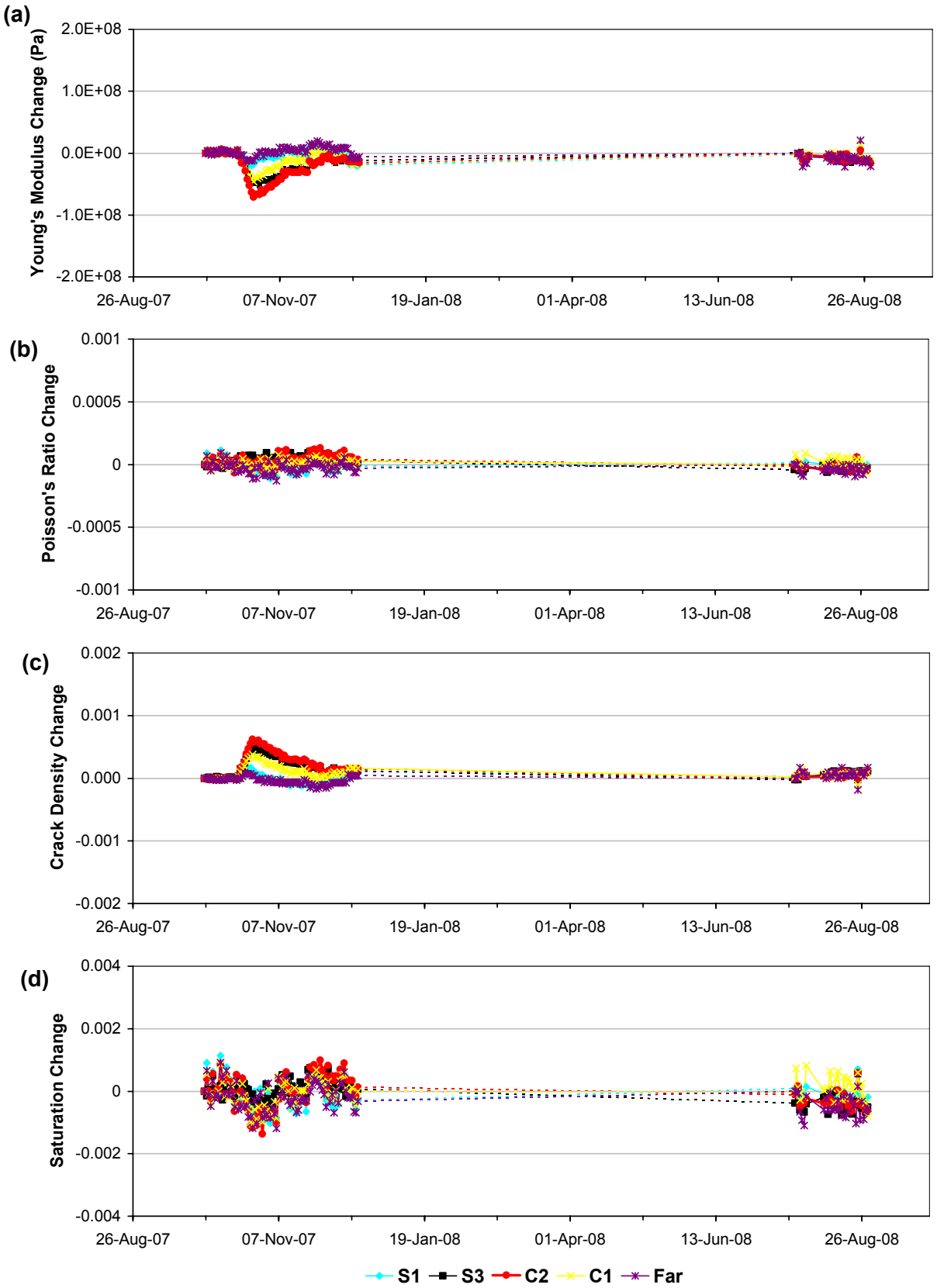

Figure 3-19: *Changes in rock parameters, calculated using average P- and S-wave velocities and amplitudes, for the five ray-path categories for (a) Young's Modulus, (b) Poisson's Ratio, (c) Crack Density and (d) Saturation in the period 1st October 2007 (start of the previous report period) to 30th September 2008 (end of this report period). Temperature (TR6045) and pressure (UFA15) are displayed on the secondary axes.*

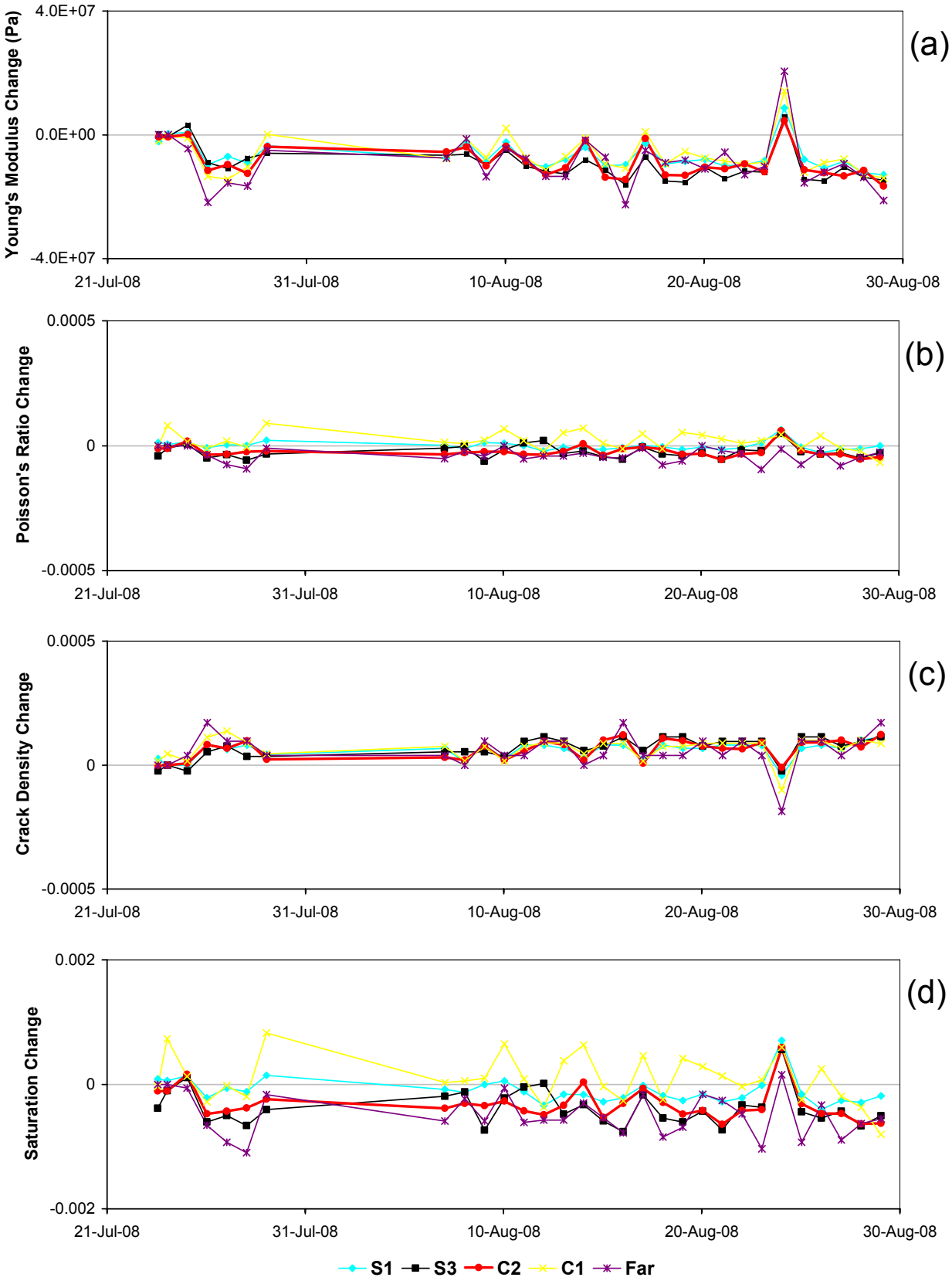

Figure 3-20: *Changes in rock parameters, calculated using average P- and S-wave velocities and amplitudes, for the five ray-path categories for (a) Young's Modulus, (b) Poisson's Ratio, (c) Crack Density and (d) Saturation for the period that data was actively captured (23rd July – 31st August 2008).*

4 Conclusions

4.1 Monitoring Between April 2008 and September 2008

- This report describes the results from acoustic emission (AE) and ultrasonic monitoring around a canister deposition hole (DA3545G01) in the Prototype Repository Experiment at SKB's Hard Rock Laboratory (HRL), Sweden. The monitoring aims to examine changes in the rock mass caused by an experimental repository environment, in particular due to thermal stresses induced from canister heating and pore pressure variation induced from tunnel sealing. Monitoring of this volume has been performed during excavation [*Pettitt et al.,* 1999] and during stages of canister heating and tunnel pressurisation [*Haycox et al.,* 2005a and 2005b; *Haycox et al.,* 2006a and 2006b; *Zolezzi et al.,* 2007 and 2008; *Duckworth et al*., 2008]. The period covered by this report is between 1st April 2008 and 30th September 2008.

- In total there were 60 acoustic emissions, all of which have been located with a high degree of confidence.

- The majority of located AEs are positioned in three tight clusters around deposition hole DA3545G01; labelled A, B and D. Cluster A is made up of 29 events and located on the SE side, Cluster B (12 events) is on the SW side, and Cluster D (4 events) is on the NE side of the deposition hole. Clusters A and B are recurring and have been observed in several reports [*Zolezzi at al*., 2007 and 2008; *Duckworth et al*., 2008]. Cluster D was first identified during the last report period [*Duckworth et* al., 2008] and is located in a region of activity which occurred during excavation [*Pettitt et al.,* 2000]. The events in each cluster are close enough together to be considered as occurring along the same geological feature and may be occurring at specific positions due to the presence of pre-existing structures, either generated during excavation or at an intersection with a pre-existing micro-fracture.

- Two AEs have located in the same position as 'Cluster T', observed during the last report [*Duckworth et al*., 2008]. The events position SE of the deposition hole around the base of the tunnel and at a depth not previously highlighted as an existing damaged region either during the excavation or the pressurisation phases.

- The AEs located during this reporting period are consistent with previous results, i.e. no events are positioned in regions where activity has not been observed in the past. The events can therefore be interpreted as a continuation of activity in the damaged zone. We observe a decrease in the number of AEs with respect to the previous monitoring period and an overall decrease throughout the current response period interpreted from previous monitoring results. After correcting for the time which the system was not operating after 31st August 2008, the rate of AE triggering is an average of 0.38 triggers recorded each day compared to 0.90 in the previous monitoring period.

- Results from the velocity analysis reveal changes in P- and S-wave velocity that closely mimic one another but with slightly larger variations observed for P-waves. The average change in velocity is approximately ±0.4ms^{-1} for P-waves and ±0.1ms^{-1} for S-waves. The magnitudes of the average velocity changes are significantly smaller than the velocity uncertainty of 2ms^{-1} estimated for ultrasonic measurements, however, changes on individual ray-paths may be more pronounced. For example, the greatest magnitude change in velocity is observed on the ray-path between transmitter three and receiver nine (on the 18th August 2008), when P-wave velocity decreases by ~10ms^{-1}.

- Similar changes are also noted in P- and S-wave amplitudes with average changes in the region of ±0.05dB - ±0.1dB for both P- and S-waves.

- The five category ray-paths show the same velocity variations for both P- and S-waves during the period for which data were actively recorded (23rd July to 31st August 2008). For P-waves, ray-path C1 exhibits the greatest variation with average changes in the region of 0.6ms^{-1} and a maximum change of ~1.7ms^{-1}. For S-waves, category Far exhibits the most variation with average changes of ~0.3ms^{-1} and a maximum change of 0.6ms^{-1}. Overall, P-wave velocities display more variation than S-waves.

- Due to the lack of survey data obtained during this monitoring period, we have assembled the data recorded here, from July and August 2008, with data recorded during the previous recording period so as to evaluate any significant changes across the time when no recording was performed. Over this time there is a small decrease in temperature of ~7°C. Pressure variations are observed, but result in a small total pressure change when the system returns to being operational (decrease of ~0.8MPa). These changes have had very small accumulated effects on the P- and S-wave velocities and amplitudes measured, and are not significant compared to the uncertainties or to changes measured in previous monitoring periods.

- A comparison of AE activity and tunnel blasting activities revealed that there is no direct correlation between the timing of blasting and increased AE activity, although a time dependent effect resulting from the new excavation cannot be ruled out.

- AE rates and changes in ultrasonic survey parameters have remained relatively small indicating that the rock mass around the deposition holes has remained stable throughout this report period.

4.2 Summary of Monitoring from the Heating and Pressurisation Phase

- Monitoring of the heating and pressurisation phase at the Prototype Repository Experiment has been conducted since March 2003. Analysis of the AEs and ultrasonic measurements is split into five response periods (following previous reports). Table 4-1 presents a summary of the observations from ultrasonic monitoring thus far and Table 4-2 provides interpretations of the rock response.

- Figure 4-1 shows average P- and S-wave velocity and amplitude recorded during the monitoring period. Figure 4-2 to Figure 4-6 provide average velocity and modulus changes for the six ray-path categories selected in terms of disturbed and damaged regions. Figure 4-7 and Figure 4-8 show all locations and the temporal distributions of located AEs recorded since March 2003. Figure 4-9 to Figure 4-12 summarise changes that take place at different regions around the deposition hole in schematic diagrams for each period, identifying the primary changes in the properties of the rock as described in Table 4-2.

4.3 Recommendations

The rock mass around the deposition holes has remained relatively stable during this monitoring period.

- There are over five years of monitoring ultrasonic survey measurements at the Prototype experiment with velocity and amplitude measurements conducted through a number of variations in pressure and temperature conditions. It would now be beneficial to perform an additional integrated interpretation of changes in these measurements with available data on the thermal and hydro-mechanical conditions in the repository, in order to better understand the rock response in the immediate vicinity of the deposition hole. This could help resolve whether pressure or temperature, or an optimal combination of the two, has a leading role in reducing crack density (and hence permeability) and thus provide a best practise for working conditions of a future repository.

- AE clustering is thought to occur in regions of pre-existing micro-cracks following the excavation phase [Pettitt et al., 2000] and might suggest a re-activation of pre-existing fractures. Clustering of AE events is observed around the walls of the deposition hole. It would be interesting to carry out further study on these events to investigate the fracture mechanism, and their temporal evolution with respect to changing environmental variables. The objective would be to resolve the primary factors responsible for causing AEs to occur in specific locations around the deposition hole.

Table 4-1: Summary of velocity, amplitude and AE variation measured during five response periods of temperature and/or pressure change.

Name / Date	Temperature/Pressure	Velocity	Amplitude	AE
PERIOD 1 25th May 2003 to 31st October 2004	Heaters in canister switched on causing an initially rapid change in temperature which gradually levels out to a constant increase. An increase of 35ºC is measured for an instrument in rock adjacent to the deposition hole. Pressure constant.	Rapid increase in P- and S-wave velocity on S3 category. Other categories show increases but to a lesser extent. Initial decrease in P-wave velocity in comparison to S-wave velocity for all ray-paths except for S3.	Amplitudes increase over this period by between 3dB and 9dB for P-wave amplitude, and 7dB and 12dB for S-wave amplitude.	AEs do not start immediately after heating. This could be a Kaiser-type effect in which AE rate remains close to background level until stress increases above the largest previous value. Peak of 13 events located on 26th June 2003. Average Event Rate = 0.5 / day.
PERIOD 2 1st November 2004 to 4th September 2005	Drainage to tunnel closed on 1st November. Pressure in tunnel increases. Pressure increases measured in the deposition-hole buffer between 3rd and 5th December. Damage observed on canister on 6th December so drainage reopened and heaters switched off. Power switched on 15th December.	Velocity increases measured close to the tunnel from 26th November. Larger increases measured on categories S1 and S3.	Amplitude increases measured close to the tunnel from 26th November.	Relatively large number of events recorded in this period. Peak rate of 32 AEs on 4th and 5th December. Events locate in clusters in previously observed damage zone. Average Event Rate = 0.4 / day.
PERIOD 3 5th September 2005 to 2nd November 2005	Additional drainage is opened in August 2005 leading to a decrease in pressure and temperature. Heaters turned off on 5th September.	P- and S-wave velocities decrease on all ray-path categories except Far.	P-wave amplitude decrease on all category ray-paths.	Slight increase in event rate above background rate recorded in previous 5 months. Average Event Rate = 0.3 / day.
PERIOD 4 3rd November 2005 to 13th April 2007	Pressure in tunnel increases. Constant increase in pressure in buffer above deposition hole. Heaters switched on again so temperature around the deposition hole increases.	P- and S-wave velocities increase on all category ray-paths. Larger increases measured on S3.	P- and S-wave amplitude increase on the majority of ray-paths.	Cluster of 202 events located on SE side of deposition hole. Similar rate of AE locations. Average Event Rate = 0.46 / day.
PERIOD 5 14th April 2007 to 30th September 2008	Short-term variations of pressure and temperature in the tunnel and deposition hole. Missing pressure data period (24/06/2007-09/09/2007). Missing ultrasonic data period (17/12/2007 – 27/07/2008).	P- and S-wave velocities generally increase on all category ray-paths. Larger increases measured on all ray-paths related to instrument 6. Largest decrease in October 2007 is observed on category C2.	P- and S-wave amplitude increase on all ray-paths. Deviation observed during short-term pressure and temperature excursions.	346 events located in 4 distinct clusters on SE, SW and NE sides of deposition hole. Peak of 21 events on 22nd January 2008 locate in one anomalous cluster some distance from the deposition hole. Average Event Rate = 0.75 / day.

Table 4-2: Summary of key interpretation of rock response from the ultrasonic measurements.

Period	Summary of Key Interpretations
1	The heaters are switched on. The S3 category passes through a volume that is unloaded and hence experiences low compressive stresses. This volume responds more rapidly to thermal stresses because existing microfractures are initially unloaded and hence more open than microfractures in the compressive region. P- and S-wave velocities decrease a similar amount during excavation as they increase during heating. This suggests very strongly that the microfractures induced in the regions of tensile damage around the deposition hole close when thermal stresses are applied. The difference in the rate of response between ray-paths in the compressive categories was interpreted as a different magnitude of response of the microfractures in the rock mass to increasing thermal stresses. In the first few months of heating, another effect is superimposed onto the rock's response to thermal stresses. This is measured as a reduction in P-wave velocities compared to S-wave velocities in the first few months of heating. This is particularly noticeable on S1 category in Figure 4-2, in which P-wave velocity decreases by about 3.5ms^{-1} while S-wave velocity remains constant. A desaturation occurs on all ray-path categories other than S3. This must be caused by a drying of the rock mass, in the zones experiencing high compressive stresses, as heat is applied to the rock (i.e. both temperature and pressure are acting to expel moisture). In the low-compressed, or tensile, region saturation increases during this period. This is probably caused by hot fluids expanding into the open microfracture fabric.
2	Pressure rose rapidly after drainage from the tunnel was closed. This resulted in damage to the canister and the heaters being temporarily switched off. Temperature around the deposition hole dropped rapidly, but started increasing again after 13 days. Significant changes to the character of many recorded ultrasonic waveforms were observed as significant increases in signal quality. This suggests that as pressure increased in the rock surrounding the deposition hole, attenuation of the ultrasonic waves is significantly reduced meaning that they can pass more efficiently through the rock medium. The pressure increase can be interpreted as increasing the stiffness of the rock with a corresponding decrease in crack density. The magnitude of increase is greater for S1 and S3 categories because the volumes through which they pass are close to the deposition holes and contain a higher proportion of microfractures in an excavation damage zone. The pressure increase acts as a confining pressure on the rock mass leading to a closure of the pre-existing microcrack fabric and therefore a reduction in crack density. We observe that only a relatively small pressure increase is sufficient to close this microcrack fabric in the volumes already under high compressive stresses, leading to an initially high rate of change in measured velocities followed by a constant level, even though pressures may keep increasing afterwards. From Figure 4-2 the required pressure increase is approximately 1.5MPa. The rapid pressure increase led to 32 events locating in clusters over the course of two days. The events are interpreted as stress changes in the rock as it responds to the sudden pressure change. This induces small scale movement on pre-existing microcracks, or induces new microfractures in weaker volumes of the rock. Pore pressure increases may also have assisted in inducing slip on pre-existing microfractures, by reducing the normal stress on the fractures. Over the rest of this period, as pressure continued to increase, fewer events were located. Another effect at this time is a rapid cooling of the rock when the heater inside the canister is switched off (for 13 days between 2nd and 15th December 2004), followed by warming as the rock is reheated. The majority of categories do not show a significant change in P- or S-wave velocity during this period indicating they are relatively insensitive to temperature changes at this time (i.e. when pressures are high). The exception is category S3, which exhibits a decrease in P- and S-wave velocity followed by an increase that mirrors the rate at which temperature changes (Figure 4-3). This category was found to be the most sensitive to thermal stresses during the initial stages of heating. When the rock cools, thermal stresses acting in this volume of low compressive (or slightly tensile) stresses reduce causing unloading of the microcracks. Microcracks close again when the rock is reheated and thermal stresses increase.

3	In September 2005 additional drainage from a permeable mat placed on the inner surface of the outer plug was opened, and heaters were switched off. This resulted in a cooling and de-pressurisation of the deposition hole. Neither temperature nor pressure reduced to the background level. The decrease in velocity on most ray-paths is generally low compared to the increases observed previously. An exception to this is category S3. This category is observed as the most sensitive. As temperature and pressure decreases, stresses again reduce in this volume causing microcracks to reopen and resulting in an increase in crack density and reduced stiffness of the rock. At the start of the period a sudden (over a few days), but relatively small change in velocity is observed, superimposed on the longer-term trends. We believe these are related to rapid changes in fluid pressure; a corresponding increase is observed at the end of the period (start of Period 4). For Period 3, an increase in Young's Modulus occurs which indicates a stiffening of the rock. This short term change is therefore likely to be a sudden reaction of the rock mass to the decrease in fluid pressure, perhaps caused by a general closing of microcracks caused by decreased pore pressures. The reverse is true for Period 4, when a pressure increase leads to a general opening of microcracks caused by increased pore pressures. This is believed to be a different response to long term trends from thermal stresses and general confining of the rock mass.
4	During the fourth period, heaters were turned back on once more causing temperature around the deposition hole to increase. Pressure increased rapidly again, probably caused by changes in the buffer temperature (changes in water volume caused by the temperature in combination with low hydraulic conductivity) [*Goudarzi* and *Johannesson*, 2006]. Velocity increases rapidly at first, then at a constant rate, following a similar pattern to the temperature and pressure. Ray-path category S3 exhibits the greatest increase in P and S-wave velocity. Similar patterns are observed on S1 and C1, and to a lesser extent on C2. Velocity on the Far ray-path category remains constant throughout the period. When temperature and pressure start to increase the stiffness of the rock increases, particularly on S3. This is accompanied by a reduction in crack density. The associated increase in stiffness and decrease in crack density can be interpreted as the closing of existing microfractures and pore spaces as observed previously. This effect has continued to the current day. Few events have been located during Periods 3 and 4. A rapid decrease, and then increase, in pressure and temperature appears to have no significant effect on the number, or distribution of AEs around the deposition hole. The AE rate marginally increased since February 2006 (Figure 4-8). The vast majority of events locate on a single cluster in the south-east of the deposition hole and at 455.1m depth. The low number of AEs suggests the rock mass has stabilised. The high pressures result in a confining pressure being placed on the rock around the deposition hole and inhibit the movement on microcracks or macrofractures.
5	During the fifth response period the excavation of a new tunnel near the prototype tunnel resulted in a gap in pressure data (from 24th June until 9th September 2007). Pressure in the tunnel backfill generally increased through the period (by ~0.5MPa) while the temperature has remained extremely stable (maximum change of only 1-2°C). Conditions in the buffer surrounding the canister remain fairly stable with the exception of two sudden drops in both temperature and pressure. The first occurred on 21st October 2007, when temperature dropped by ~5°C and pressure by ~8MPa, these changes coincide with decreases in P- and S-wave velocity and amplitude. The second occurred on 10th June 2008, at a time when no ultrasonic survey data was captured. As temperature and pressure decreases, stresses reduce in the volume causing microcracks to reopen and resulting in an increase in crack density and reduced stiffness of the rock. It is unclear whether the drop in pressure or temperature is responsible for the observed changes in velocity and amplitude, but both are likely to affect the stress field in some manner. In the first six months of this period (April 2007 – September 2007) the velocity and amplitude for both P- and S-waves increases between 20th and 24th April 2007. P-waves show higher variation than S-waves. The most sensitive ray-paths to the changes are those related with sensor 6. Analysis of the different ray-paths reveal that category Far shows the maximum velocity changes for both P- and S- waves while category C1 shows minor changes. The minimum variation in signal amplitudes is observed for S3 category. In the following six months (October 2007 – March 2008) velocity and amplitude for both P- and S-waves decrease for a period between 21st and 26th October 2007 then increase more gradually, with only minor variations observed, until the end of March 2008. P-wave velocity increases suddenly to a period high on 21st November 2007. The most sensitive ray-path categories (with most observable variation) are C2, S3 and to a lesser extent C1. Data for velocity and amplitude are not obtainable from ultrasonic surveys after 17th December 2007 due to a power malfunction. In the following six months (April 2008 – September 2008) we observe small changes in P-and S-wave amplitude and velocity, and changes in rock properties that are similar to the previous six months, although category C1 displays the most variation. The AE rate increases since the last response period (by ~40%). Events generally locate in clusters around the deposition hole: three of these clusters are recurring in active volumes, one occurring in a volume around the canister deposition hole not previously seen, and one anomalous cluster representing a newly activated volume in the tunnel floor. The increase in AE activity would suggest that the rock mass has undergone some new fracturing or movement on existing fractures. Blasting records give no indication that nearby tunnel excavation is directly responsible for this increase; although a time dependent stress effect could play a role. Towards the end of the response period the AE rate decreases. The relatively low number of AEs suggests the rock mass is generally stable.

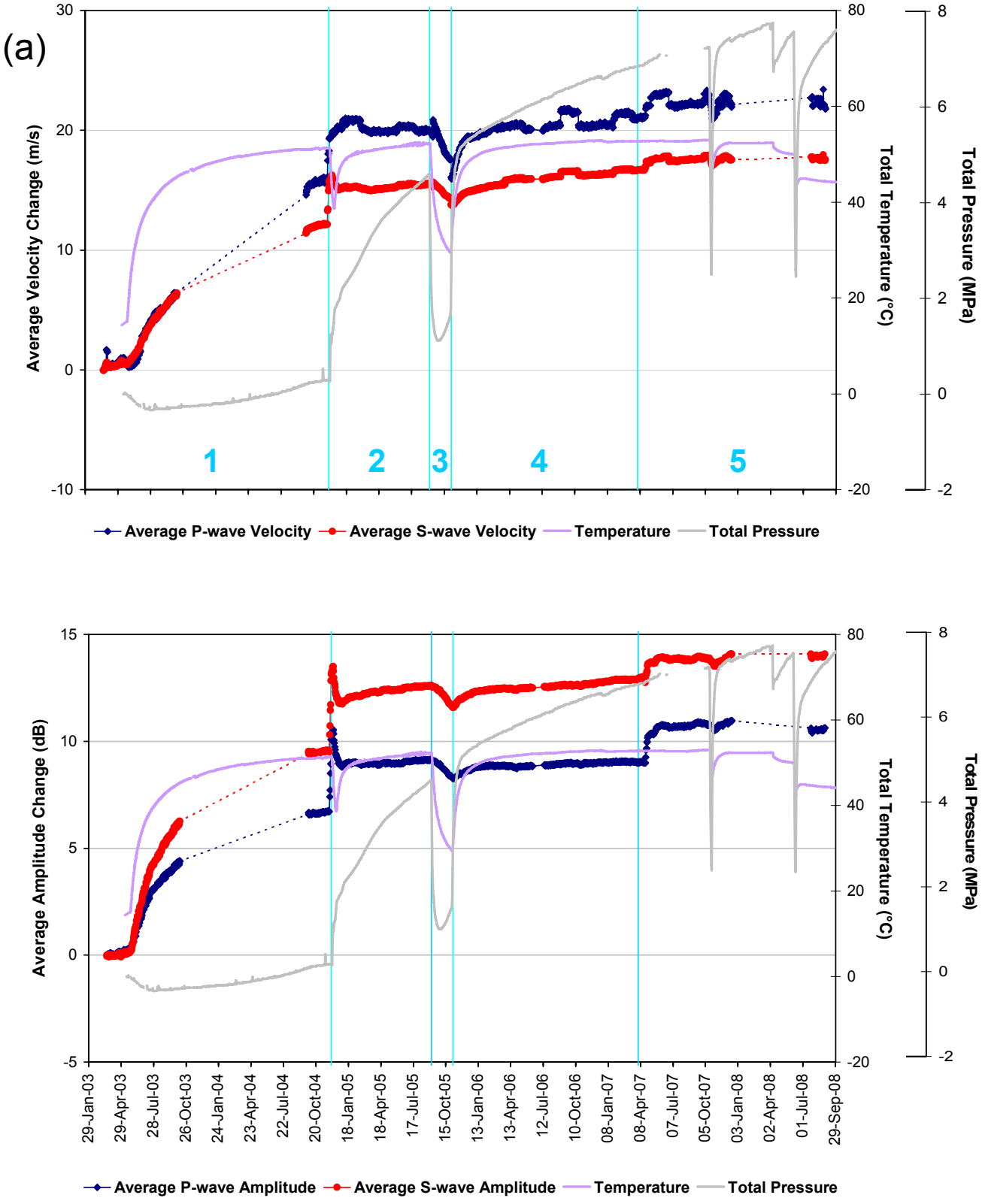

Figure 4-1: *P- and S-wave velocity change (a) and amplitude change (b) from the start of monitoring (20th March 2003), plotted alongside temperature (TR6045) and pressure (PB616) measurements in deposition hole DA3545G01. The vertical blue lines separate periods of similar environmental conditions as defined in Table 4-1.*

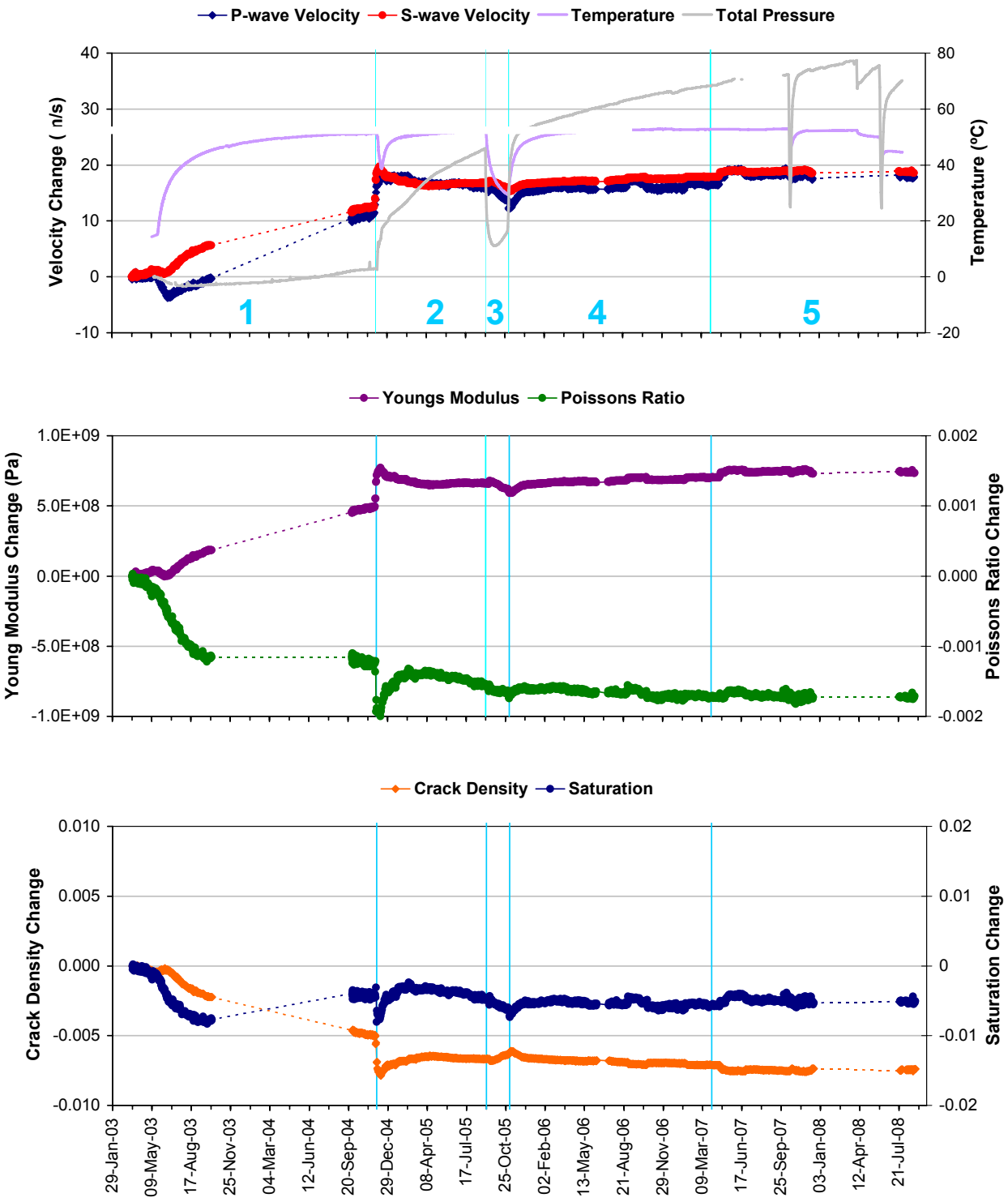

Figure 4-2: *Changes in rock properties and velocity along the S1 category of ray-paths. Average P- and S-wave velocity change shown with temperature (instrument TR6045) and total pressure (instrument PB616) (top), Young's Modulus and Poison's Ratio change (middle), and Crack Density and Saturation change (bottom). Periods representing similar environmental conditions, as defined in Table 4-1, are separated by the vertical blue lines.*

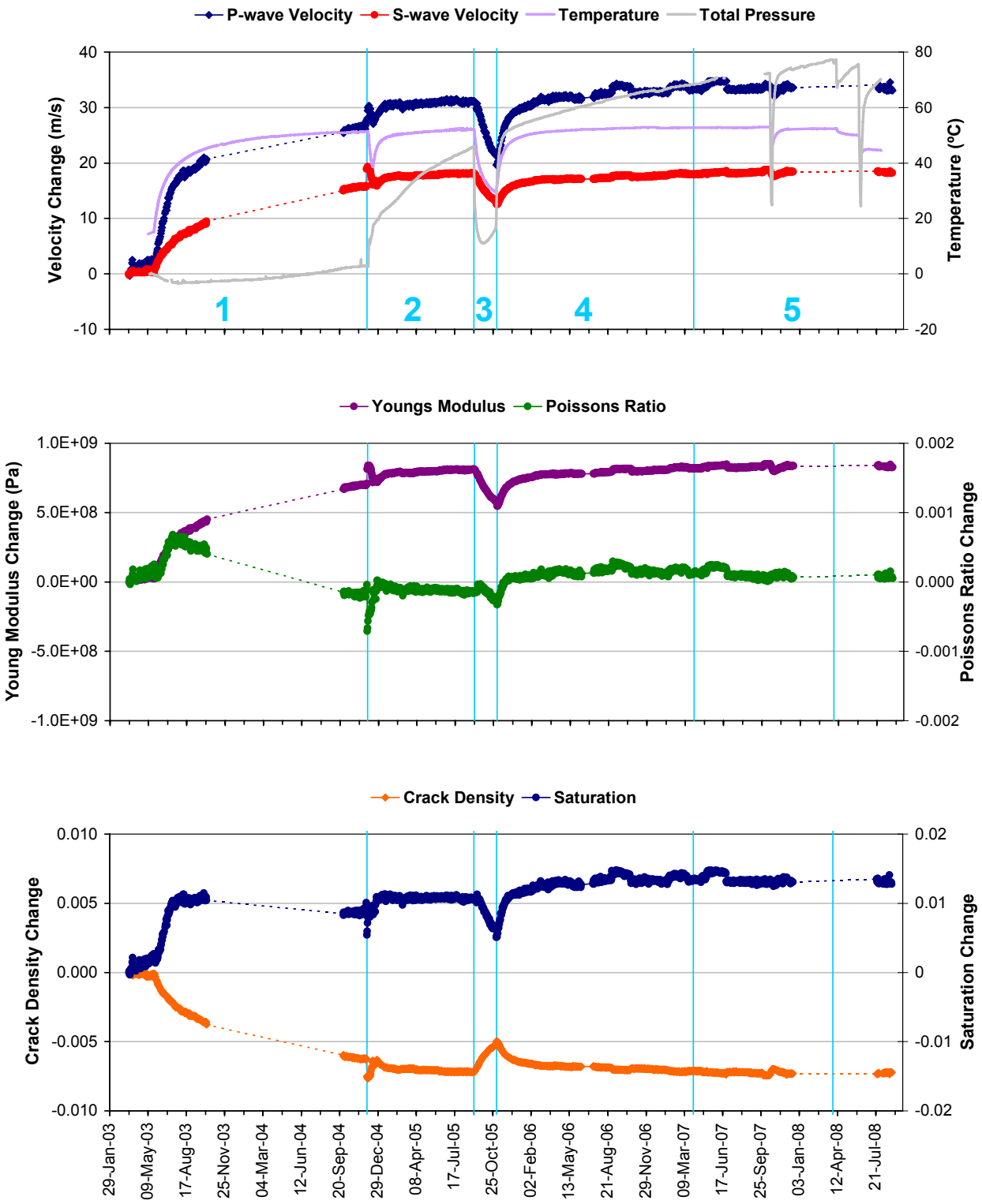

Figure 4-3: *Changes in rock properties and velocity along the S3 category of ray-paths. Average P- and S-wave velocity change shown with temperature (instrument TR6045) and total pressure (instrument PB616) (top), Young's Modulus and Poison's Ratio change (middle), and Crack Density and Saturation change (bottom). Periods representing similar environmental conditions, as defined in Table 4-1, are separated by the vertical blue lines.*

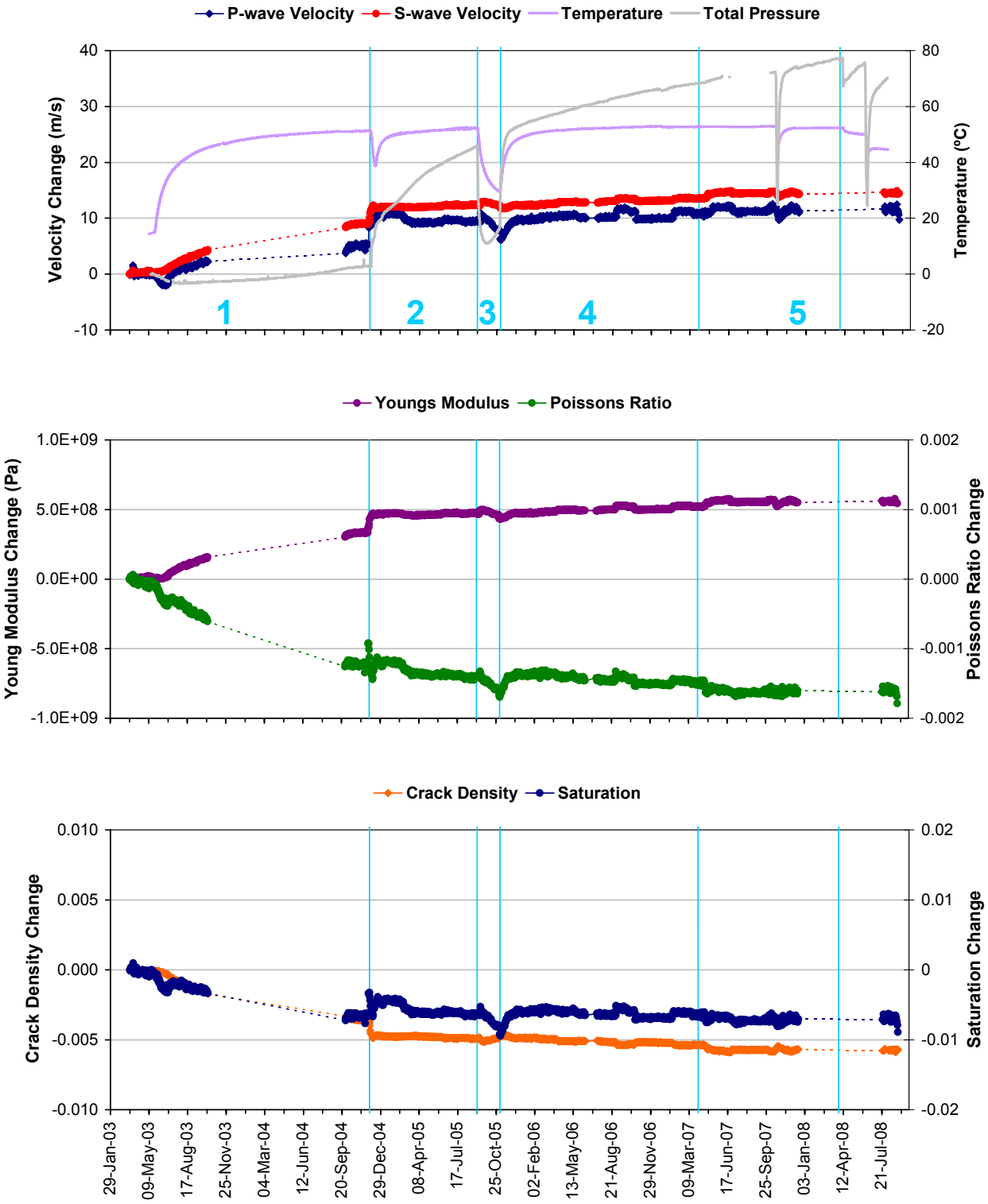

Figure 4-4: *Changes in rock properties and velocity along the C1 category of ray-paths. Average P- and S-wave velocity change shown with temperature (instrument TR6045) and total pressure (instrument PB616) (top), Young's Modulus and Poison's Ratio change (middle), and Crack Density and Saturation change (bottom). Periods representing similar environmental conditions, as defined in Table 4-1, are separated by the vertical blue lines.*

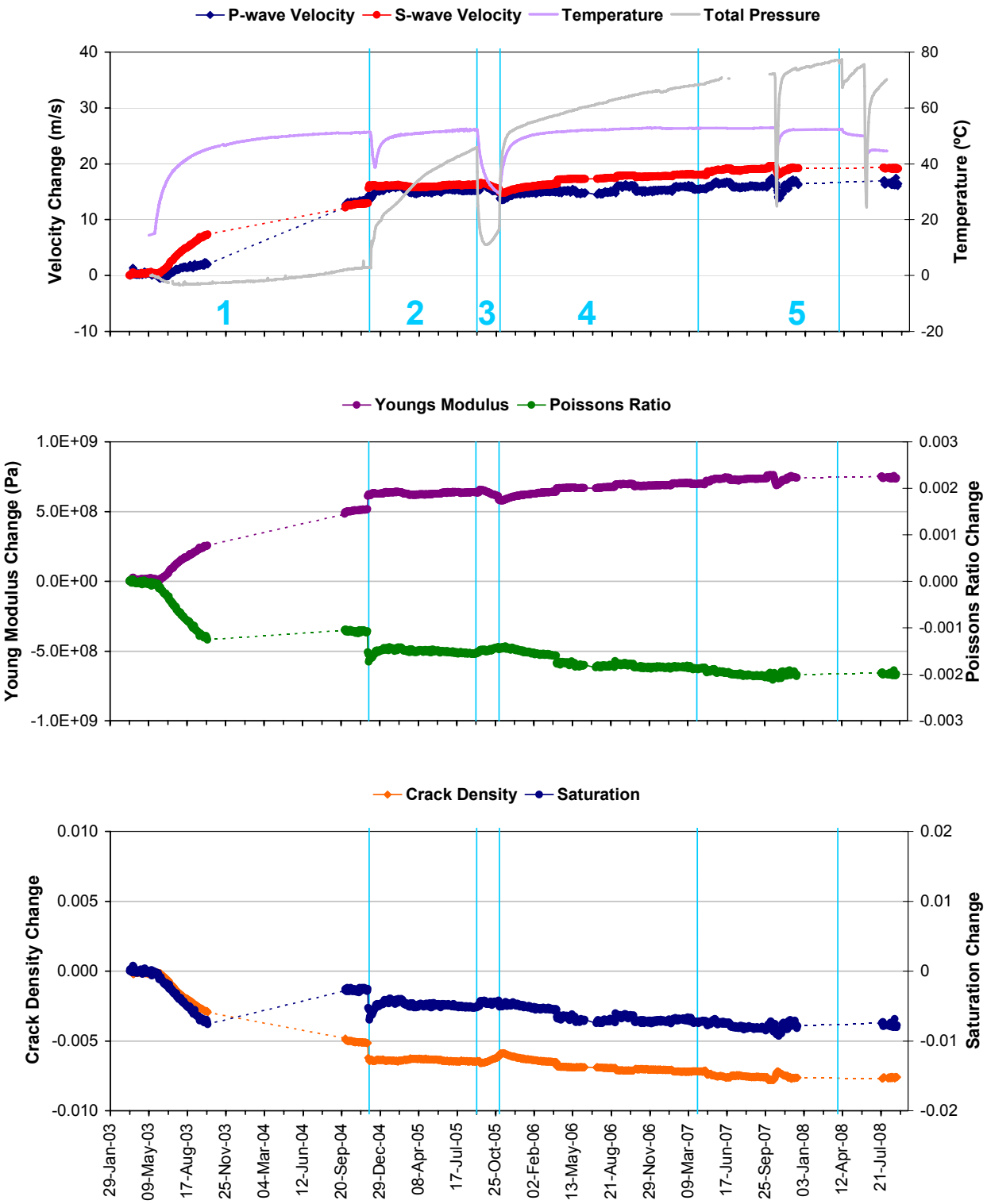

Figure 4-5: *Changes in rock properties and velocity along the C2 category of ray-paths. Average P- and S-wave velocity change shown with temperature (instrument TR6045) and total pressure (instrument PB616) (top), Young's Modulus and Poison's Ratio change (middle), and Crack Density and Saturation change (bottom). Periods representing similar environmental conditions, as defined in Table 4-1, are separated by the vertical blue lines.*

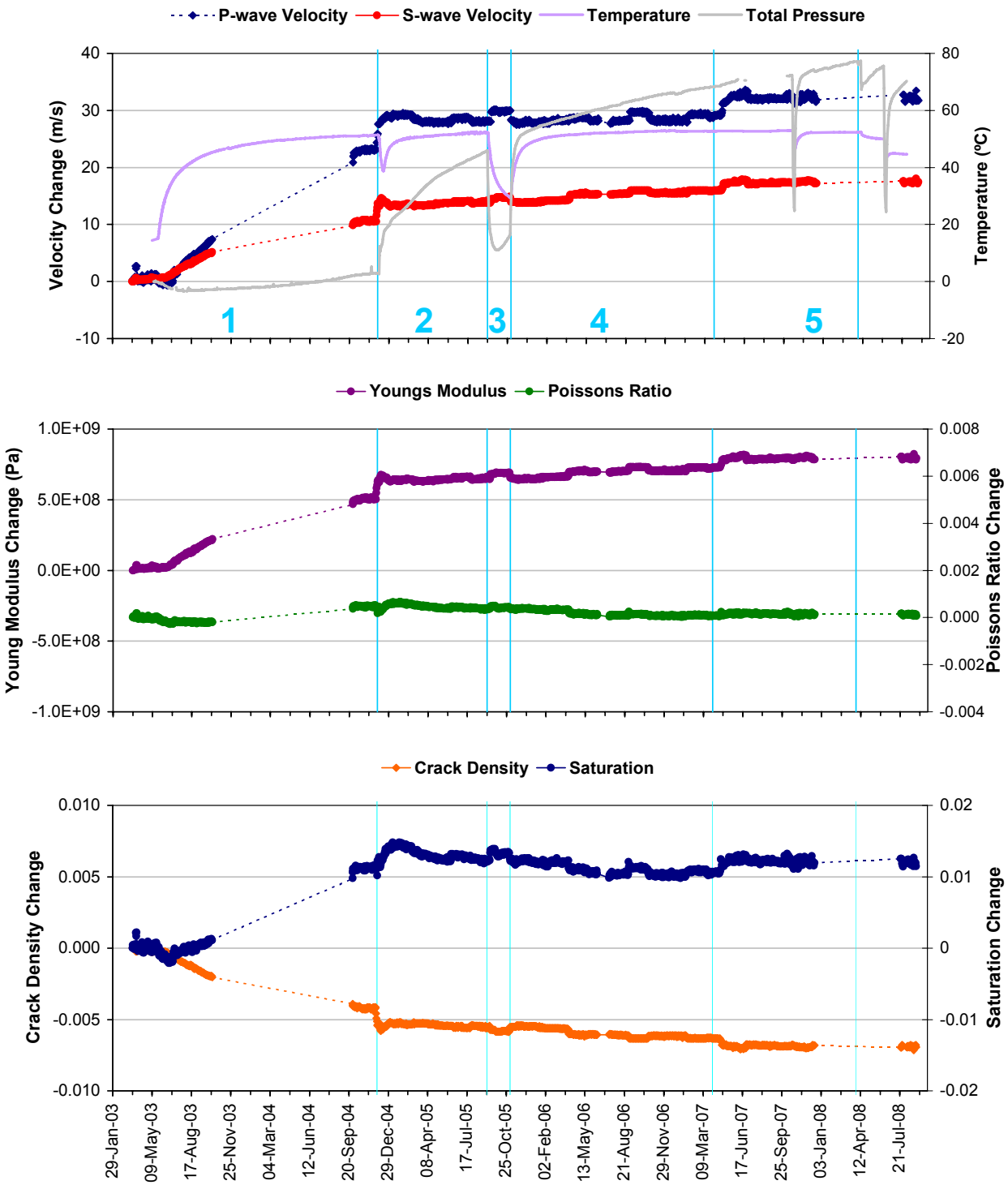

Figure 4-6: *Changes in rock properties and velocity along the Far category of ray-paths. Average P- and S-wave velocity change shown with temperature (instrument TR6045) and total pressure (instrument PB616) (top), Young's Modulus and Poison's Ratio change (middle), and Crack Density and Saturation change (bottom). Periods representing similar environmental conditions, as defined in Table 4-1, are separated by the vertical blue lines.*

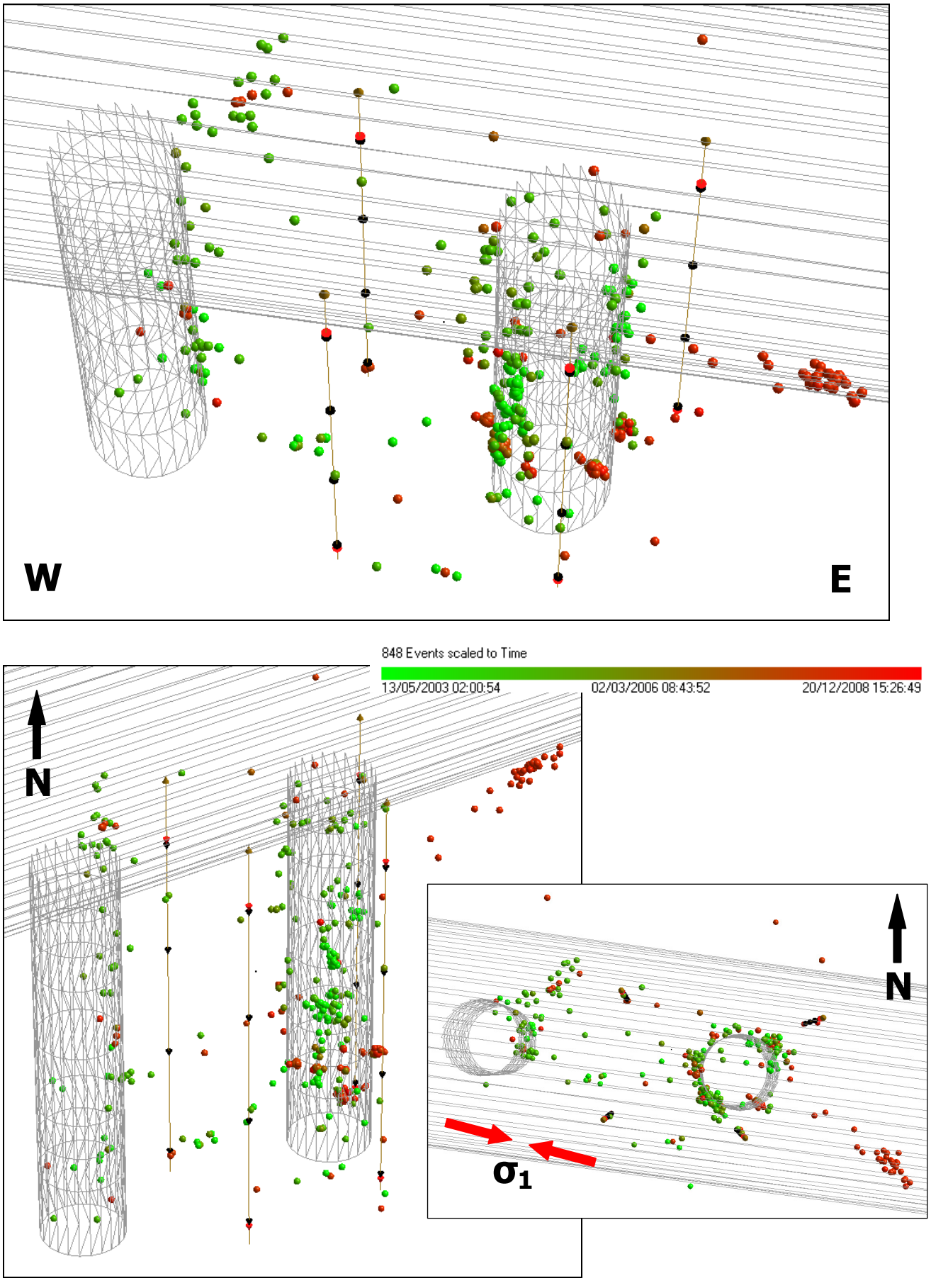

Figure 4-7: *Projections of all AEs located during the heating phase (20th March 2003 to 30th September 2008). In total there have been 848 events over the last six years of monitoring (events are scaled by time).*

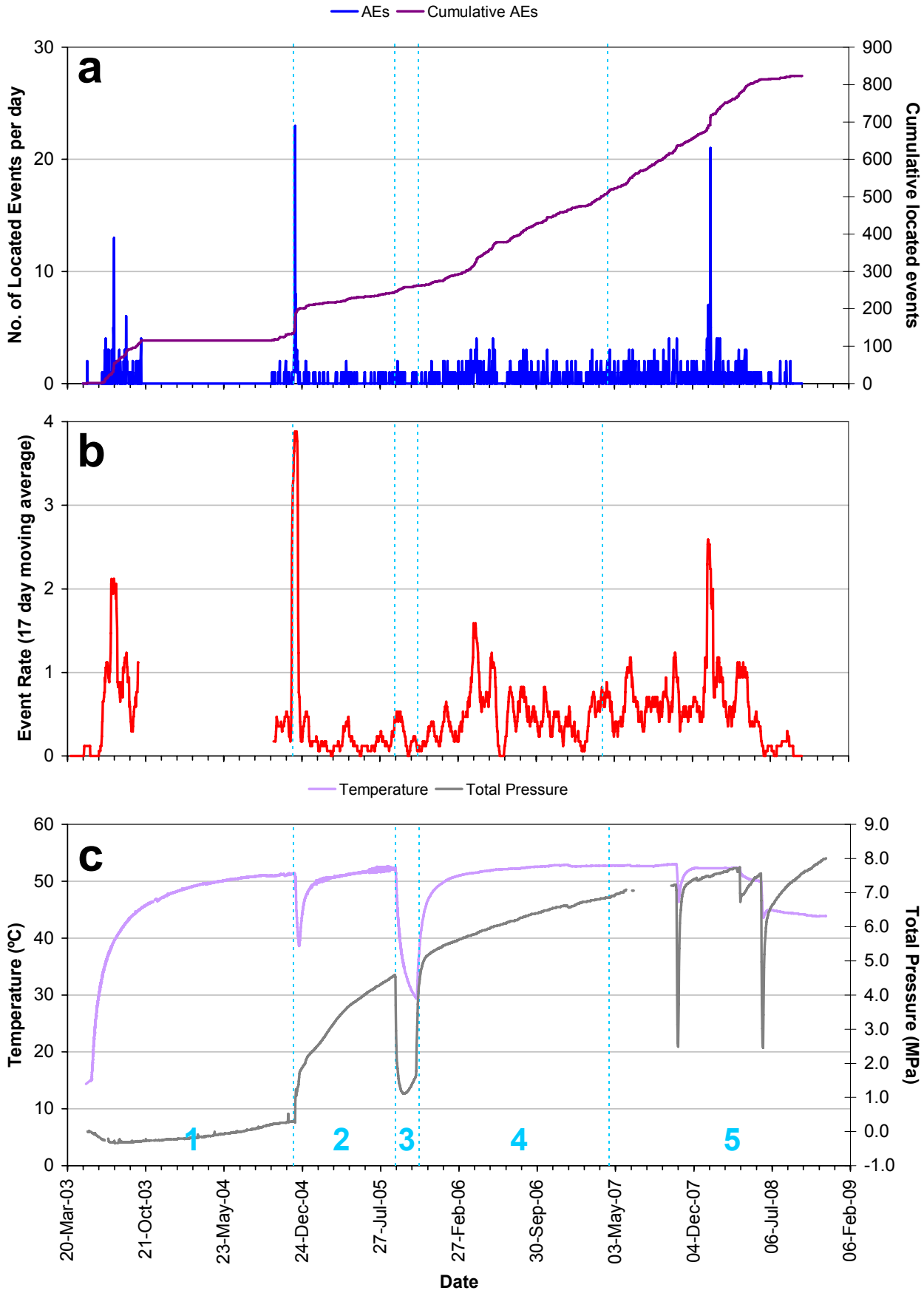

Figure 4-8: *(a) Number and cumulative number of located events from the start of monitoring in March 2003, (b) 17 day moving average of located AEs and (c) temperature (TR6045) and pressure (PB616) measurements in deposition hole DA3545G01.*

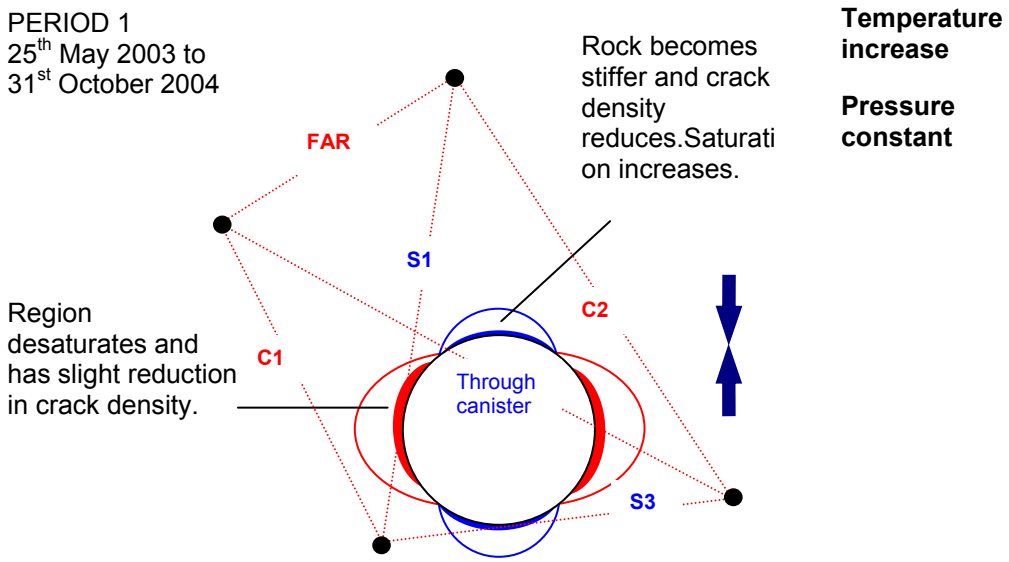

Figure 4-9: *Schematic diagram of the deposition hole and explanation of changes experienced during Period 1.*

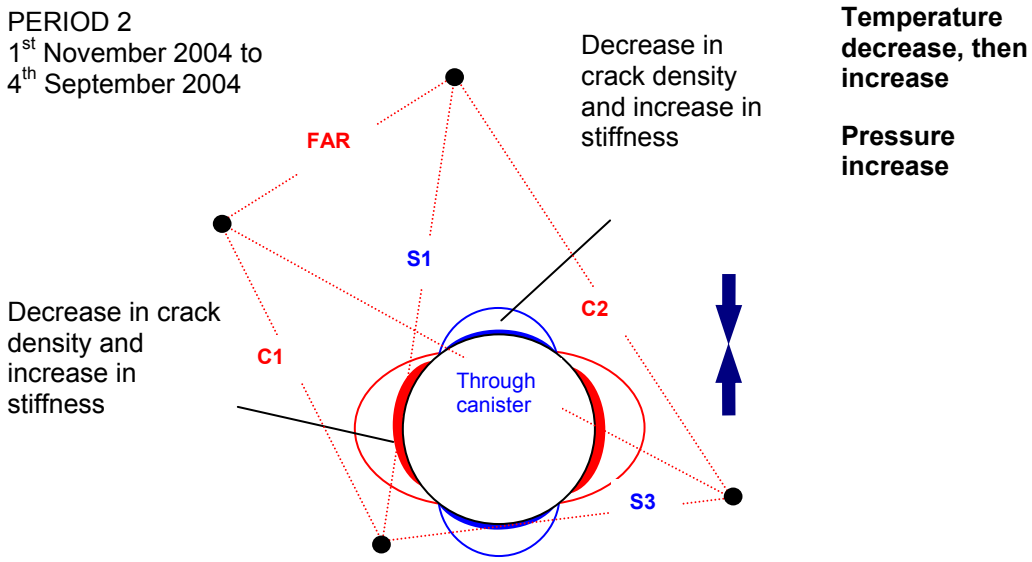

Figure 4-10: *Schematic diagram of the deposition hole and explanation of changes experienced during Period 2.*

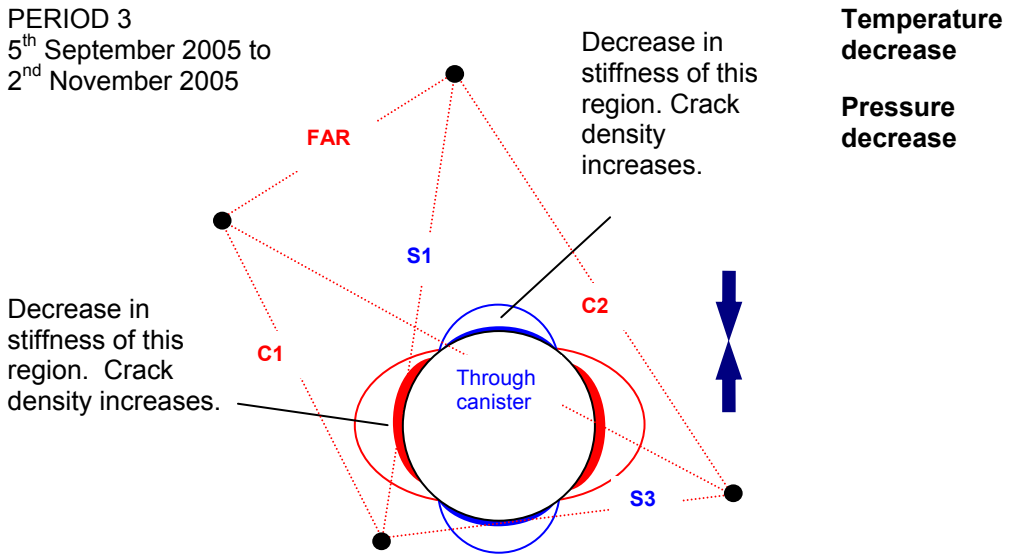

Figure 4-11: *Schematic diagram of the deposition hole and explanation of changes experienced during Period 3.*

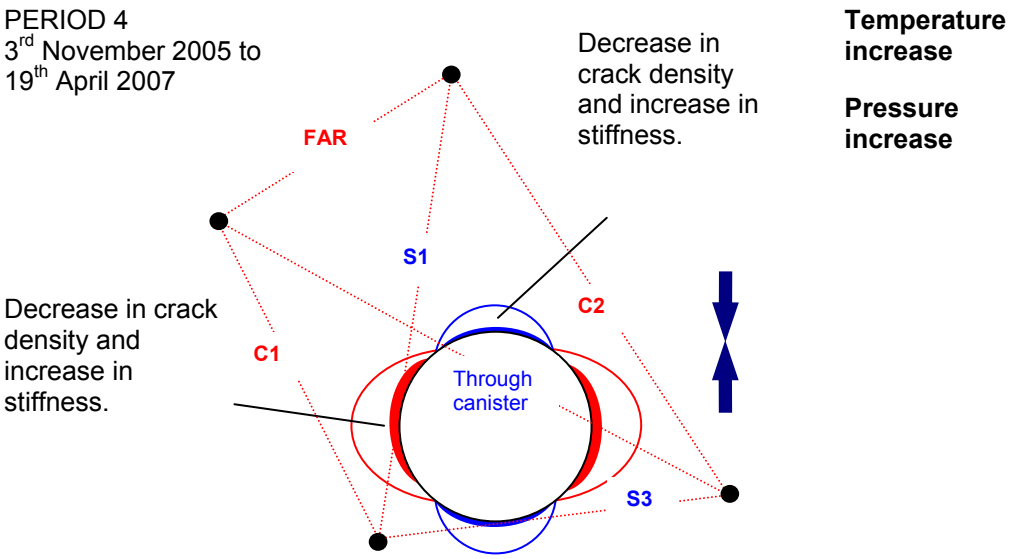

Figure 4-12: *Schematic diagram of the deposition hole and explanation of changes experienced during Period 4.*

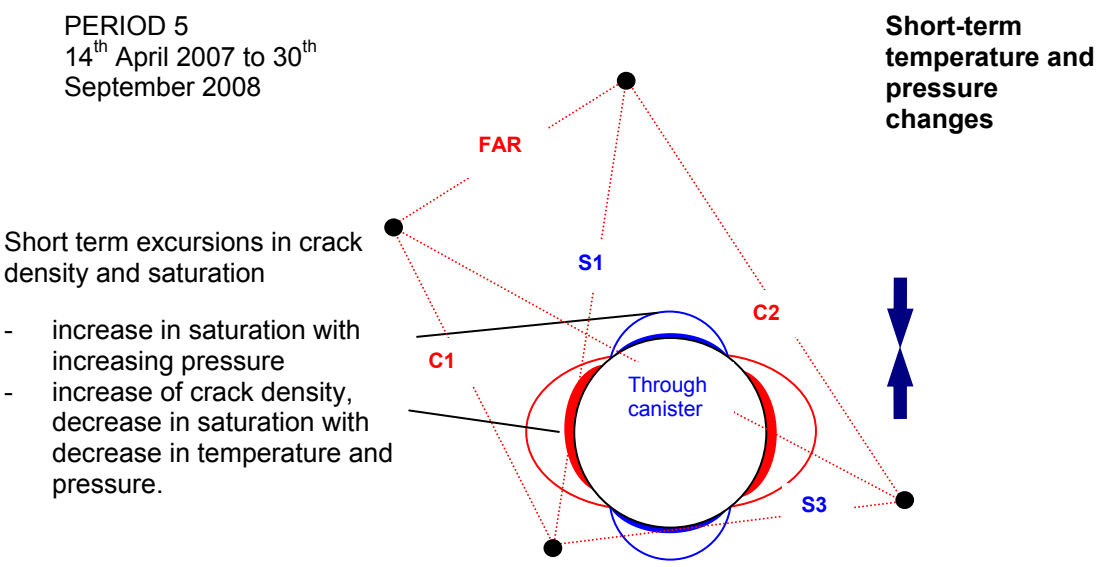

Figure 4-13: *Schematic diagram of the deposition hole and explanation of changes experienced during Period 5.*

References

Duckworth, D., Haycox J.R., and Pettitt W.S., 2008: Acoustic Emission and Ultrasonic Monitoring Results from Deposition Hole DA3545G01 in the Prototype Repository between October 2007 and March 2007, Applied Seismology Consultants, Shrewsbury, UK.

Goudarzi, R., and Johannesson, L-E., 2006: Sensor Data Report (Period: 010917-061201). Prototype Repository, Report No: 16, International Progress Report IPR-07-05, Äspö Hard Rock Laboratory, Swedish Nuclear Fuel and Waste Management Company, Sweden.

Haycox, J.R., Pettitt, W.S., and Young, R.P., 2005a: Acoustic Emission and Ultrasonic Monitoring During the Heating of Deposition hole DA3545G01 in the Prototype Repository to March 2005, International Progress Report IPR-05-30, Äspö Hard Rock Laboratory, Swedish Nuclear Fuel and Waste Management Co. Sweden.

Haycox, J.R., Pettitt, W.S., and Young, R.P., 2005b: Acoustic Emission and Ultrasonic Monitoring Results from Deposition Hole DA3545G01 in the Prototype Repository between April 2005 and September 2005, International Progress Report IPR-05-31, Äspö Hard Rock Laboratory, Swedish Nuclear Fuel and Waste Management Co. Sweden.

Haycox, J.R., Pettitt, W.S., and Young, R.P., 2006a: Acoustic Emission and Ultrasonic Monitoring Results from Deposition Hole DA3545G01 in the Prototype Repository between October 2005 and March 2006, International Progress Report IPR-06-23, Äspö Hard Rock Laboratory, Swedish Nuclear Fuel and Waste Management Co. Sweden.

Haycox, J.R., Pettitt, W.S., and Young, R.P., 2006b: Acoustic Emission and Ultrasonic Monitoring Results from Deposition Hole DA3545G01 in the Prototype Repository between April 2006 and September 2006, International Progress Report IPR-06-36, Äspö Hard Rock Laboratory, Swedish Nuclear Fuel and Waste Management Company, Sweden.

Maxwell, S.C., and Young, R.P., 1995: A controlled in-situ investigation of the relationship between stress, velocity and induced seismicity, Geophys. Res. Lett, 22, pp. 1049-1052.

Patel, S., Dahlstrom, L.-O., and Stenberg, L., 1997: Characterisation of the Rock Mass in the Prototype Repository at Äspö HRL Stage 1, Äspö Hard Rock Laboratory Progress Report HRL-97-24, Swedish Nuclear Fuel and Waste Management Company, Sweden.

Pettitt, W.S., Baker, C., and Young, R.P., 1999: Acoustic emission and ultrasonic monitoring during the excavation of deposition holes in the Prototype Repository, International Progress Report IPR-01-01, Äspö Hard Rock Laboratory, Swedish Nuclear Fuel and Waste Management Company, Sweden.

Pettitt, W.S., Baker, C., and Young, R.P., 2000: Analysis of the in-situ principal stress field at the HRL using acoustic emission data, International Progress Report IPR-01-09, Äspö Hard Rock Laboratory, Swedish Nuclear Fuel and Waste Management Company, Sweden.

Pettitt, W.S., Baker, C., Young, R.P., Dahlstrom, L., and Ramqvist, G., 2002: The assessment of Damage around Critical Engineering Structures Using Induced Seismicity and Ultrasonic Techniques, Pure and Applied Geophysics, 159, 179-195.

Pettitt, W.S., and Young, R.P., 2007: InSite Seismic Processor – User Operations Manual Version 2.14, Applied Seismology Consultants Ltd. Shrewsbury, UK.

SKB, Äspö Hard Rock Laboratory: Current Research Projects 1999: Swedish Nuclear Fuel and Waste Management Company, Sweden.

Telford, W.M., Geldart, L.P., and Sheriff, R.E., Applied Geophysics: Second Edition, Cambridge University Press, 1990.

Young, R.P., and Pettitt, W.S., 2000: Investigating the stability of engineered structures using acoustic validation of numerical models, in Geotechnical Special Publication No 102, edited by J.F. Labuz, S.D. Glaser and Dawson.
ASCE, USA, pp. 1-15.

Zimmerman, R.W., and King M.S., 1985: Propagation of acoustic waves through cracked rock, 20th Symposium on Rock Mechanics, Rapid City, SD.

Zolezzi F., Haycox J. R., and Pettitt W.P., 2007: Acoustic Emission and Ultrasonic Monitoring Results from Deposition Hole DA3545G01 in the Prototype Repository between October 2006 and March 2007, International Progress Report IPR-06-23, Äspö Hard Rock Laboratory, Swedish Nuclear Fuel and Waste Management Co. Sweden.

Zolezzi F., Haycox J.R., and Pettitt W.P., 2008: Acoustic Emission and Ultrasonic Monitoring Results from Deposition Hole DA3545G01 in the Prototype Repository between April 2007 and September 2007, Applied Seismology Consultants, Shrewsbury, UK.

Appendix I Previous Monitoring at the Prototype Repository

Ultrasonic monitoring has been conducted at the Prototype Repository since September 1999. During excavation, monitoring of both deposition holes in Tunnel Section 2 (DA3551G01 and DA3545G01) was undertaken to delineate zones of stress related fracturing and quantitatively measure fracturing in the damaged zone [*Pettitt et al.,* 1999]. Monitoring has been undertaken on a single deposition hole (DA3545G01) since 2003, and the response of the surrounding rock to changes in temperature and pressure has been measured with reporting of results every six months (see Table 4-3). This report presents new results from the period 1st April 2008 to 30th September 2008.

Table 4-3: Summary of ultrasonic monitoring at the Prototype Repository to-date.

Report	Monitoring Period	Location	Response Period
Pettitt et al., [1999]	25/08/1999 to 18/09/1999	DA3551G01 and DA3545G01	Excavation
Haycox et al., [2005a]	20/03/2003 to 09/10/2003	DA3545G01	1
	29/04/2004 to 31/03/2005	DA3545G01	1, 2
Haycox et al., [2005b]	01/04/2005 to 30/09/2005	DA3545G01	2, 3
Haycox et al., [2006a]	01/10/2005 to 31/03/2006	DA3545G01	3, 4
Haycox et al., [2006b]	01/04/2006 to 30/09/2006	DA3545G01	4
Zolezzi et al., [2007]	01/10/2006 to 31/03/2007	DA3545G01	4
Zolezzi et al., [2008]	01/04/2007 to 31/09/2007	DA3545G01	4,5
Duckworth et al., [2008]	01/10/2007 to 31/03/2008	DA3545G01	5
Duckworth et al., [2009] *(this report)*	01/04/2008 to 30/09/2008	DA3545G01	5

A temporary ultrasonic array was installed around the rock volume when deposition hole DA3545G01 and its neighbour DA3551G01, were first excavated in September 1999 [*Pettitt et al.,* 1999]. A total of 2467 AE triggers were obtained during monitoring of the two deposition holes. Of these 1153 were located. There was significantly more AE activity around the second deposition hole (labelled DA3545G01) than the first (DA3551G01). This difference is likely to depend upon intersection of the excavation with a greater number of pre-existing fractures. These fractures may be preferentially located in the side wall of the deposition hole or preferentially orientated to the *in situ* stress field. Fracturing associated with excavation-induced stresses was observed with AEs distributed mainly in regions orthogonal to the maximum principal stress, σ_1. This

was consistent with observations from the Canister Retrieval Tunnel and from dynamic numerical models. AEs, and hence microcrack damage, were shown to locate in clusters down the deposition hole and not as a continuous 'thin skin'. *Pettitt et al.,* [2000] showed that these clusters were associated with weaknesses in the rock mass generated by excavation through pre-existing fractures. Damage in the side wall of the deposition holes depended significantly on these pre-existing features. The *in situ* stress field was a contributing factor in that induced stresses were sufficiently high to create damage in these weakened regions although not sufficiently high to create significant damage in the rock mass as a whole.

A permanent ultrasonic array, with transducers grouted into instrumentation boreholes, was installed in the rock mass in June 2002. In this arrangement, ultrasonic monitoring has been conducted between 20th March and 9th October 2003, and then from 29th September 2004 to the present. A gap in monitoring occurred when the ultrasonic acquisition system was used for another experiment in the HRL (Pillar Stability Experiment). Processing and reporting of results has been undertaken, as shown in Table 4-3, and is further discussed in Section 4.2. A description of instruments measuring other environmental factors (such as temperature and pressure) and their locations can be found in *Goudarzi and Johannesson* [2006].

Appendix II Methodology

Data Acquisition

The ultrasonic array consists of twenty-four ultrasonic transducers configured as eight transmitters and sixteen receivers installed into four instrumentation boreholes. The transducers are fixed into the boreholes using specially designed frames (Figure 4-13) – two transmitters and four receivers per frame. The boreholes are vertical, 76mm in diameter and approximately 10 meters in length distributed around each deposition hole volume. The array has been designed to provide good coverage for AE locations and to provide 'skimming' ray-paths that pass within a few centimetres of the deposition-hole void so as to sample the rock immediately adjacent to the deposition-hole wall. The layout of the instrumentation boreholes is shown in Figure 4-14 and described further in Table 4-4. Each of the ultrasonic transducers has a hemispherical brass cap fixed over its active face and is then spring-loaded against the borehole surface so as to obtain good coupling to the rock mass. The boreholes have then been filled with a slightly expansive grout so as to permanently fix the transducers in place, reduce the likelihood of damage to the transducers and to remove the borehole voids.

Figure 4-13: *Top: Schematic diagram of the locations of all transducers on a single frame. Left: Photo of a section of the transducer assembly. Right: The transducer assembly during installation.*

The piezoelectric transducers operate by converting a transient elastic wave into an electric signal or visa versa. The monitoring system is then operated in one of two modes. The first is used to passively monitor AE activity preferentially within the array volume. AEs release elastic energy in the same way as 'earthquakes' but over a very small scale. At these frequencies AEs have a moment magnitude (M_w) of approximately -6. They occur either during the creation process of new fractures within the medium, or on pre-existing fractures due to small scale movements. Each receiver has a frequency response of approximately 35-350 kHz and contains a 40dB pre-amplifier. This minimises a reduction in signal-to-noise between the sensors and the acquisition system. The sensors have a vulcanised surround and a high pressure reinforced cable to protect them from water infiltration. In addition, polyamide tubes and *Swagelok* connectors have been fitted to the cables to reduce the likelihood of breakage.

Figure 4-15 shows a schematic diagram of the acquisition system used. Cables from each transducer pass through the pillar between the PRT and the G-tunnel. Data acquisition uses a Hyperion Ultrasonic System controlled by a PC, set up within a cabin provided by SKB. This has 16 receiving channels and 8 transmitting channels. An AE is recorded when the amplitude of the signal on a specified number of channels exceeds a trigger threshold within a time window of 5ms. The system then records the full-waveform signals from all 16 transducers. In this case a trigger threshold of 50mV on three channels was used. This allows the system to have sufficient sensitivity to record high quality data without recording an abundance of activity that cannot be processed due to very small signal to noise on only a few channels. The captured signals are digitised with a sampling interval of 1μs and a total length of 4096 data points. In general, low noise levels were observed (<2mV) giving high signal to noise and good quality data. AE monitoring is set to switch off during daytime working hours (6am-8pm) so as to minimise the amount of noise recorded from human activity.

A second operating mode actively acquires ultrasonic waveforms by scanning across the volume. This allows measurements of P- and S-wave velocities and signal amplitudes over a possible 128 different ray-paths. By repeating these ultrasonic surveys at increments in time, a temporal analysis is obtained for the variation in medium properties. Ultrasonic surveys are conducted daily at 1am in order to measure changes in P- and S-wave signals. At that time of night, no human activity will cause noise that can interfere with the signals received. A Panametrics signal generator is used to produce a high frequency electric spike. This is sent to each of the 8 transmitters in turn. The signal emitted from each transmitter is recorded over the 16 receivers in a similar fashion to that described above. An external trigger pulse from the signal generator is used to trigger the acquisition system and identifies the transmission start time to an accuracy of one sample point. In order to decrease random noise the signal from each transmitter is stacked 100 times.

Table 4-4: Boreholes used for AE monitoring of deposition hole DA3545G01.

SKB Borehole designation	ASC Borehole reference	Transducer Numbers
KA3543G01	1	T1, T2, R1-R4
KA3545G02	2	T3, T4, R5-R8
KA3548G03	3	T5, T6, R9-R12
KA3548G02	4	T7, T8, R13-R16

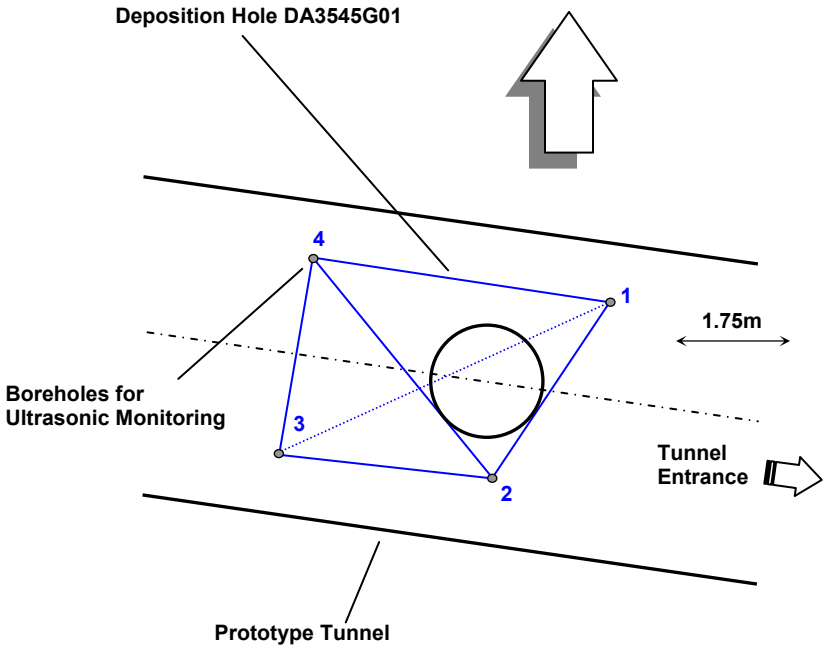

Figure 4-14: *Plan view of the array geometry for Deposition Hole DA3545G01 during heating in the Prototype Tunnel. The blue solid lines represent direct ray-paths between sondes illustrating their 'skimming' nature. The blue dashed line represents a ray-path that travels through the deposition hole.*

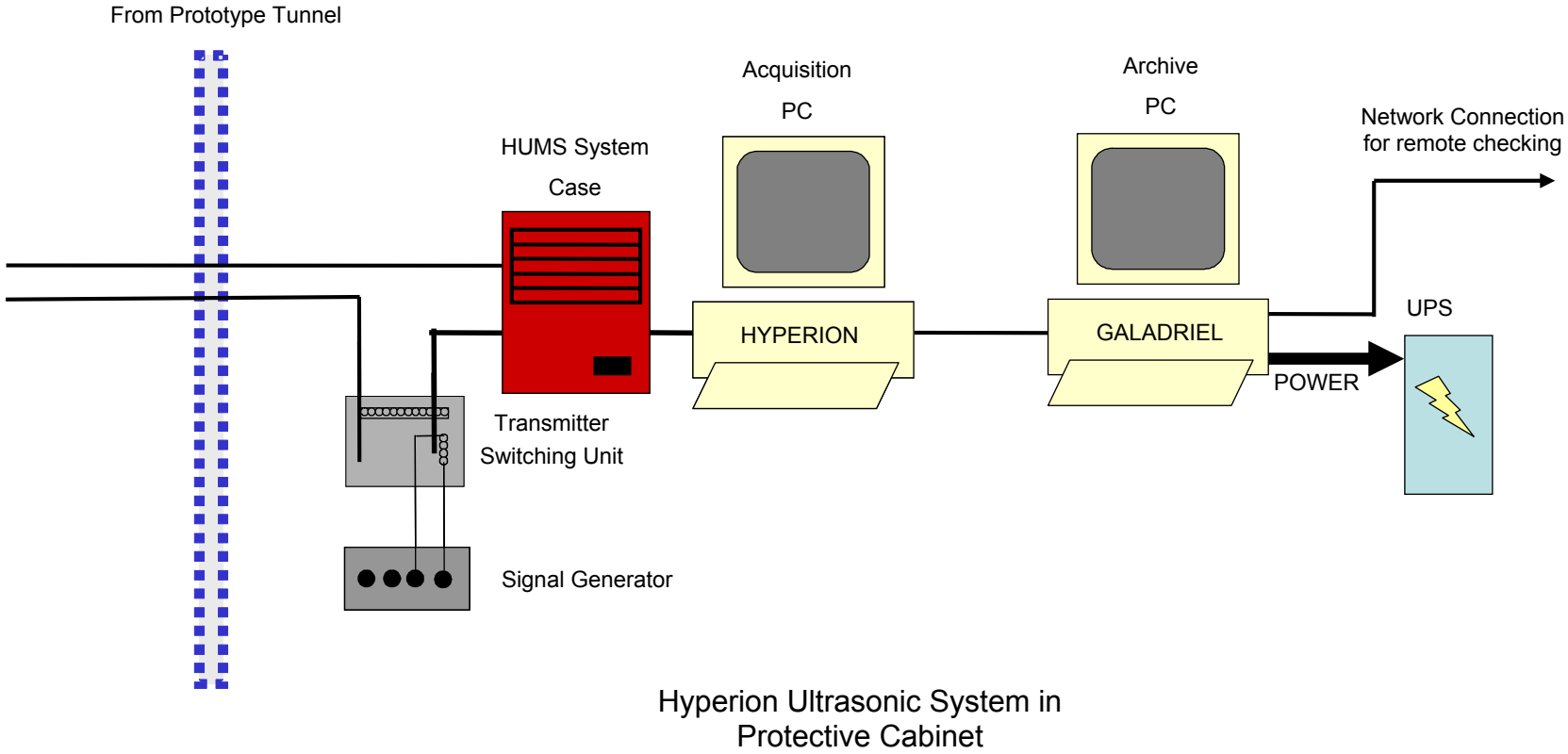

Figure 4-15: *Schematic diagram of the hardware used for the heating stage in the Prototype Repository. The ultrasonic pulse generator sends a signal to each transmitter and the resulting signal is recorded on each receiver. The receivers are also used to listen for AE activity. The archive PC is required to make a copy of the data for backup purposes.*

Processing Procedure

Overview

ASC's InSite Seismic Processor has been used to automatically process both the AE and ultrasonic survey data. Appendix IIIA and Appendix IIIB give the processing parameters used. *Pettitt et al.,* [2005] provides a detailed description of this software.

Ultrasonic Data Procedure

The ultrasonic survey full-waveform data was initially stored with the AE data. This was automatically sorted and the survey data extracted to a separate processing project. A reference survey, taken from previous monitoring periods was imported into the project and used to process the ultrasonic results. The reference survey was recorded on 8th December 2004 and has had first P- and S-wave arrivals manually picked from the waveform [*Haycox et al.,* 2006a]. Since transmitter and receiver locations are known, the ultrasonic velocity for each ray-path can be calculated with an estimated uncertainty of ±30 ms^{-1} (±3 data points). Cross-correlation can then be used to automatically process subsequent surveys. This technique cross-correlates P- and S-wave arrivals from a transmitter-receiver pair with arrivals recorded on the same transmitter-receiver pair from the reference survey. Note that when the transmitter and receiver are on the same borehole, the ray-path is not used due to the introduction of transmission effects from the instrumentation borehole, grout and transducer frames.

Manual picking of arrivals by the examiner can often be erroneous due to random noise superimposed on the first few data points of the first break. By using the cross-correlation procedure it reduces this uncertainty and allows high-resolution analysis, with an estimated uncertainties of ± 2 ms^{-1} between surveys on individual ray-paths, to be performed and hence small changes in velocity to be observed. This is extremely important when changes in rock properties occur over only a small section (~5%) of the ray-path.

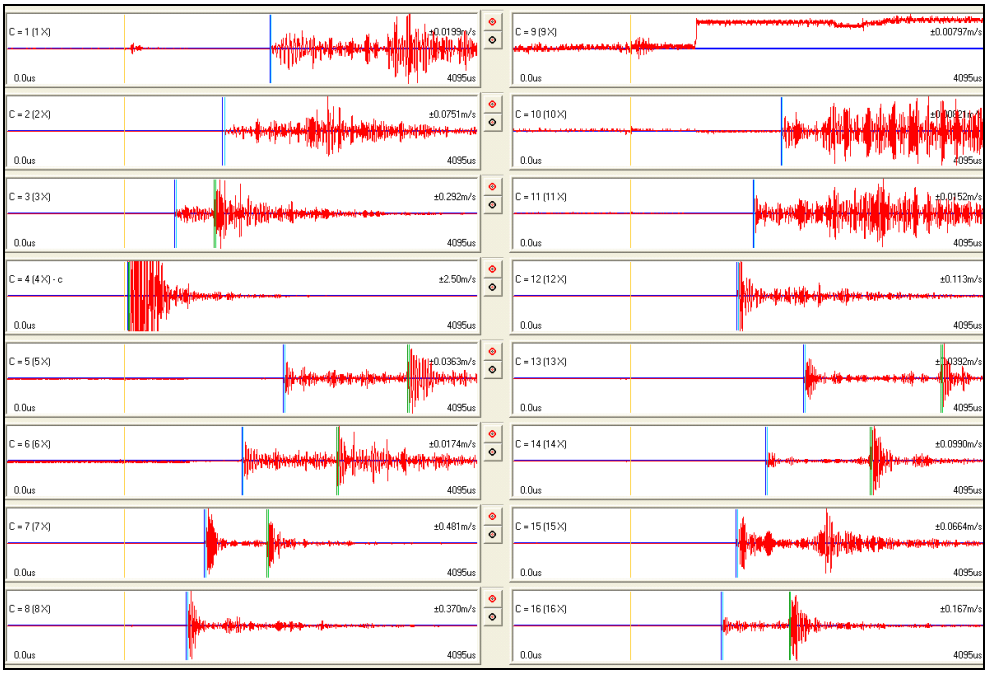

Figure 4-16: *Waveforms recorded from one transmitter on the array of sixteen receivers. The gold markers indicate the transmission time. The blue and green markers indicate picked P- and S-wave arrivals respectively.*

Figure 4-16 gives example waveforms recorded from one of the transmitters during this reporting period. Each waveform is first automatically picked to obtain an estimate of the P-wave or S-wave arrival. A window is then automatically defined around the arrival and a bell function is applied, centred on the automatic pick. The data at the ends of the window then have a much smaller effect on the cross-correlation. The windowed data is then cross-correlated [*Telford et al.,* 1990] with a similar window constructed around the arrival on the reference survey. The change in arrival time is then converted to a change in velocity knowing the manually-picked arrival time for the reference survey. Waveforms that do not provide automatic picks are not cross-correlated. This gives an automatic discrimination of signals that have very poor signal to noise ratios and could give spurious cross-correlation results from poor discrimination of the first arrival. During the automatic processing an arrival amplitude is also calculated from within a processing window defined by a minimum and maximum transmission velocity. This provides a robust measure of arrival amplitudes between surveys.

When calculating average velocities and amplitudes, ray-paths passing through the deposition hole are removed due to the uncertain transmission paths produced by the wave travelling in the rock around the deposition hole and through the bentonite, fluid and canister fill. Therefore the majority of ray-paths between boreholes 1 and 3 (transmitters 1, 2, 5, 6 and receivers 1, 2, 3, 4) are not used in the analysis. An exception is made for the deepest ray-paths that pass under the deposition hole entirely through rock.

The dynamic Young's modulus E, and dynamic Poisson's Ratio, σ, can be calculated from the velocity measurements using Equation 1 and Equation 2.

$$E = \rho V_S^{\,2}\left(\frac{3V_P^{\,2} - 4V_S^{\,2}}{V_P^{\,2} - V_S^{\,2}}\right) \qquad \text{Equation 1}$$

$$\sigma = \frac{V_P^{\,2} - 2V_S^{\,2}}{2\left(V_P^{\,2} - V_S^{\,2}\right)} \qquad \text{Equation 2}$$

V_P and V_S values are also used to model for crack density (c) and saturation (s) in the rock mass using the method of *Zimmerman and King* [1985]. The crack density parameter is defined by the number of cracks (penny-shaped) per unit volume multiplied by the mean value of the cube of the crack radius (Equation 3). This method assumes the elastic modulus E and σ in the damaged material normalized to the undisturbed material, decrease exponentially with crack density. Also assumed are the shear modulus (μ) is unaffected by s, and the bulk modulus (k) increases linearly with s, equalling that of uncracked rock when s=1. Equation *4* shows the calculation used to determine saturation.

$$c = \frac{9}{16}\ln\left(\frac{2\mu}{E_0 - 2\mu v_0}\right) \qquad \textit{Equation 3}$$

$$s = \frac{k(c,s) - k(c,0)}{k_0 - k(c,0)} \qquad \textit{Equation 4}$$

The calculations require an estimation of the completely undisturbed rock (i.e. an unsaturated, uncracked and intact rock mass). This study assumes values of V_{0P} = 6660ms^{-1}, and V_{0S} = 3840ms^{-1} for the undisturbed material taken from laboratory tests on a similar granite, summarized in *Maxwell and Young* [1995]. A value of 2650 kg m^{-3} is presented by *Pettitt et al.,* [2002] for the density of the rock mass.

Young's Modulus and Poisson's ratio are calculated from measured velocities by making the assumption that the transmission medium is isotropic elastic. Under this assumption a rock can be completely characterised by two independent constants. One case of an isotropic elastic medium is a rock with a random distribution of cracks embedded in an isotropic mineral matrix. Under the application of a hydrostatic compressive stress, the rock will stay isotropic but become stiffer (characterised by increased velocity (V_P and V_S) and therefore increased Young's Modulus). In contrast, under the application of a uniaxial compressive stress, cracks with 'normals' parallel or nearly parallel to the applied stress will preferentially close and the rock will take on a transversely isotropic symmetry. Under this situation P- and S-wave velocities become variable with orientation. The crack density and saturation calculations also assume an isotropic elastic medium.

It should be noted that E and σ calculated in this report are dynamic measurements due to the small strains exerted on the rock mass at high frequencies from the passing ultrasonic waves. Static E and σ measurements, made from uniaxial laboratory tests on rock samples, may be different from dynamic values – even if sample disturbance is minimal – due to the larger strains exerted over relatively long periods of time.

Acoustic Emission Procedure

The procedure used to process the AEs in this reporting period has been undertaken as follows:

1. Calibration surveys from the installation phase (when the deposition hole was open) have been used to optimise an automatic picking and source location algorithm and check location uncertainties. ASC's InSite seismic processing software was used for location and visualisation.

2. Where possible, P- and S-wave arrival times were measured for each AE using the automatic picking procedure.

3. AEs with ≥6 P-wave arrival times were input into a downhill-simplex location algorithm [*Pettitt et al.,* 2005]. This has the option of incorporating either a three-dimensional anisotropic velocity structure or an isotropic structure. Velocities calculated from the ultrasonic surveys were used.

4. The waveforms from all events were visually inspected to ensure they were 'real' acoustic emissions. Events were removed if they had the appearance of noise spikes (increase in amplitude is recorded on all channels at the same time) or they were the result of human noise (long period events that occur at close intervals during the day).

5. The acoustic emissions that remained had their arrivals manually picked to obtain the best possible location. Any events that located outside the expected region of activity were further checked to ensure accuracy. Experience from previous studies around deposition holes showed that large source location errors were produced if significant portions of a ray-path passed through the excavated deposition hole void. This only becomes a problem for the largest AEs. AEs were reprocessed with these ray-paths removed.

6. Finally, a filter was applied to remove all AEs with a location error greater than 1.0.

During the equipment installation phase, calibration shots were undertaken to assess the sensitivity of the system to AEs and to determine the accuracy with which real events could be located by the array of sensors. A series of tests, called 'shots', were performed on the wall of deposition hole DA3545G01 (Figure 4-17). The shots consisted of undertaking 10 'pencil lead breaks' and 10 hits with a screw-driver at 1 metre intervals down 4 lines along the wall of the deposition hole. The pencil-lead tests involved breaking the 0.5 mm lead from a mechanical pencil against the borehole wall. This is a 'standard' analogue for an AE as it generates a similar amount of high-frequency energy. An example of a pencil lead break test is shown in Figure 4-18. This was made at 6 metres below the tunnel surface on the wall of the deposition at a point adjacent to borehole KA3548G02. This corresponds to an AE source dimension on the millimetre scale (grain size).

The screw-driver hits provided a good amplitude signal for assessing the accuracy with which events can be located within the volume surrounded by the array. Figure 4-17 shows the results from one processed set of locations for a line of shots down the deposition hole. This shows that the array is able to locate events with good accuracy and consistency within an estimated uncertainty of approximately 10cm.

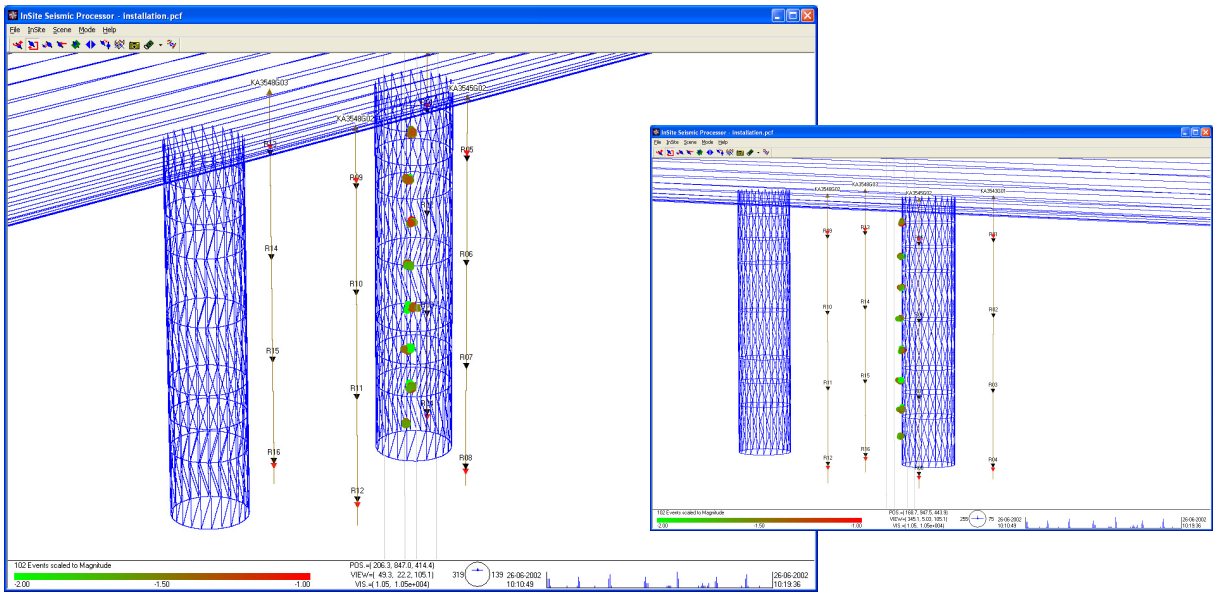

Figure 4-17: *Locations of calibration shots obtained from a series of tests at 1 metre intervals down the wall of deposition hole DA3545G01. The two views show that these line up and are located close to the surface of the hole.*

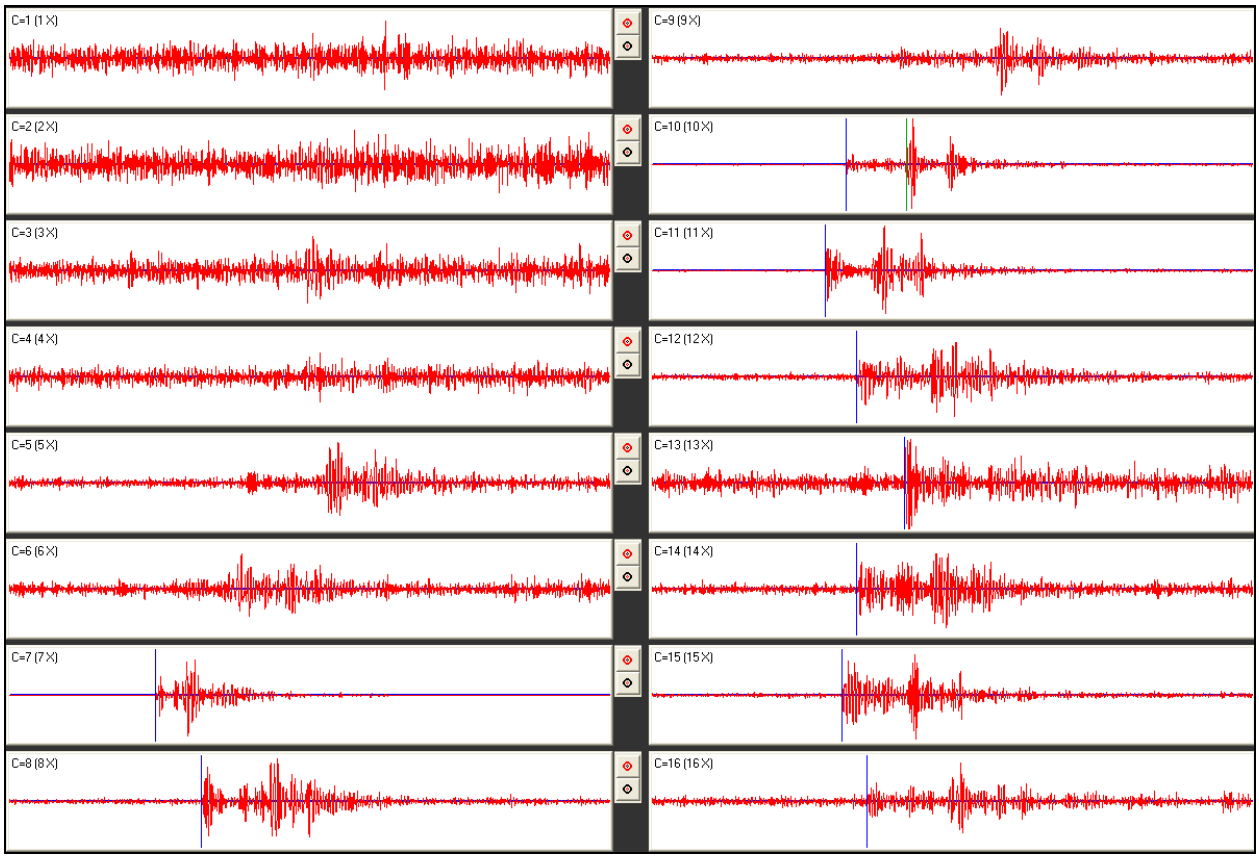

Figure 4-18: *Example waveforms from each of the 16 receiving channels for a 'pencil-lead break' test undertaken against the Deposition Hole (DA3545G01) wall 6 metres below the tunnel floor.*

Appendix III Processing Parameters

A: Ultrasonic survey processing parameters:

PROCCESSING PARAMETERS **Velocity survey processing**

EVENT INITIALISATION	
View/process waveforms by	Channel
Channel-view Width-to-height ratio	6
Waveform Response type	Set from sensor
Sampling time	1
Time units	Microseconds
Pre-signal points	200
Spline sampling time	0.2
Waveform To point	1023
P-Time correction	0
S-Time correction	0
Automatically update Channel Settings	NOT SET
Project Files	NULL

AUTO PICKING	
Allow P-wave-autopicking	YES, Use first peak in the auto-pick function
Back-window length	100
Front-window length	35
Picking Threshold	4
Min. Peak-to-Peak amplitude	0
Allow S-Wave Autopicking	YES, Use first peak in the auto-pick function
Back-window length	100
Front-window length	35
Picking Threshold	3
Min. Peak-to-Peak amplitude	0
Allow Automatic Amplitude Picking	YES
Use Velocity Window Picking	YES
P-wave Min. Velocity/Max. Velocity	4500, 6500
S-wave Min. Velocity/Max. Velocity	2500, 3500

CROSS-CORRELATION	
CCR Events	Referenced to a Survey
Reference Component	20041208005920
Reference Event	NULL
Window construction method	Front to Back
Window comparison method	Fixed to reference picks
Window Parameters	Back-window length = 20 Front-window length=30 Rise-time multiplier = NULL Power to raise waveform =1 Split to a Spline function = YES Obtain absolute waveform= NOT SET

LOCATER	***(not used in velocity surveys)***
Method	SIMPLEX INTO GEIGER
Method settings Simplex settings Geiger settings 	Tolerance = 0.01 LPNorm = 1 P-wave weighting = 1 S-wave weighting = 1 Use Outlier Identification = NOT SET Arrival error factor = ×2 Tolerance (Loc. units) = 0.01 Step size (Loc.units) = 0.1 Max. Iterations = 100 Conditional No. Limit = 10000000000
Velocity Structure	Homogeneous Isotropic
Velocity Structure settings	P-wave velocity = 6000 ms^{-1} S-wave velocity = 3350 ms^{-1} Attenuation = 200 Q(S) value = 100
Data to use	P-wave Arrivals Only
Distance units	Metres
Working time units	Microseconds
Min P-wave arrivals	0
Min S-wave arrivals	0
Min Independent arrivals	5
Max. Residual	20
Start point	Start at the centroid of the array
Write report to RPT	NOT SET
Source parameters	Set to calculate automatically

B: AE processing parameters:

PROCCESSING PARAMETERS **AE processing**

EVENT INITIALISATION	
View/process waveforms by	Channel
Channel-view Width-to-height ratio	6
Waveform Response type	Set from sensor
Sampling time	1
Time units	Microseconds
Pre-signal points	200
Spline sampling time	0.2
Waveform To point	1023
P-Time correction	0
S-Time correction	0
Automatically update Channel Settings	SET
Project Files	NULL

AUTO PICKING	
Allow P-wave-autopicking	YES, Use max peak in the auto-pick function
Back-window length	100
Front-window length	35
Picking Threshold	5
Min. Peak-to-Peak amplitude	0
Allow S-Wave Autopicking	YES, Use max peak in the auto-pick function
Back-window length	100
Front-window length	35
Picking Threshold	5
Min. Peak-to-Peak amplitude	0
Allow Automatic Amplitude Picking	NOT SET
Use Velocity Window Picking	YES
P-wave Min. Velocity/Max. Velocity	4500, 6500
S-wave Min. Velocity/Max. Velocity	2500, 3500

CROSS-CORRELATION	***(not used in AE processing)***
CCR Events	NOT SET
Reference Component	NOT SET
Reference Event	NULL (not activated)
Window construction method	Individual
Window comparison method	Fixed to reference picks
Window Parameters	Back-window length = 20 Front-window length = 30 Rise-time multiplier = NULL Power to raise waveform =1 Split to a Spline function = NOT SET Obtain absolute waveform= NOT SET

LOCATER	
Method	SIMPLEX INTO GEIGER
Method settings Simplex settings Geiger settings 	Tolerance = 0.01 LPNorm = 1 P-wave weighting = 1 S-wave weighting = 1 Use Outlier Identification = NOT SET Arrival error factor = ×2 Tolerance (Loc. units) = 0.01 Step size (Loc.units) = 0.1 Max. Iterations = 100 Conditional No. Limit = 10000000000
Velocity Structure	Homogeneous Isotropic
Velocity Structure settings	P-wave velocity = 5986.106 ms^{-1} S-wave velocity = 3349.171 ms^{-1} Attenuation = 200 Q(S) value = 100
Data to use	P-wave Arrivals Only
Distance units	Metres
Working time units	Microseconds
Min P-wave arrivals	0
Min S-wave arrivals	0
Min Independent arrivals	5
Max. Residual	20
Start point	Start at the centroid of the array
Write report to RPT	NOT SET
Source parameters	Set to calculate automatically

EVENT FILTER	
Date and Time	NOT SET
Location volume	Minimum = (235, 880, 420)
	Maximum = (300, 964, 463)
L. Magnitude	NOT SET
Location Error	1
Independent Instruments	Minimum = 0

SOURCE PARAMETERS	
Automatic source-parameter windows	P-wave back window = 10
	P-wave front window = 50
	S-wave back window = 10
	S-wave front window = 50
Source parameter calculations	Min number to use = 3
Automatic source-parameter windows	Apply Q correction = SET
	Source density = 2640
	Source shear modulus = 39131400000
	Av. radiation coefficient: Fp = 0.52 ,Fs = 0.63
Source parameter calculations	Source coefficient: kp = 2.01 , ks = 1.32
Magnitude calculations	Instrument magnitude = 1 * log (ppV) +0
	Moment magnitude = 0.666667 * log(Mo) + -6